MULTIDISCIPLINARY AND MULTIOBJECTIVE DESIGN OPTIMIZATION OF AN UNMANNED COMBAT AERIAL VEHICLE (UCAV)

A THESIS SUBMITTED TO
THE GRADUATE SCHOOL OF NATURAL AND APPLIED SCIENCES
OF
MIDDLE EAST TECHNICAL UNIVERSITY

BY

NESRİN ÇAVUŞ

IN PARTIAL FULFILLMENT OF THE REQUIREMENTS
FOR
THE DEGREE OF MASTER OF SCIENCE
IN
AEROSPACE ENGINEERING

FEBRUARY 2009

Approval of the thesis:

MULTIDISCIPLINARY AND MULTIOBJECTIVE DESIGN OPTIMIZATION OF AN UNMANNED COMBAT AERIAL VEHICLE (UCAV)

submitted by **NESRİN ÇAVUŞ** in partial fulfillment of the requirements for the degree of **Master of Science in Aerospace Engineering Department, Middle East Technical University** by,

Prof. Dr. Canan Özgen
Dean, Gradute School of **Natural and Applied Sciences** _____

Prof. Dr. İsmail Hakkı Tuncer
Head of Department, **Aerospace Engineering** _____

Prof. Dr. Ozan Tekinalp
Supervisor, **Aerospace Engineering Dept., METU** _____

Dr. İlkay Yavrucuk
Co-supervisor, **Aerospace Engineering Dept., METU** _____

Examining Committee Members:

Assoc. Prof. Dr. Serkan Özgen
Aerospace Engineering Dept., METU _____

Prof. Dr. Ozan Tekinalp
Aerospace Engineering Dept., METU _____

Assoc. Prof. Dr. Altan Kayran
Aerospace Engineering Dept., METU _____

Assist. Prof. Dr. Oğuz Uzol
Aerospace Engineering Dept., METU _____

Dr. Küçük Ayşe İlhan
Turkish Aerospace Industries, Inc. _____

Date: 6 February 2009

I hereby declare that all information in this document has been obtained and presented in accordance with academic rules and ethical conduct. I also declare that, as required by these rules and conduct, I have fully cited and referenced all material and results that are not original to this work.

Name, Last Name: NESRİN ÇAVUŞ

Signature :

ABSTRACT

MULTIDISCIPLINARY AND MULTIOBJECTIVE
DESIGN OPTIMIZATION OF
AN UNMANNED COMBAT AERIAL VEHICLE (UCAV)

Çavuş, Nesrin
M.S., Department of Aerospace Engineering
Supervisor : Prof. Dr. Ozan Tekinalp
Co-Supervisor: Dr. İlkay Yavrucuk

February 2009, 150 pages

The Multiple Cooling Multi-Objective Simulated Annealing Algorithm is used for the conceptual design optimization of a supersonic Unmanned Combat Aerial Vehicle (UCAV). Single and multiobjective optimization problems are addressed while limiting performance requirements between desired bounds to obtain viable aircraft configurations. A conceptual aircraft design code was prepared for planned but flexible combat missions. The results demonstrate that the optimization technique employed is an effective tool for the conceptual design of aircrafts.

Keywords: Airplane Design, Multidisciplinary Design, Unmanned Combat Aerial Vehicle (UCAV), Multi-Objective Optimization, Simulated Annealing

öz

BİR İNSANSIZ MUHARİP HAVA ARACININ
ÇOK DİSİPLİNLİ VE ÇOK AMAÇLI
TASARIM ENİYİLEMESİ

Çavuş, Nesrin
Yüksek Lisans, Havacılık ve Uzay Mühendisliği Bölümü
Tez Yöneticisi : Prof. Dr. Ozan Tekinalp
Ortak Tez Yöneticisi : Dr. İlkay Yavrucuk

Şubat 2009, 150 sayfa

Çoklu Soğutma-Çok Amaçlı Tavlama Benzetimi Algoritması bir sesötesi insansız muharip hava aracının kavramsal tasarım eniyilemesi için kullanılmıştır. Bir ve çok amaçlı eniyileme problemleri performans gereksinimleri istenilen sınırlar arasında tutulurken uygun uçak yapılandırmaları sağlayacak şekilde ele alınmıştır. Daha önceden planlanmış fakat esnetilebilir muharebe rotası için bir kavramsal uçak tasarım kodu hazırlanmıştır. Elde edilen sonuçlar kullanılan eniyileme tekniğinin çok amaçlı kavramsal uçak tasarımı için etkin bir araç olduğunu göstermektedir.

Anahtar kelimeler: Uçak Tasarımı, Çok Disiplinli Tasarım, İnsansız Muharip Hava Aracı, Çok Amaçlı Eniyileme, Tavlama Benzetimi Yöntemi

To my father, NUH ÇAVUŞ,
who taught me the importance of knowledge
and the importance to possess it.

And to my mother, Ayşe Çavuş,
and my brother, Mehmet Çavuş,
thanks for their existences…

TABLE OF CONTENTS

LIST OF TABLES

TABLES

LIST OF FIGURES

FIGURES

NOMENCLATURE

a	Speed of sound
a_t	Tail lift curve slope
A	Area
AR	Aspect ratio
b	Span
c	Chord
c_d	Airfoil drag coefficient
c_{d0}	Airfoil drag coefficient at zero angle of attack
c_l	Airfoil lift coefficient
c_{l0}	Airfoil lift coefficient at zero angle of attack
$c_{l\alpha}$	Airfoil lift curve slope
$c_{m\alpha}$	Airfoil pitching moment curve slope
c_r	Root chord length
c_t	Tip chord length
$\bar{c}$	Mean aerodynamic chord length
c_D	Drag coefficient
$c_{D\alpha}$	Airplane drag curve slope
c_{D0}	Drag coefficient at zero angle of attack
$c_{DL\&P}$	Drag coefficient with leakages and protuberances
c_f	Flat-plate skin-friction drag coefficient
c_L	Lift coefficient
$C_{L\,\alpha}$	Airplane lift curve slope
d	Combat time
D	Drag, Diameter
e	Oswalds efficiency
E	Endurance
F_M	Total force on the two main wheels
F_N	Force on nose wheel
g	Gravitational acceleration
H	Height, Hour

K_{vs}	Variable sweep constant
L	Lift, length
l_t	Tail arm
M	Moment, Mach number
n	Load factor
N_z	Ultimate load factor
q	Dynamic pressure
Q	Interference factor
R	Radius, range, hourly rate
Re	Reynolds number
s_L	Landing distance
s_{TO}	Take-off distance
S	Reference area
t	Time
T	Thrust
T_{av}	Thrust available
T_i	Turbine inlet temperature
V	Velocity
V_f	Fuel volume
w	Width
W	Weight
W_0	Take-off gross weight
W_{dg}	Design gross weight
W_e	Empty weight
W_f	Fuel weight
xx	Number of combat turns
x_{acwb}	Aerodynamic center of the wing-body
x_n	Neutral point
$\bar{x}$	Mean aerodynamic chord x location
$\bar{y}$	Mean aerodynamic chord y location
$\bar{z}$	Mean aerodynamic chord z location
θ	Pitch angle
ρ	Density
Δ	Change

μ	Friction coefficient
λ	Taper ratio
Λ	Sweep angle
τ	Ratio of tip and root thickness ratios
Γ	Dihedral angle
β	Prandtl Glauert
σ	Density ratio
ω	Rate of turn
#	Number of
0	Sea level
A	Aft , Avionics
ac	Aerodynamic center
c	Chord , combat
cg	Center of gravity
cr	cruise
d	dash
D	Development
e	engineering
E	Engine (production)
eng	Engine
exp	Exposed
F	Flight test
fus	Fuselage
HT	Horizontal tail
L	Landing
LE	Leading edge
LG	Landing gear
ltr	loiter
M	Mid-body, Manufacturing
max	maximum
min	Minimum
misc	Miscellaneous
net	Net

N	Nose
plf	Planform
q	Quality control
r	Root
Ref	Reference
s	Steady state
sh	Sears-Haack body
t	Thickness , tooling
TO	Take-off
VT	Vertical tail
w	Wing
wb	Wing-body
wet	Wetted
∞	Free stream
BPR	Bypass Ratio
FF	Fitness Function
FTA	Number of flight test aircraft
ROC	Rate of climb
SFC	Specific fuel consumption
TOG	Take-off ground roll
UCAV	Unmanned Combat Aerial Vehicle

CHAPTER 1

INTRODUCTION

1.1 Literature Survey

1.1.1 History of Unmanned Aerial Vehicles (UAV)

Flying, a dream of human beings, was experimented by a Turkish scientist Hezarfen Ahmet Çelebi as early as 1630 with homemade wings from the top of the Galata Tower to Doğancılar Square above Üsküdar in İstanbul [24]. Even in those days after this brave move, people believed that flying was not just a dream. Afterwards, lots of attempts had been made by people to attain this enjoying experience.

In 1804 George Cayley flew the first fixed wing unmanned model glider in Yorkshire, England. Later, John Stringfellow performed the first flight of a powered unmanned aircraft, with a 12-foot spanned wing [41].

In December 17th of 1903 the Wright brothers, Orville and Wilbur, achieved the first successfully sustained powered flight with the first working airplane of human history.

On January 7th 1918 the Dayton Wright Airplane Company was awarded for the first production contract of an unmanned aircraft. The first successful flight was achieved on October 4th. Before this flight, a powered, full-size, unmanned aircraft by the Curtiss Sperry Aerial Torpedo performed the first successful flight on 6th of March of 1918 in New York. Subsequently, the British RAE 1921 Target,

a radio controlled unmanned aircraft, had the first successful flight without a safety pilot onboard on September 3rd 1924 [41].

Then, in 1933 Fairey Queen used an unmanned aircraft as a target drone over the Mediterranean Sea. Afterwards, on June 12th 1944 German Fi-103 "V-1" was used as a cruise missile in a combat. Similarly, the U.S. Navy TDR-I attack drone was used for a strike firstly as an unmanned aircraft in a combat on October 19th 1944 [41].

The first scientific research using an unmanned aircraft, a modified version of the Northrop P-61 Black Widow, was done on April 1946 to collect meteorological data. The Northrop Radioplane SD-1 Falconer/Observer was used for exploration in 1955. On the other hand, the first unmanned helicopter flight was done by the Gyrodyne QH-50A in 1960, 12th of August. Then, the first trans-Atlantic crossing by an unmanned aircraft was performed on 20-21 August 1998 by the Insitu Group's Aerosonde™ Laima, whereas the first trans-Pacific crossing by an unmanned aircraft was performed about three years later on 22-23 April 2001 by the Northrop Grumman Global Hawk [41].

Then on May 22, 2002 the first flight of an unmanned combat aerial vehicle was completed by X-45A built by Boing Company [70]. The purpose of this technology program was to produce a defence tool against any enemy missions [63].

Today many aerospace companies try to produce unmanned aerial vehicles having the characteristics of combat aerial vehicles, with various specifications; emphasizing concepts with *stealth* properties on top.

1.1.2 Unmanned Combat Aerial Vehicle (UCAV) Specifications

An unmanned combat air vehicle (UCAV) is a class of unmanned aerial vehicle (UAV). Like UAVs, UCAVs can also send observation results to ground stations. They differ from ordinary UAVs, because they are also designed to deliver weapons (attack targets) and have higher agility, possibly with a great degree of autonomy [67].

As the developed cruise missiles like Tomahawk, UCAVs are capable of attacking variety of targets. However, UCAVs have superiority on cruise missiles because of their air-to-ground and air-to-air attacking capability. These tasks become attainable with precision guidance and advanced control algorithms. Furthermore, after completing their tasks UCAVs can fly back to their base and not be disposed after the mission.

Current UCAVs are aimed to operate virtually autonomously. They can be programmed with route and target details, and then conduct the mission even without help of human pilots [67].

Unmanned air vehicles have the advantage that they can challenge high g-loads and therefore include high maneuvering capability. Because they do not have a pilot onboard, the design is limited by the engine performance and the structure. On the other hand, no pilot means no cockpit so cleaner aerodynamic shape, less avionics and as a result a lighter aircraft. In addition, the aircraft can be made stealthier because of the freedom to design a geometry with lower radar cross section.

Since, there is no pilot the aircraft can be built smaller than other fighter aircraft or it may have larger wings to carry more missiles. The wing span and shape are designed without concerning a pilot's visibility.

UCAVs are also capable of flying without risking a human life onboard. Moreover, no pilot training will be required to operate these vehicles. Therefore, the range, the endurance, the combat time and the cruise ceiling are only limited with the aircraft performance.

In summary, the important properties of the UCAVs are defined as precision, agility, stealthiness, and low operating cost. By eliminating human-related structures and systems, an aircraft becomes much lighter, stealthier and also much cheaper. Together with pinpoint attacking features these modern combat vehicles have the attributes to be the best choice for the Defence Systems in the 21st century.

The features of existing UCAVs are added in Appendix B. The aircraft included are: Boeing X-45C, Northrop Grumman X-47B, and General Atomics Aeronautical Systems MQ-9 Reaper.

1.1.3 Aircraft Design

As mentioned in the previous section an UCAV has many advantages, which may be exploited for an excellent result. The following lines describe how this might be achieved.

An aircraft design begins with establishing the requirements. These requirements must be technologically and economically feasible.

The steps of designing a new UAV are summarized in Figure 1.1.

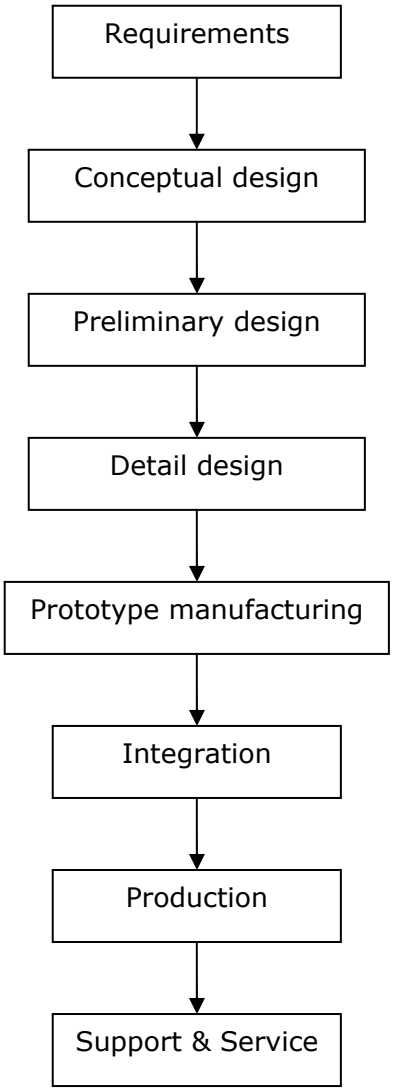

Figure 1.1 Design steps for a new UAV [33]

An unmanned aerial vehicle design process is described more in detail in Ref. [33]. While designing an aircraft many disciplines are involved in the process. This can be illustrated in the Figure 1.2.

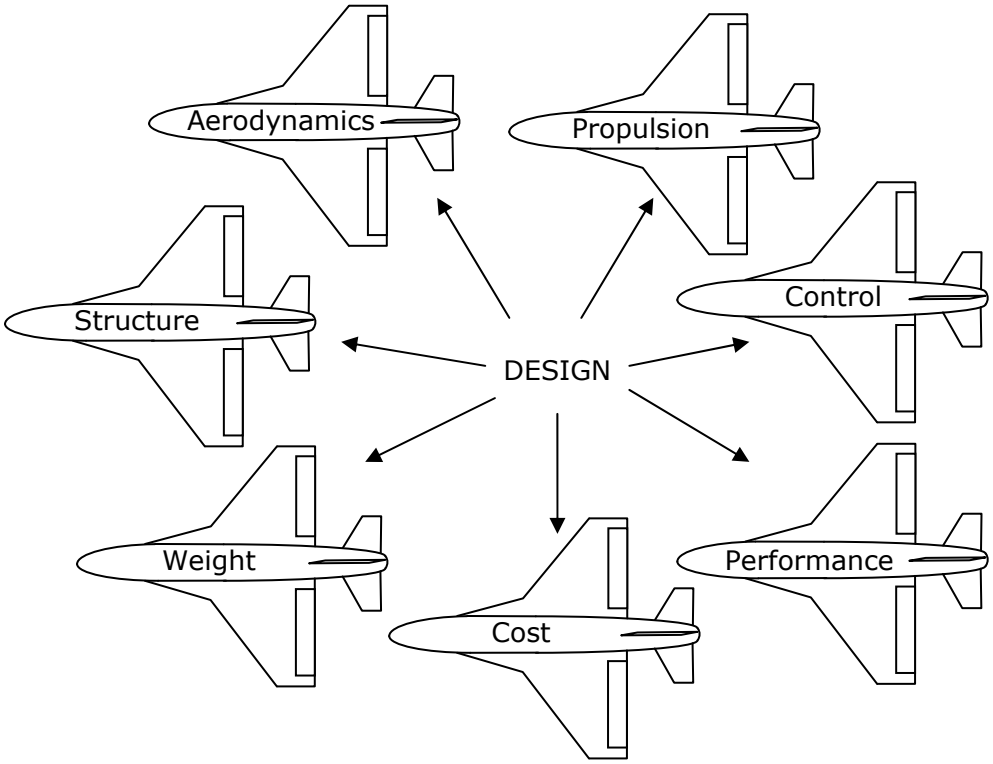

Figure 1.2 Aircraft design areas

All these disciplines are integrated and must work well in order to reach a successful design. Each of these disciplines is vital and should not be underrated. Nevertheless, some of them can be considered more important than others during the design process.

In the following, some aircraft design studies were summarized to conceive how people deal with the importance and priorities of these disciplines. Each of these efforts was based on the mentioned disciplines fundamentally with dealing one or more at a time.

Ref. [52] developed a methodology for a morphing UCAV for the mission requirements and related conceptual design. By designing this kind of UCAV, performance was aimed to be better for the planned mission. The mission requirements are determined according to the given objectives by this method.

After finding these requirements the initial shape and size of a morphing aircraft is designed conceptually, then the geometry is varied parametrically for the given mission.

Ref. [39] examined the aerodynamic performance and stability for different types of wing planforms for UCAVs. It was proved that, by beginning with basic concepts wing planform, performance and stability can be predicted efficiently to compare them with each other.

Ref. [68] represented a conceptual design study of the 1303 UCAV configuration where two conceptual design trade-offs were examined. With the determined UCAV planform shape, different sizes of UCAVs are analyzed for the performance requirements to find the trigger design parameters for a UCAV.

Ref. [40] considered flow improvement at high lift conditions for UCAVs. Leading edge vortex flaps for moderate sweep wings were applied. And aerodynamic performance results are obtained using Euler analysis.

Ref. [50] studied a UCAV configuration computationally using a high-order Overset-Grid Algorithm. A 1303 UCAV configuration was selected as a sample to simulate the complex flow field around it.

Ref. [11] searched for advanced task assignment scenarios for UCAVs running for two objectives: overall minimum weapon cost and survivability after completing the mission. Besides these two objectives, determination weapon requirements for each type of target, assigning priorities to the target types, carriage of different types of weapons and constraints for usage of these weapons to specific target types were also concerned and studied.

From all of these studies and researches it is understood that aircraft design involves lots of disciplines contradicting each other. In Ref. [71], it is stated that the powerful design tool for the aerospace community is the optimization methodology, for a multidisciplinary system. The successful techniques in this area are capable of finding good results for both in the preliminary and detailed design stages [71].

1.1.4 Aircraft Design Optimization

Aircraft are developed as a result of large amounts of accumulated knowledge, lots of effort and expenses. The developers as well as the customers want to get the best result in terms of performance and cost. The set of viable solutions is known as a "feasible" design. The design will be a result of a set of conflicting requirements. For example, one might want to have a military aircraft that has long range, a high endurance compared to its competitors, but also cheap. This is possible from a performance stand-point, but the cost and the dimension of the aircraft will also be large; therefore these parameters will contradict with each other while the aircraft is being developed.

To get the best result that meets all requirements to its best, some optimization techniques must be used to find an optimized aircraft configuration.

Ref. [31] applied different configurations for aircraft conceptual design to obtain performance parameters. A numerical optimization procedure was used to investigate the effect of different geometrical and technological parameters on take off gross weight for an aircraft.

Ref. [35] examined the aerodynamic optimization on Eurofighter project within multidisciplinary design environment.

Ref. [8] introduced a multi-variable optimization program for a modern combat aircraft. Some properties of previous combat aircraft, such as low observability were selected in order to reach a viable shape for this objective. An existing design program was developed and then combined with a general-purpose gradient search code for non-linear optimization. This optimization was based on changing design variables and getting the sensitive performance parameters and minimizing the empty weight.
Ref. [45] examined the role of various optimization techniques on the aerodynamic design of military combat aircraft. Throughout the paper aerodynamic optimization was applied in multi-objective environment. Design requirements were grouped into three as to find the resultant aircraft having transonic, supersonic and with good transonic performance and a supersonic

dominant performance. The used multi-objective design optimization based on shape optimization for performance and controllability in these conditions.

Ref. [14] applied Pareto frontier methods to optimize the wing of a generic modern military delta aircraft in multi-disciplinary environment. They used two optimizers: a multi objective genetic algorithm (MOGA) and a simple gradient-based method.

Ref. [42] examined the three dimensional configurations for aerodynamic optimizations. Non-linear solutions were tried to be caught by this aerodynamic optimization method. The problems in hand were a biconic re-entry capsule, a supersonic commercial transport wing and a supersonic commercial transport wing/body configurations. The applied optimization method was based on Euler/Navier Stokes equations.

Ref. [49] reported Alenia multi-disciplinary design optimization for transonic 2D and 3D optimization problems. A wing-body configuration was optimized aerodynamically and structurally. The applied optimization method uses a quasi-Newton method for unconstrained problems and Zoutendijk's feasible direction algorithm [60] for constrained problems.

Ref. [38] designed and optimized wings for subsonic and transonic regimes. For optimization finite difference based commercial code had been used with added option to use the Newton method. The type and number of design variables were also considered and the Bèzior polynomia was used to get the points defining the initial geometry.

Ref. [61] optimized the planform and wing section in the multiobjective environment by using genetic algorithms in transonic regimes. An interpolation technique was used for approaching the Pareto fronts. And a hybrid optimization method was presented.

Ref. [58] applied micro genetic algorithm and artificial neural networks to inverse and direct airfoil design optimization. These two methods were studied to show the improvement of the performance of these genetic algorithms.

Ref. [51] did multi-objective aeroelastic optimization for maximizing aerodynamic roll rate and minimizing the structural weight at supersonic regimes for the X31 delta wing configuration. A gradient based optimization algorithm, Genetic Algorithm was used in the multi-objective environment to achieve the best structural and control surface configuration with given requirements on performance and weight.

Ref. [4] used multi-objective design optimization to obtain the design points, which are feasible to the presented target requirements for an UCAV. Pre-concept design was applied considering survivability against surface to air missiles. Including a probabilistic analysis, robust design points were tried to be caught to reach the customers' requirements. Design process was consisting of performance parameters on flight velocity and manoeuvrability.

Ref. [43] evaluated different multidisciplinary optimization techniques to aircraft conceptual design. Supersonic business jet configuration was taken as a sample for conceptual design applications. Comparisons were made to express the affectivity of these multi-disciplinary optimization techniques.

Ref. [69] presented a study of an UCAV configuration with performance trade-offs. The study was based on tailless namely flying wing aircraft configuration with a highly integrated propulsion system. UCAVs are optimized to size for minimum empty weight. Aerodynamics, mass and propulsive performance were calculated. At the end of the study, it was concluded that performance requirements and their incidence really affect the size of the UCAV and gained benefit from the planform including aerodynamic efficiency.

Ref. [20] used a new class of optimization technique in multi-criteria and multidisciplinary design of UAV intelligent systems. The used evolutionary algorithm is named as Hierarchical Asynchronous Parallel Evolutionary Algorithm, which requires no derivatives or gradients of the objective function and it was asserted as the global optimum could be reached with this methodology practically and robustly between the local optimums and non-dominated individuals on Pareto trade-offs were produced.

Ref. [30] applied a robust multi-objective Evolutionary Algorithm to airfoil sections and wing planform design of an UCAV. The results are optimized for improvement of aerodynamic performance and stealth. With using this Hierarchical Asynchronous Parallel Evolutionary Algorithm non-dominated results were found as a set of shock-free airfoils and supercritical aero-diamond wings. Ref. [29] was also used this advanced evolutionary algorithm to optimize blended wing body in multi-objective multidisciplinary environment with giving importance on aerodynamic efficiency and reduction of Radar Cross Section.

Ref. [10] used three CFD based optimization techniques to minimize 3D wing drag. First technique is gradient based search technique uses the continous adjoint equation and named as SYN107 built by Intelligent Aerodynamics Int'l; second technique was constructed on response-surface method and named as MDOPT made by the Boing Company; and third one is called as OPTIMAS by Israel Aerospace Industries which uses a floating-point Genetic Algorithm. Then the optimization results were compared in this study aiming to find an effective tool for an aerodynamic shape optimization problem.

Ref. [25] examined both aerodynamic and structural design variables on supersonic fighter wing optimization. A genetic algorithm helped to control the weight of the multiple objectives while optimization. This multi-objective multidisciplinary design optimization was based on response surface methodology. With this work the basic geometry for fighter at a conceptual design stage was tried to be reached. Because a supersonic fighter has to be able to maneuver in different flight conditions this work is a good sample in multi-objective design and optimization environment.

Ref. [32] did a multidisciplinary design optimization investigation on a high speed civil transport with considering the effect of the constraints. Used disciplines were selected as performance, control, aerodynamics and structures. The objective was to minimize the take of gross weight only while finding wing planform and thickness distribution, fuselage shape, engine placement and thrust. Twenty-nine design variables and seventy constraints were used in this study, which admirable.

Ref. [18] took aircraft design optimization with numerical noise issue. Two types of noise-free mathematical models were created for aircraft optimization: a classical statistical technique with least squares surface fitting for polynomial approximation and Bayesian statistics with Kriging process in Geostatics for exponential interpolation to reach the results. Subsonic and supersonic aerodynamic performance of the high-speed civil transport aircraft configuration was selected for optimization while reducing the detrimental effects of numerical noise.

Ref. [9] focused on non-linear multi-objective optimization methods for optimizing a typical wide-body transport where conflicting figures of merit were considered simultaneously. A new method was developed for eliminating separate optimizations for each objective.

Ref. [7] aimed to build up a optimal design framework running under MATLAB for aircraft conceptual design for families of aircrafts. Genetic Algorithm was used for multi-objective multidisciplinary design optimization.

Ref. [47] examined multidisciplinary optimization methods on four kinds of aircraft: an advanced multi-role export fighter, a commercial airliner, a flying wing UAV, and a general aviation twin of novel asymmetric configuration. Different optimization methods were used to optimize these aircrafts: Full-factorial Orthogonal Steepest Descent, Monte Carlo, a mutation based Evolutionary Algorithm, and three types of the Genetic Algorithm with options. All of these methods were compared to find the best multidisciplinary optimization method for aircraft conceptual design.

Ref. [23] made a research for analysis and optimization of subsonic Fixed-wing UAVs in multidisciplinary design environment. A genetic algorithm was used to minimize the design gross weight for a given mission requirement and technology set. The High-Altitude Long Endurance (HALE) Global Hawk, Medium-Altitude Endurance (MAE) Predator, and Tactical Shadow 200 classes were selected to study on the following areas: avionics, aerodynamics, subsystems, design, payloads, propulsion, and structure technology. The results were evaluated to project through the year 2025.

Ref. [22] studied on constraint functions and their differentiations for structural optimization of fighter aircraft design. The optimization problem was also concerned from the aspect of computer time saving which was achieved by representing physical formulations mathematically.

Ref. [44] applied multidisciplinary design optimization technologies to design of a Business Jet. While gathering the different disciplines they used low and high fidelity computational fluid dynamics codes. The optimization was built up of two stages: first, reaching the optimum design by low fidelity codes; second, refining the preliminary design with high fidelity codes.

Ref. [28] worked on multidisciplinary optimization methods for aircraft preliminary design. With the help of a genetic algorithm a decomposition tool was developed to design and simplify the complex system between numerous disciplines. Then the design problem was transformed to collaborative tasks for the optimization.

Ref. [17] studied on optimizing of conceptual aircraft design for stability, control and performance. The airplane was sized to meet the requirements. Sizing was based on determining the dimensions and locations of tail surfaces, control surfaces, landing gear, and planning the systems and components to find the optimal solutions.

Ref. [21] used multi-criteria evolutionary algorithm to optimize UAV in multidisciplinary design environment. The framework for the UAV design and optimization was studied for requirements and initial development at preliminary design stage of aeronautical systems. Evolutionary algorithm was selected for not requiring derivations or gradients of objective functions and robustness while finding optimal solutions.

In this thesis Multiple Cooling Multi Objective Simulated Annealing Algorithm (MC-MOSA) was used for single, two and three objective optimizations of a supersonic UCAV. The significant difference of this work from mentioned studies perhaps its flexibility to deciding on the number of objectives; and also including numerous disciplines considering cost with performance, weight, stability,

aerodynamics, propulsion, sizing and configuration of the aircraft including flexible distances for mission segments. While optimizing with this new method two kinds of fitness functions were used and compared to find the optimal UCAV optimization method.

1.1.5 Multiple Cooling Multi Objective Simulated Annealing

Multiple Cooling Multi Objective Simulated Annealing (MC-MOSA) mimics the physical Simulated Annealing. It is a kind of generic probabilistic meta-algorithm for a global optimization problem. The Simulated Annealing idea comes from the roughly analogous process of heating and the slowly cooling of the substance to obtain a strong crystalline structure. The cooling process continues until the system is frozen. In the simulated annealing optimization method, the cost function replaces the energy of the system, and the optimization variables are represented by atoms [26]. Discrete combinatorial optimization problems were solved by Kirkpatrick et al. using this algorithm. This algorithm was then used by other researchers and verified by solving single and multi objective optimization problems.

MC-MOSA, like Hide and Seek, is a continuous Simulated Annealing algorithm, uses adaptive cooling schedules and random walk to generate the trials. In this algorithm, continuous optimization problems with many fitness functions are used in parallel, which can be structured by using different weight sets [54].

In the algorithm, temperature is cooled when an improvement in the fitness functions is encountered, and the related trial point is recorded. MC-MOSA algorithm assigns each fitness function separate temperatures which are cooled if the related fitness function is improved. In the optimization loop the fitness function could be introduced as a linear weight sum or elliptically; or else ellipsoidal for a 3-objective optimization problem. The specialty of elliptic and ellipsoidal fitness functions are capable of catching the points which are laying on the non-convex fronts.

Linear weight sum approach uses tangent lines to move towards the points on the Pareto front, while elliptic and ellipsoidal fitness functions uses family of ellipses or ellipsoids, respectively. These ellipses' or ellipsoids' centers are placed uniformly by an algorithm on a quarter-circle for a two-objective problem or eight of a sphere for a three-objective problem. Then, the purpose becomes to minimize the semi major axes to reach the points on the Pareto front.

The MC-MOSA algorithm uses random walk like Hide-and-Seek algorithm while finding next values for design variables so that next test point; next aircraft design point for the problem of this research. And the algorithm uses adaptive cooling procedures as well.

While formulating the problem the aim may be to minimize or maximize the objectives, or else mix their weights. Objective functions, that need to be maximized, can be turned into minimization problems by multiplying the function by a negative sign. Then, available minimization process works for maximizing these objectives.

This MC-MOSA algorithm was first introduced in Ref. [54], and used for some optimization problems which also include elliptic and ellipsoidal fitness function samples presented in Ref.[54,55] successfully. Even, the design of an agricultural aerial robot was optimized with this algorithm presented in Ref. [56].

The originality of this study from other applications of MC-MOSA algorithm is stated in the next section.

1.2 Original Contributions and Purpose

In this thesis the MC-MOSA algorithm is employed to optimize a supersonic unmanned combat aerial vehicle (UCAV). Single, two and three objective optimization are carried out. For the two and three objective optimization studies three kinds of fitness functions are used and compared; these are linear fitness functions which use tangent lines to search for the Pareto front and elliptic

fitness functions that use ellipses for two objective optimizations and ellipsoids for the three objective optimizations to reach the Pareto front. For two and three objective optimizations non-dominant points were also separated from dominant points by a prepared subroutine and results are pictorially shown.

The code is written in FORTRAN which is composed of two main parts; optimization and design.

The optimization includes the algorithms of MC-MOSA, and the aircraft design part was formed by the following design components:

International Standard Atmosphere (ISA)
Initial sizing
Wing configuration
Fuselage configuration
Propulsion
Horizontal and vertical tail sizing
Landing gears
Aerodynamics
Weight and stability
Performance
Structural load
Costs

All of these design components are explained in detail in Chapter 2.

The contribution of this work may be illustrated through the sample aircrafts with top and side views. This shows that the developed program gives not just the points on the graphs, but also meaningful aircraft shapes. A simple Excel sheet was prepared for this purpose.

In this study the effectiveness of the MC-MOSA Algorithm is aimed to be justified in finding the optimal designs for aircraft conceptual designs.

1.3 The Scope of the Thesis

In the first chapter, Introduction, a literature survey is provided. A general knowledge about how to develop an aircraft with aircraft design samples were pointed out. Then the need for multidisciplinary optimization methods for aircraft design optimization mentioned with numerous examples done by other researches in this area. Original contributions, purpose and the scope of the thesis was also included in the introduction part.

In the second chapter, Aircraft Design, the planned requirements and mathematical models were described in the following sections: mission analysis, initial sizing, wing configuration, fuselage configuration, propulsion system, horizontal and vertical tail configuration, landing gears, aerodynamics, weight and stability, performance, structural load, and cost. All the planned sizing parameters and needed performance characteristics with determined parameters were described in details in these sections. Then to prove the correctness of the aircraft design algorithm a sample run was made for correlating one of a similar and well known aircraft, F-16. The inputs and outputs with the resultant top and side views were presented in this part.

In the third chapter, Optimization, the optimization technique, selected design variables, constraints, objectives were tabulated. And the single, two and three objective optimization examples using different fitness functions were illustrated with charts and sample aircraft figures.

In the last chapter, Conclusion, the results were evaluated and the possible future work was advised.

CHAPTER 2

AIRCRAFT DESIGN

2.1 Defining the Requirements of an UCAV

In this thesis, a multi-role supersonic unmanned combat aerial vehicle conceptual design optimization problem is addressed. The aircraft shall be capable to combat, maneuver, resist high maneuver loads, carry bombs, drop bombs, cruise at high altitudes and have long endurance without refuelling.

It will autonomously locate its targets, navigate autonomously, but also be able to be flown by a remotely controlled pilot with a ground station system.

It is planned to have a simple and fixed shape during the flight. In other words, except the control surfaces (flaps, ailerons, elevator and rudder) it shall not have any moving components (i.e., fixed swept wing and fixed tail configuration). The basic view of this concept is illustrated in the figures 2.1 and 2.2.

The mission is composed of 14 segments: engine start and warm-up, taxi, take-off, climb, cruise-out, loiter, descent, dash-out, combat (strafe), dash-in, climb, cruise-in, descent, landing-taxi and shutdown. The segment characteristics were described in details in the next section.

It should be able to carry weapons until the end of the flight if the mission is aborted. This payload will be carried externally under the wings. The detailed placement is not addressed in this work. It was assumed that they will be installed properly without affecting the static and dynamic stability of the UCAV. Two kinds of weapons were selected for the mission: a weapon below 2000 lb and Aim9 (Sidewinder) (200 lb).

The positions of the wings, horizontal and vertical tails, and landing gears with respect to the fuselage are calculated in the Aircraft Design Code prepared. The fuel will be carried internally in the wings; no external fuel tanks are planned.

The engine sizing is automatically done in the code which gives its dimensions and its thrust. The calculations were based on a rubber engine with turbofan characteristics which has constant bypass ratio and specific fuel consumption.

Landing gears were planned to be tricycle and retractable, and designed to find the dimensions according to the changing aircraft configurations. The placements were changed for different aircraft configurations with center of gravity.

Cost is another important parameter in aircraft design and it was taken into account in this study. A subroutine in the code calculates the total acquisition cost.

Proper mathematical models were selected and coded in separate subroutines. The main program picks up values of some parameters from an input file and then does the calculations; afterwards gives results to an output file. While calculating, subroutines are called by the main program in an order assigned by the programmer, before. Throughout the program some parameters need to be updated, this is coped with calling the required subroutine in the concerning subroutine again.

How the subroutines of the aircraft design part communicate with each other are shown by a flow chart in Figure 2.3.

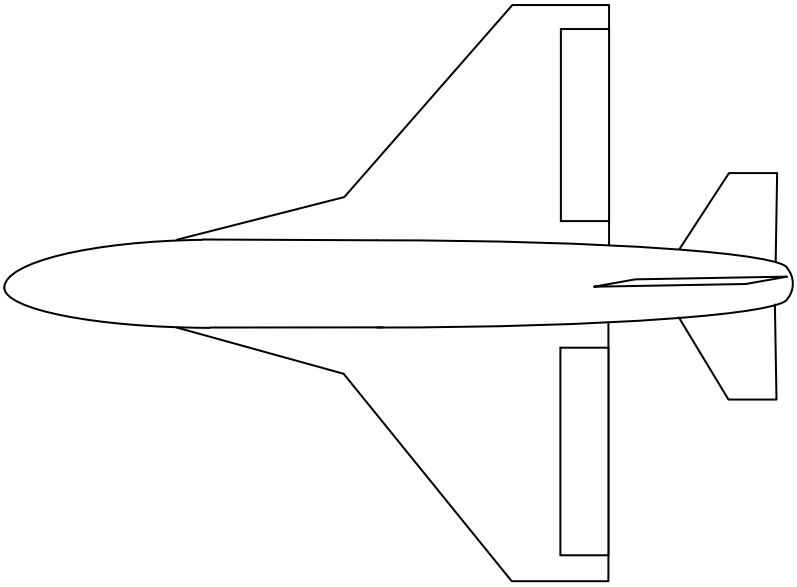

Figure 2.1 The sketch of the basic UCAV concept (top view)

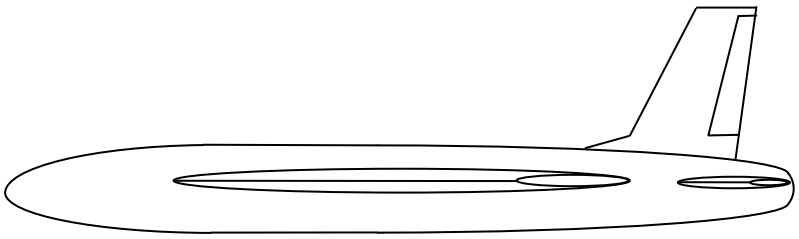

Figure 2.2 The sketch of the basic UCAV concept (side view)

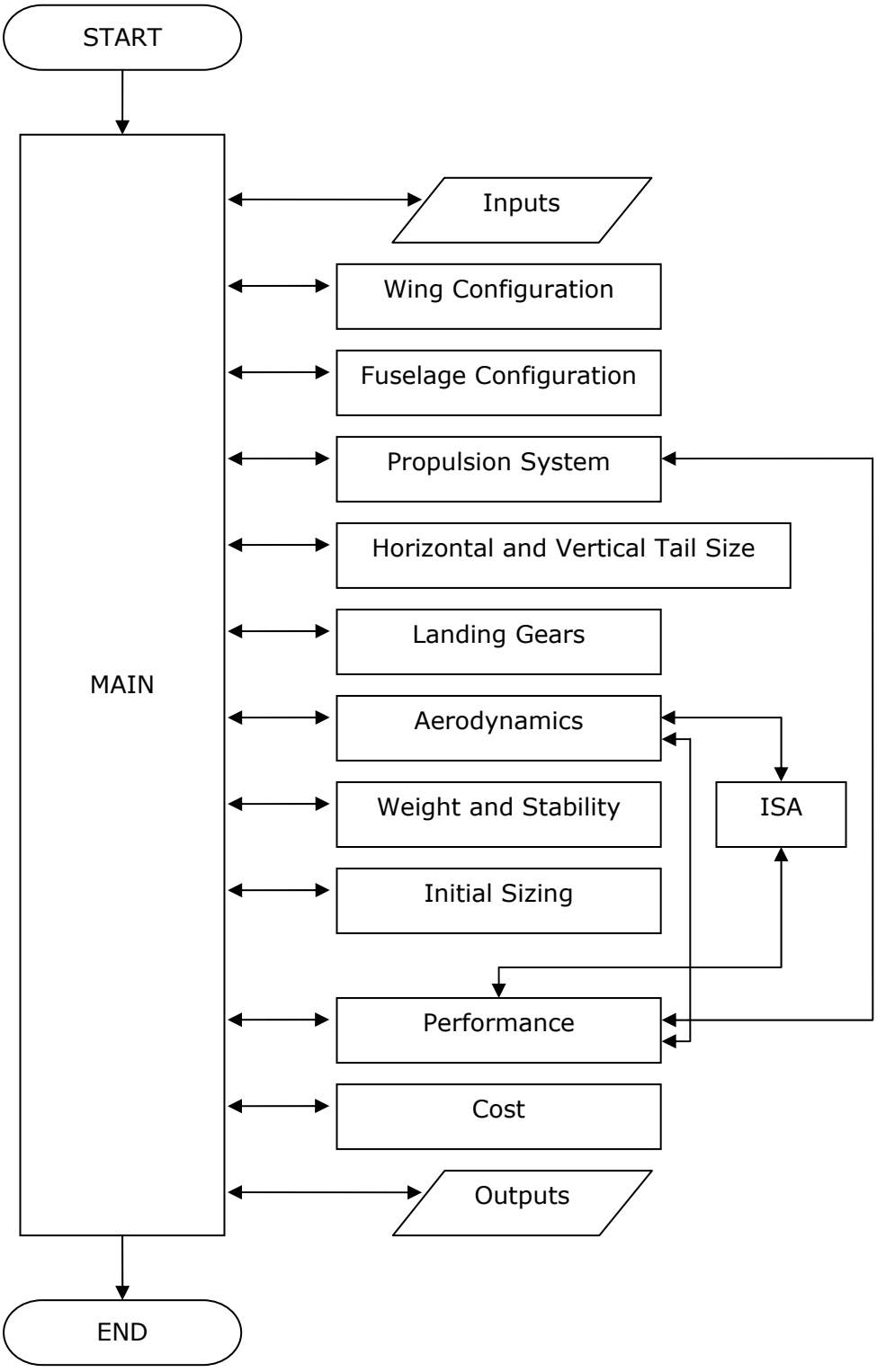

Figure 2.3 Flow Chart of the Aircraft Design Algorithm

Propulsion System and Aerodynamics subroutines are called more frequently because of frequently updated variables like Mach number, thrust and induced drag.

The detailed information about the conceptual design phases with equations, requirements, limits and constants are given in the following sections.

2.2 Mission Profile

Figure 2.4 illustrates the planned mission profile for the UCAV.

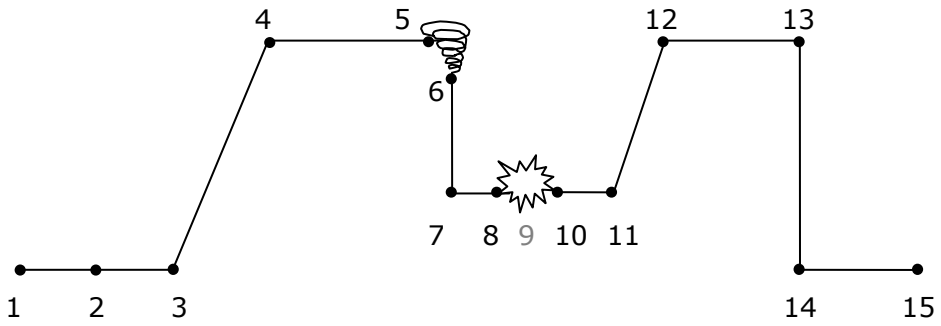

Figure 2.4 UCAV's mission segments

Each segment can be described as:

0-1 : Engine Start and Warm-up
1-2 : Taxi
2-3 : Take-off
3-4 : Climb
4-5 : Cruise-out
5-6 : Loiter
6-7 : Descent
7-8 : Dash-out

8-10 : Combat (strafe)
10-11 : Dash-in
11-12 : Climb
12-13 : Cruise-in
13-14 : Descent
14-15 : Landing, Taxi and Shutdown

This is a typical mission profile for combat air vehicles including all the required segments [46,48].

In combat, the UCAV is designed for air-to-air and air-to-ground attacks i.e. strafe and dog fights which include kinds of maneuvers that result in high g forces.

Mission segments' details may be understood better in the following sections.

2.3 Initial Sizing

Airplanes must normally meet very stringent range, endurance, speed and cruise speed objectives while carrying a given payload. It is important, to be able to predict the minimum airplane and fuel weights needed to accomplish a given mission [48].

Besides, a typical UCAV mission includes a combat consisting of either certain number of turns or a certain number of minutes at maximum power, a weapons drop, a cruise back and a loiter. The weapons drop refers to the firing of the gun and/or missiles [46].

In this thesis, aerial refuelling and external fuel tanks were not considered and it is assumed that the fuel consumed is only which the wings can hold.

While estimating the mission fuel fractions, reserved and trapped fuel as required by civil or military design specifications were taken into consideration

by 6 % percentage of the used fuel at the end of the mission.

Under these assumptions, the fuel fractions were found for each segment with the help of the given tables and the equations in referenced design books [46, 48], and used tables from these references are Table 2.1 and Table 2.2.

Table 2.1 Historical mission segment weight fractions [46]

Mission segment	(W_i/W_{i-1})
Warmup and Takeoff	0.970
Climb	0.985
Landing	0.995

Table 2.2 Suggested fuel-fractions for several mission phases [48]

	Engine Start, Warmup	Taxi	Takeoff	Climb	Descent	Landing, Taxi Shutdown
Fighters	0.990	0.990	0.990	0.96-0.99	0.990	0.995

For these segments, the following equations are used:

Engine Start and Warm-up:

$$\frac{W_1}{W_0} = 0.990 \tag{2.1}$$

Taxi:

$$\frac{W_2}{W_1} = 0.990 \tag{2.2}$$

Takeoff:

$$\frac{W_3}{W_2} = 0.990 \tag{2.3}$$

For performance calculations, the weight at the beginning of the climb is, W_3:

$$W_3 = \frac{W_3}{W_2}.\frac{W_2}{W_1}.\frac{W_1}{W_0}.W_0 \tag{2.4}$$

Climb:

$$\frac{W_4}{W_3} = 0.985 \tag{2.5}$$

Under the light of Ref. [46], lift to drag ratios for loiter and cruise were decided for maximum performance. To maximize loiter efficiency it is assumed that the aircraft will be able to fly approximately with the velocity that gives maximum lift to drag ratio, L/D. And similarly, it will be able to fly with the velocity standing for an L/D of 86.6% of the maximum L/D for the most efficient cruise [46]:

$$\left.\frac{L}{D}\right)_{cr} = 0.866.\left.\frac{L}{D}\right)_{\max} \text{ and } \qquad \left.\frac{L}{D}\right)_{ltr} = \left.\frac{L}{D}\right)_{\max} \tag{2.6) and (2.7}$$

Cruise:

$$\frac{W_5}{W_4} = e^{\frac{-R.SFC}{V(L/D)}} \tag{2.8}$$

Loiter:

$$\frac{W_6}{W_5} = e^{\frac{-E.SFC}{L/D}} \tag{2.9}$$

Descent:

$$\frac{W_7}{W_6} = 0.990 \tag{2.10}$$

Dash out:

$$\frac{W_8}{W_7} = e^{\frac{-R.SFC}{V(L/D)}} \tag{2.11}$$

Combat & Strafe:

The fuel consumed at combat time was assumed as 1 at the beginning, and then it was calculated according to the remaining fuel, later.

Combat (and Strafe):

$$\frac{W_{10}}{W_8} = 1 \tag{2.12}$$

Dash in:

$$\frac{W_{11}}{W_{10}} = e^{\frac{-R.SFC}{V(L/D)}} \tag{2.13}$$

Climb:

$$\frac{W_{12}}{W_{11}} = 0.985 \tag{2.14}$$

Cruise:

$$\frac{W_{13}}{W_{12}} = e^{\frac{-R.SFC}{V(L/D)}} \tag{2.15}$$

Descent:

$$\frac{W_{14}}{W_{13}} = 0.990 \tag{2.16}$$

Landing:

$$\frac{W_{15}}{W_{14}} = 0.995 \tag{2.17}$$

Total weight ratio:

$$\frac{W_{15}}{W_0} = \frac{W_{15}}{W_{14}} \cdot \frac{W_{14}}{W_{13}} \cdot \frac{W_{13}}{W_{12}} \cdot \frac{W_{12}}{W_{11}} \cdot \frac{W_{11}}{W_{10}} \cdot \frac{W_{10}}{W_8} \frac{W_8}{W_7} \cdot \frac{W_7}{W_6} \cdot \frac{W_6}{W_5} \cdot \frac{W_5}{W_4} \cdot \frac{W_4}{W_3} \cdot \frac{W_3}{W_2} \cdot \frac{W_2}{W_1} \cdot \frac{W_1}{W_0} \tag{2.18}$$

Total fuel fraction excepting combat time was calculated with:

$$\frac{W_f}{W_0} = 1.06 \left(1 - \frac{W_{15}}{W_0}\right) \tag{2.19}$$

For combat the available fuel was found by considering the maximum fuel capacity of the wings and the required fuel for other segments. And also, 6% more fuel for reserved and trapped fuel was also taken into account. Then, the fuel burned during combat becomes:

$$W_{fc} = \frac{W_{f\max w} - W_f}{1.06} \tag{2.20}$$

However, it was planned that there is a time at which all the bombs would have been dropped, point 9. And, at that point the weight of the aircraft was defined as W_9.

Which is:

$$W_9 = W_8 - W_{payload} \tag{2.21}$$

One other assumption was made for the segment 8-9 as at payload drop the fuel consumed was little when compared to other segments [48], and:

$$\frac{W_9}{W_8} = 1 \tag{2.22}$$

And at point 10:

$$W_{10} = W_8 - W_{payload} - W_{fc} \tag{2.23}$$

For combat the fuel fraction can now be found as following.

Combat (and Strafe):

$$\frac{W_{10}}{W_8} = 1 - \left(\frac{W_{fc}}{W_9}\right) \tag{2.24}$$

The total fuel fraction was updated by including the combat time fuel fraction:

$$W_f = W_f + 1.06W_{fc} \tag{2.25}$$

Then, W_0 is found by iterating the following equation:

$$W_0 = \frac{W_{payload}}{\left(1 - \frac{W_f}{W_0} - \frac{W_e}{W_0}\right)} \tag{2.26}$$

2.4 Wing Configuration

While configuring the wing, the first decision to make is the selection of the airfoil. The airfoil selection should be made carefully because the airfoil affects the cruise speed, takeoff and landing distances, stall speed, and overall aerodynamic efficiency during all phases of flight. In supersonic flow, the aircraft encounter bow shocks which results in extra drag, also. To prevent this, an airfoil which has a sharp or nearly sharp leading edge should be used and/or wing sweep can be given [46].

The competitor aircrafts use NACA six-digit series airfoils. These airfoils have lower drag at higher speeds compared to four or five digits series. Among these airfoils NACA 64A210 may be chosen for the UCAV, whose data may be taken from Table 2.3, Ref. [48], and was illustrated in Figure 2.5.

Table 2.3 Six-Digit NACA airfoils [48]

Airfoil	$\alpha_{0\ell}$ (deg)	c_{m0}	$c_{\ell\alpha}$ (deg^{-1})	a.c. (tenths c)	$\alpha_{c\ell\max}$ (deg)	$c_{l\max}$	α (deg)
63A010	0	.005	.105	.254	13.0	1.20	10.0
63A210	-1.5	-.040	.103	.257	14.0	1.43	10.0
64A010	0	0	.110	.253	12.0	1.23	10.0
64A210	-1.5	-.040	.105	.251	13.0	1.44	10.0
64A410	-3.0	-.080	.100	.254	15.0	1.61	10.0

Figure 2.5 NACA 64A210

It is proposed that the airfoil can be chosen from an airfoil database which can be inserted to program and may be left as a future work. In this work, it is assumed that there is an airfoil which can meet the calculated performance parameters. For that reason, in the program some checks are made by the programmer in order to stay in the feasible region. So, NACA 64A210 may also be considered as a sample for this purpose.

Another concern was the leading edge sweep for this supersonic aircraft in order to reduce the drag. The leading edge sweep was calculated for straight trailing edge as in Figure 2.6 [46]:

$$\tan \Lambda_{LE} = \tan \Lambda_{c/4} + \left[\left(1 - \lambda\right) / AR\left(1 + \lambda\right) \right] \tag{2.27}$$

Where, the quarter chord sweep angle and the aspect ratio were selected as design variable in the Fortran Code.

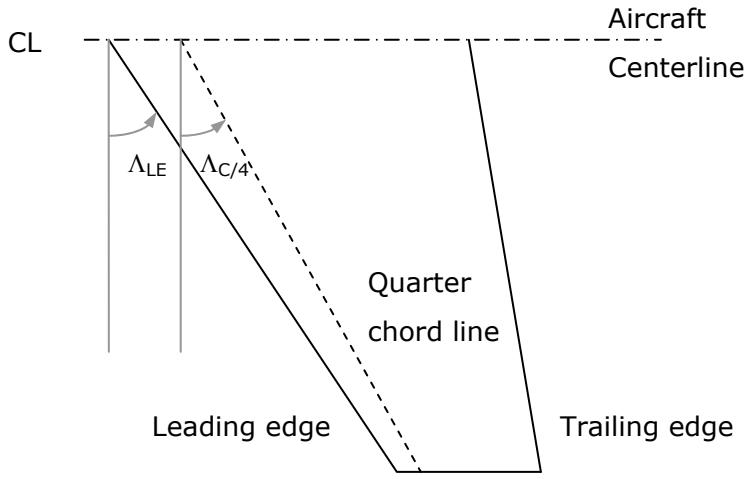

Figure 2.6 Wing Sweep Λ [46]

Taper effects the distribution of lift along the span of the wing. It is known that while designing a wing of an aircraft the purpose is to obtain maximum lift with minimum drag. The minimum drag due to lift or induced drag occurs when the lift is distributed in an elliptical fashion. However, an elliptical wing planform is difficult to produce and expensive to manufacture [46]. In order to catch this elliptical wing benefit, the taper ratio is increased. To have the desirable taper ratio interpolation from Figure 2.7 Ref.[46]was made as:

$$\lambda \cong 0.6.\left(\frac{\Lambda_{c/4} - 90}{100}\right)^2 \tag{2.28}$$

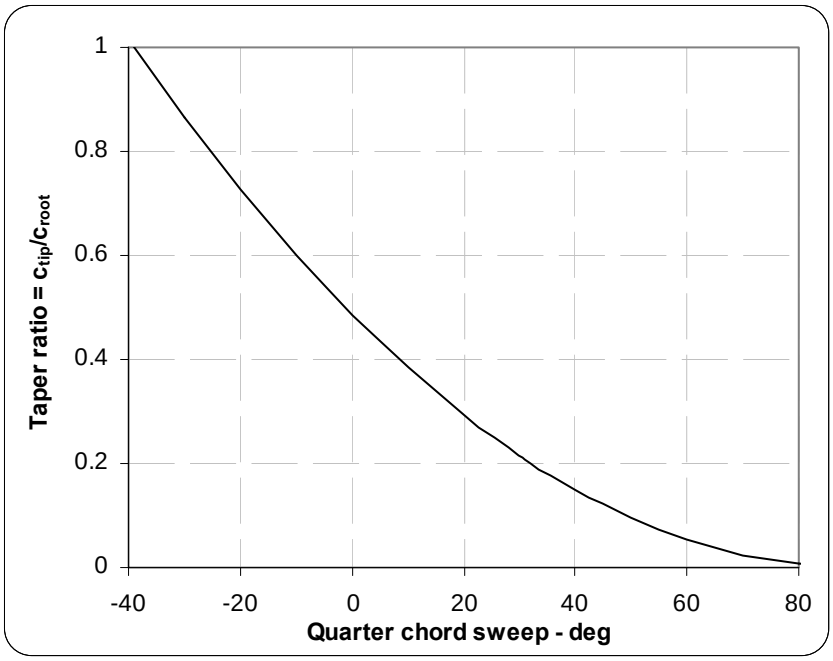

Figure 2.7 Effect of sweep on desired taper ratio [46]

To see the effect of wing dihedral angle on the UCAV design, it was taken as a design variable changing according to the Table 2.4 [46] for supersonic swept wing. Initially it was started from 0°.

$$\Gamma_w = 0° \tag{2.29}$$

Table 2.4 Dihedral guidelines [46]

	Wing position		
	Low	Mid	High
Unswept (civil)	5 to 7	2 to 4	0 to 2
Subsonic swept wing	3 to 7	-2 to 2	-5 to -2
Supersonic swept wing	0 to 5	-5 to 0	-5 to 0

It was assumed that the length of fuselage-wing intersection on the fuselage width was:

$$w_{f\max} = 0.5.D_{f\max} \tag{2.30}$$

So that, in order to be able to get the desired intersection length, the wing position on the fuselage was determined as above the centre line of the fuselage, which means a high wing configuration. This configuration also serves to carry high volume of missiles under the wing, safely. This idea would be understood from the front view of the fuselage, Figure 2.8.

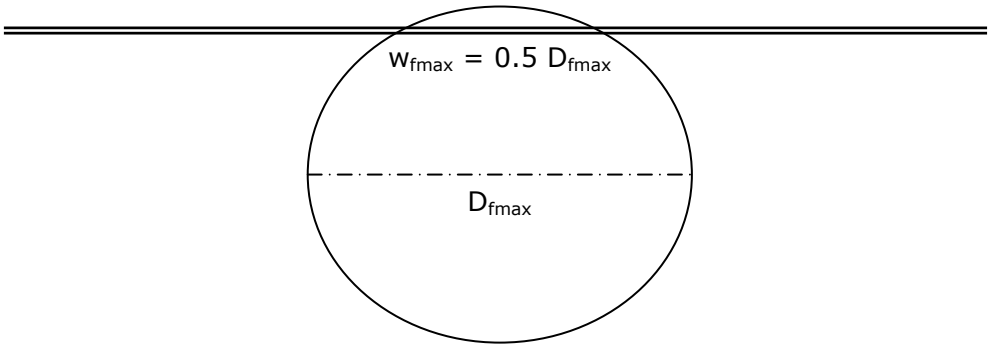

Figure 2.8 Wing Configuration

One more assumption was made for the maximum thickness ratio as constant:

$$\left.t/c\right)_{rw} = \left.t/c\right)_{tw} = \left.t/c\right)_{w} \tag{2.31}$$

Referenced wing area:

$$S = \frac{b^2}{AR} \tag{2.32}$$

And the control surface area was calculated according to the competitor aircrafts as:

$$S_{csw} = 0.1.S \tag{2.33}$$

The required data calculated from the equations for wing configuration as given in Ref.[46]:

$$c_r = \frac{2.S}{b(1+\lambda)} \tag{2.34}$$

$$c_t = \lambda.c_r \tag{2.35}$$

$$\bar{c} = \left(\frac{2}{3}\right).c_r.\left(\frac{1+\lambda+\lambda^2}{1+\lambda}\right) \tag{2.36}$$

$$\bar{y} = \left(\frac{b}{6}\right).c_r.\left(\frac{1+2.\lambda}{1+\lambda}\right) \tag{2.37}$$

$$\bar{x} = \bar{y}.\tan\Lambda_{LE} \tag{2.38}$$

The wing root at wing-fuselage intersection:

$$c_{r\,fw} = c_r.\left[1-\left(\frac{w_{f\max}}{b}(1-\lambda)\right)\right] \tag{2.39}$$

The exposed wing taper ratio:

$$\lambda_{fw} = \frac{c_t}{c_{r\,fw}} \tag{2.40}$$

The exposed wing root thickness ratio:

$$\left.t/c\right)_{fw} = \frac{\left.t/c\right)_{rw} - \frac{w_{f\max}}{b}.\left[\left.t/c\right)_{rw} - \lambda_{fw}.\left.t/c\right)_{tw}\right]}{1 - \frac{w_{f\max}}{b}.\left(1-\lambda_{fw}\right)} \tag{2.41}$$

The ratio of the tip and root thickness ratios of the exposed wing:

$$\tau_{fw} = \frac{\left.t/c\right)_{tw}}{\left.t/c\right)_{fw}} \tag{2.42}$$

The exposed wing area:

$$S_{netw} = \frac{\left(c_{rfw} + c_t\right)}{2}.\frac{b - w_{f\max}}{\cos\Gamma_w} \tag{2.43}$$

The wetted wing area [48, 57]:

$$S_{wetw} = 2S_{netw}\left[1 + 0.25\left.t/c\right)_{fw}.\left(\frac{1+\tau_{fw}.\lambda_{fw}}{1+\lambda_{fw}}\right)\right] \tag{2.44}$$

The wetted aspect ratio:

$$AR_{wet} = \frac{b^2}{S_{wetw}} \tag{2.45}$$

Maximum lift to drag ratio was interpolated from Figure 2.9 [46] for military jets as:

$$\left.\frac{L}{D}\right)_{\max} \cong \frac{AR_{wet} - 0.4}{0.142} + 9.0 \tag{2.46}$$

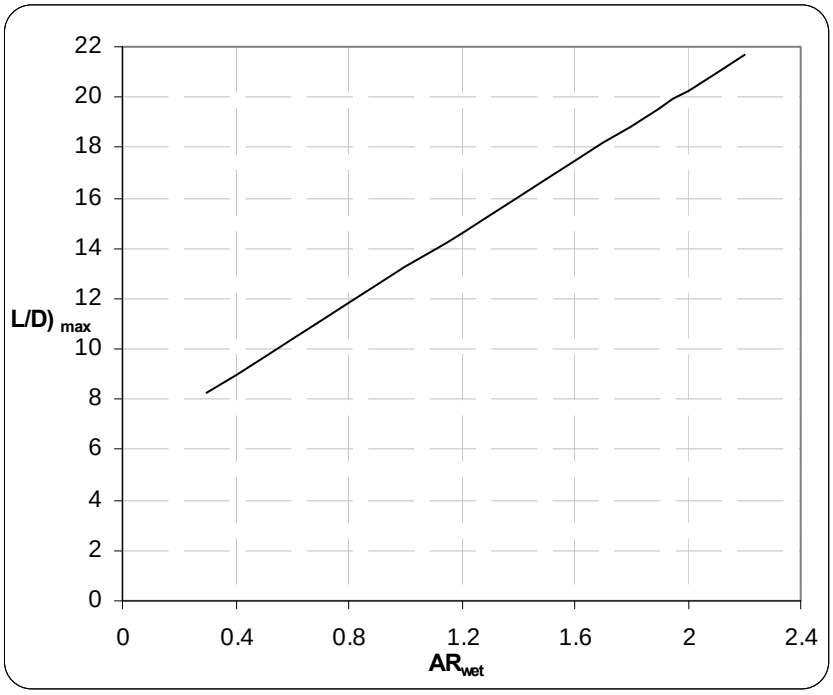

Figure 2.9 Maximum lift-to-drag ratio trends for Military Jets [46]

Fuel Capacity of the wing was found from Figure 2.10 [48, 57]:

$$V_{Fuel\tan kw} = 0.54.\frac{S^2}{b}.\left(t/c\right)_r.\frac{1+\lambda\sqrt{\tau}+\lambda^2\tau}{(1+\lambda)^2} \qquad (2.47)$$

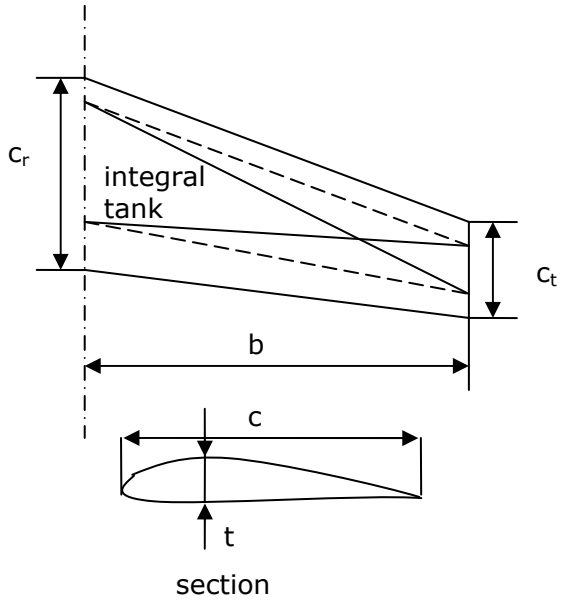

Figure 2.10 Approximation for integral fuel tank volume, available in a linear lofted wing [48, 57]

The UCAV was planned to use JP-4 as a fuel type as its competitors.
From Table 2.5 Ref.[46] fuel density was taken as 0.78 kg/lt (=780 kg/m^3).

Table 2.5 Fuel densities (kg/liter) [46]

	Average actual density		
	0°F	100°F	Mil-spec density
Aviation gasoline	0.73	0.68	0.72
JP-4	0.80	0.77	0.78
JP-5	0.86	0.82	0.82
JP-8/JETA1	-----	-----	0.80

Then, the total fuel mass capacity of the wing was found with:

$$W_{f\max w} = 780.V_{fuel\tan kw} \tag{2.48}$$

2.5 Fuselage Configuration

The fuselage was designed to have approximately a circular cross section, to include the engine and also all the instruments that is needed.

The fuselage max cross-sectional area was calculated as:

$$A_{\max} = \pi\left(\frac{D_{f\max}}{2}\right)^2 \tag{2.49}$$

Table 2.6 Ref. [46] gives the statistical values for fuselage length from takeoff gross weight. And this value was multiplied by a factor of 0.7 for an inhabited structure, as considering a competitor aircraft, X-45C from Ref. [15], also included in Appendix B. Then for an unmanned jet fighter, the length was calculated for the UCAV as:

$$L_f = (0.389\ W_0^{0.39}).0.7 \tag{2.50}$$

Table 2.6 Fuselage length (m) vs. W_0 (kg) [46]

Length = aW_0^C (m)	a	C
Jet Trainer	0.333	0.41
Jet Fighter	0.389	0.39
Military Cargo/Bomber	0.104	0.50
Jet Transport	0.287	0.43

The supersonic drag is minimized by a fineness ratio of about 14 [46], to be able to see this effect the fineness ratio was also found:

$$FinenessRatio = \frac{L_f}{D_{f\max}} \tag{2.51}$$

The fuselage was composed of nose, mid-section and aft as illustrated in Figure 2.11.

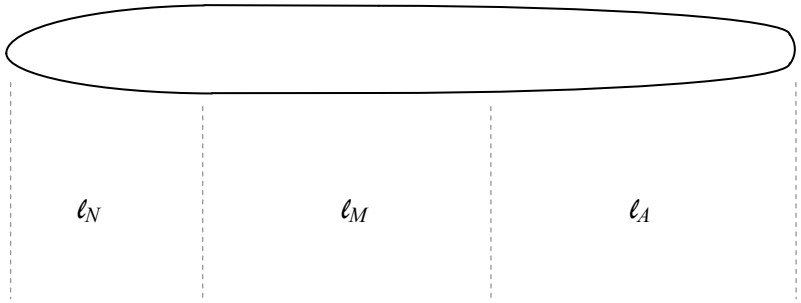

Figure 2.11 Fuselage

Where,

$$\ell_N = 1.75 D_{f\max} \tag{2.52}$$

$$\ell_A = 2.75 D_{f\max} \tag{2.53}$$

$$\ell_M = L_f - \ell_N - \ell_A \tag{2.54}$$

Volume and wetted area of the fuselage were calculated with the help of Ref. [48, 57] as follows.

For a fuselage with a circular mid-section (finenessratio > 4.5) :

$$Volume = \frac{\pi}{4} {D_{f\max}}^2 L_f \left(1 - \frac{2}{FinenessRatio}\right) \tag{2.55}$$

$$S_{wet.f} = \pi D_{f\max} L_f \left(1 - \frac{2}{FinenessRatio}\right)^{2/3} \left(1 + \frac{1}{FinenessRatio^2}\right) \tag{2.56}$$

For a fuselage without a circular mid-section (finenessratio ≤ 4.5) :

$$Volume = \frac{\pi}{4} {D_{f\max}}^2 L_f \left(0.50 + 0.135 \frac{\ell_N}{L_f}\right) \tag{2.57}$$

$$S_{wet.f} = \pi D_{f\max} L_f \left(0.50 + 0.135 \frac{\ell_N}{L_f}\right)^{2/3} \left(1.015 + \frac{0.3}{FinenessRatio^{3/2}}\right) \tag{2.58}$$

The fuselage was configured more in detail while adding other components of the aircraft. They were mentioned in the next sections.

2.6 Propulsion System

The engine inlet was planned to be on the nose of the fuselage as illustrated in Figure 2.12 [46]. It was designed as, the optimized UCAV only one engine mounted in the fuselage to use. So as, all the related equipments will be covered by the fuselage, also. And it is expected that, the effect of engine weight to the stability of the UCAV while maneuvering will be minimized with this basic configuration. Further, it is possible to integrate S-shape inlet duct for stealth.

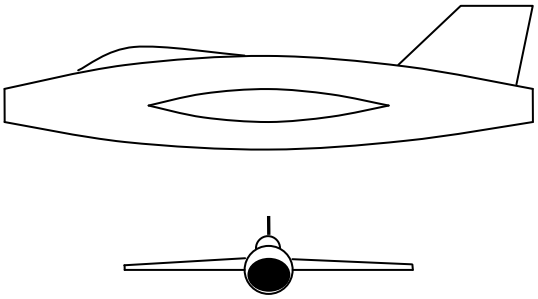

Figure 2.12 Inlet locations - buried engines (Nose) [46]

Thrust to weight ratio directly affects the performance of the aircraft. It may be grasped as; an aircraft which accelerates more quickly, climbs more rapidly, reaches a higher maximum speed, and sustains higher turn rates might have higher thrust to weight ratio, also. However, one more point should be considered that the larger engines will consume more fuel throughout the mission which also increases the takeoff gross weight [46].

Meanwhile, thrust to weight ratio is changing throughout the mission. Since, throughout the mission the fuel is consumed so that weight changes, and the altitude changes, basically.

For the first estimate, takeoff thrust to weight ratio was calculated from Table 2.7 [46].

For dog fighter,

$$a = 0.648 \tag{2.59a}$$

$$C = 0.594 \tag{2.59b}$$

$$\frac{T}{W_0} = a.M^C \tag{2.59c}$$

Table 2.7 T/W_0 vs. M_{max} [46]

$T/W_0 = aM_{\max}^{C}$ (m)	a	C
Jet Trainer	0.488	0.728
Jet Fighter (dogfighter)	0.648	0.594
Jet Fighter (other)	0.514	0.141
Military Cargo/Bomber	0.244	0.341
Jet Transport	0.267	0.363

Then, the takeoff thrust:

$$T_{TO} = \frac{T}{W_0}.W_0 \tag{2.60}$$

Noting that, take of weight was selected as an objective and also normalized with upper and lower bounds, this was guarantied that takeoff thrust would fall in reasonable limits, always.

And the maximum thrust available is [46]:

$$T_{av} = 0.75.T_{TO}\left[\frac{5+BPR}{4+BPR}\right] \tag{2.61}$$

Also, the decrease in thrust due to the altitude change was taken into account as stated in Ref.[5]:

$$\frac{T}{T_0} = \frac{\rho}{\rho_0} \tag{2.62}$$

In the program, for combat conditions thrust available was used for the maximum performance results. And for cruise the equation from Ref. [46] was used for afterburning engines:

$$T_{cruise} = 0.59\ T^{0.74}e^{0.023BPR} \tag{2.63}$$

And for the other segments of the mission thrusts were calculated with the following proportion:

$$\frac{T}{W_i} = \frac{T}{W_0} \cdot \frac{1}{W_i / W_0} \tag{2.64}$$

However, especially for combat conditions the engine uses afterburner, this means more power. This effect was calculated with the help of Figure 2.13 taken from Ref. [62] for turbofan engines as:

$$\frac{T_{ab}}{T_{dry}} \cong 0.8792.\left(M - 0.784\right)^2 + 0.7 \tag{2.65}$$

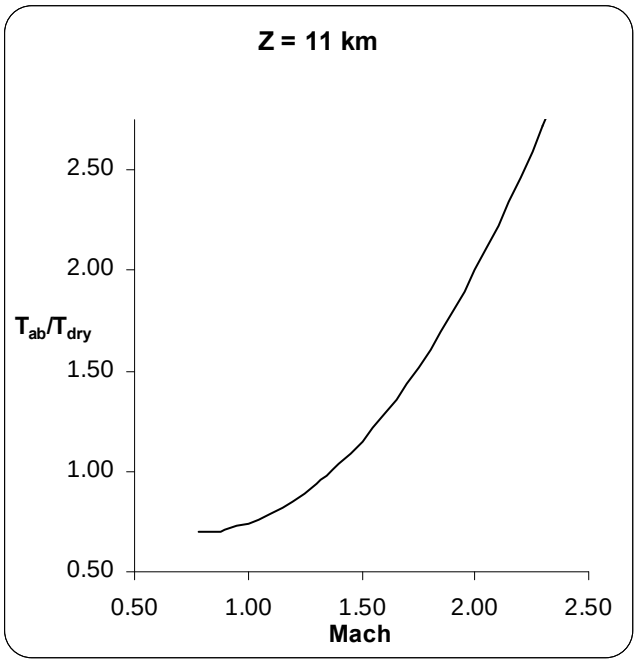

Figure 2.13 Thrust of an Afterburning Turbofan [62]

Specific fuel consumption is another point that should be concerned. At combat conditions the UCAV consumes more fuel than normal conditions in one second. While flying with maximum thrust the specific fuel consumption was calculated as Ref.[46] with 20% reduction for next-generation engines:

$$SFC_{\max T} = 0.8\ \left[60e^{-0.12BPR}\right] = SFC_c \tag{2.66}$$

For other mission segments, SFC was taken as constant and equal 0.64 mg/Ns as competitors' engines have, approximately.

For the length and the diameter of the engine the equations from Ref. [46] were used with including 20% reduction for next-generation engines.

$$L_{eng} = 0.8\ \left[0.68\ T^{0.4}M^{0.2}\right] \tag{2.67}$$

$$D_{eng} = 0.8\ \left[0.11\ T^{0.5}e^{0.04BPR}\right] \tag{2.68}$$

Then, the fuselage diameter was calculated as:

$$D_{f\max} = D_{eng} + 0.10 \tag{2.69}$$

2.7 Horizontal and Vertical Tail Configuration

The new generation combat aircrafts mostly have tailless configuration. However, tails provide for trim, stability and control. Especially, vertical tail plays a key role in spin recovery. And, these efficiencies can be optimized with the tail configuration. As a first decision, the conventional tail was selected for the UCAV because of its simplicity, light weight and adequate stability and control [46].

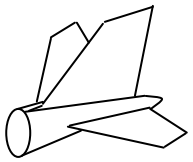

Figure 2.14 Conventional tail [46]

The airfoil of the UCAV's tail should be capable of maneuver in supersonic conditions. For that reason, the airfoil proposed for the wings, NACA 64A210, may be selected for the vertical and horizontal tail of the UCAV.

Tail aspect ratios and taper ratios were selected from Table 2.8 [46] as constants.

Table 2.8 Tail aspect Ratio and Taper ratio [46]

	Horizontal tail		Vertical tail	
	AR	λ	AR	λ
Fighter	3-4	0.2-0.4	0.6-1.4	0.2-0.4
Sail plane	6-10	0.3-0.5	1.5-2.0	0.4-0.6
Others	3-5	0.3-0.6	1.3-2.0	0.3-0.6
T-Tail	------	------	0.7-1.2	0.6-1.0

$$AR_{VT} = 1.4 \tag{2.70}$$

$$AR_{HT} = 3.4 \tag{2.71}$$

And,

$$\lambda_{VT} = 0.3 \tag{2.72}$$

$$\lambda_{HT} = 0.4 \tag{2.73}$$

Vertical tail sweep angle, Λ_{VT}, was selected as 45° for the initial value and taken as design variable changing between 35° to 55°.

Horizontal tail sweep angle, Λ_{HT}, was thought as 5° more than the wing sweep, as usual for other aircrafts. It is planned that this selection makes the tail stall after the wing, and also provides the tail with a higher Critical Mach Number than the wing, which avoids loss of elevator effectiveness due to shock formation [46].

$$\Lambda_{HT} = \Lambda_{c/4} + 5° \tag{2.74}$$

Like the wing dihedral, the vertical and the horizontal tail dihedrals taken as design variables. Initially they were thought as zero.

$$\Gamma_{VT} = 0°$$
$$\Gamma_{HT} = 0°$$

The vertical and horizontal tail volume coefficients for jet fighter were decided from Table 2.9 [46] and they were taken as constants.

$$V_{VT} = 0.07$$
$$V_{HT} = 0.40$$

Table 2.9 Tail volume coefficient [46]

	Typical values	
	V_{HT}	V_{VT}
Jet Trainer	0.70	0.06
Jet Fighter	0.40	0.07
Military Cargo/Bomber	1.00	0.08
Jet Transport	1.00	0.09

While optimizing the UCAV, one of the important variables is changing the placements of the vertical and the horizontal tails.

Stability of the aircraft is also affected by the tail because of the lift it produces, its weight and the tail moment arm measured from the center of gravity. These three parameters were related with the following equations taken from Ref.[46]:

$$S_{VT} = \frac{V_{VT}.b.S}{l_{VT}} \tag{2.75}$$

$$S_{HT} = \frac{V_{HT}.\bar{c}.S}{l_{HT}} \tag{2.76}$$

In the above equation the moment arms, ℓ_{VT} and ℓ_{HT} , were treated as the distance from the tail quarter-chord to the wing quarter chord as stated in Ref. [46] and illustrated in Figure 2.15.

However, running the design code with different moment arm values showed that these moment arms really affect the results. So that, tail moment arms were decided to be proportional with the fuselage length multiplied by l_{VTco} and l_{HTco}. These proportions added in design variables to change each time. As a result tail moment arms were calculated as:

$$l_{VT} = l_{VTco}.L_f \tag{2.77}$$

$$l_{HT} = l_{HTco}.L_f \tag{2.78}$$

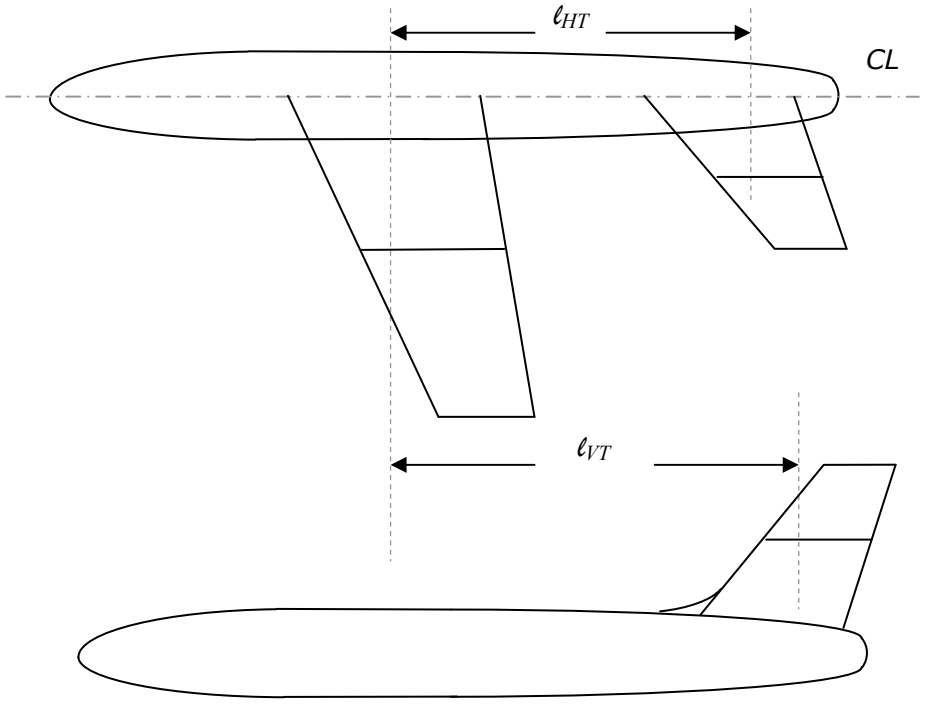

Figure 2.15 Initial tail sizing [46]

Other variables were calculated depending on the equations from Ref. [5, 46, 48, 57] as below.

Vertical tail:

$$h_{VT} = \sqrt{AR_{VT}.S_{VT}} \tag{2.79}$$

$$c_{rVT} = \frac{2.S_{VT}}{h_{VT}\left(1+\lambda_{VT}\right)} \tag{2.80}$$

$$c_{tVT} = \lambda_{VT}.c_{rVT} \tag{2.81}$$

$$\bar{c}_{VT} = \left(\frac{2}{3}\right).c_{rVT}.\left(\frac{1+\lambda_{VT}+\lambda_{VT}{}^{2}}{1+\lambda_{VT}}\right) \tag{2.82}$$

$$\bar{z}_{VT} = 2.\left(\frac{h_{VT}}{6}\right).c_{rVT}.\left(\frac{1+2.\lambda_{VT}}{1+\lambda_{VT}}\right) \tag{2.83}$$

The vertical tail root at vertical tail-fuselage intersection:

$$c_{r.fVT} = c_{rVT}.\left[1-\left(\frac{\left(1-\frac{\sqrt{3}}{2}\right).D_{f\max}.\left(\frac{c_{rVT}-\bar{c}_{VT}}{l_A}\right)}{h_{VT}}\right).\left(1-\lambda_{VT}\right)\right] \tag{2.84}$$

The exposed vertical tail taper ratio:

$$\lambda_{fVT} = \frac{c_{tVT}}{c_{r.fVT}} \tag{2.85}$$

Assuming constant thickness to chord ratio throughout the vertical tail:

$$\left.t/c\right)_{rVT} = \left.t/c\right)_{tVT} = \left.t/c\right)_{VT} \tag{2.86}$$

The exposed vertical tail root thickness to chord ratio:

$$\left.t/c\right)_{fVT} = \left.t/c\right)_{VT} \tag{2.87}$$

The ratio of the tip and root thickness ratios of the exposed vertical tail:

$$\tau_{fVT} = \frac{\left.t/c\right)_{fVT}}{\left.t/c\right)_{rVT}} \tag{2.88}$$

Exposed vertical tail area:

$$S_{netVT} = \left(\frac{c_{r.fVT}+c_{tVT}}{2}\right).\left(\frac{h_{VT}-\left(1-\frac{\sqrt{3}}{2}\right).D_{f\max}.\left(\frac{c_{rVT}-\bar{c}_{VT}}{l_A}\right)}{\cos\left(\Gamma_{VT}\right)}\right) \tag{2.89}$$

Vertical tail wetted area:

$$S_{wetVT} = 2.S_{netVT}.\left[1 + 0.25.\left(t/c\right)_{fVT}.\left(\frac{1+\tau_{fVT}.\lambda_{fVT}}{1+\lambda_{fVT}}\right)\right] \tag{2.90}$$

Horizontal tail:

$$b_{HT} = \sqrt{AR_{HT}.S_{HT}} \tag{2.91}$$

$$c_{rHT} = \frac{2.S_{HT}}{b_{HT}\left(1+\lambda_{HT}\right)} \tag{2.92}$$

$$c_{tHT} = \lambda_{HT}.c_{rHT} \tag{2.93}$$

$$\bar{c}_{HT} = \left(\frac{2}{3}\right).c_{rHT}.\left(\frac{1+\lambda_{HT}+\lambda_{HT}^{\ 2}}{1+\lambda_{HT}}\right) \tag{2.94}$$

$$\bar{y}_{HT} = \left(\frac{b_{HT}}{6}\right).c_{rVT}.\left(\frac{1+2.\lambda_{HT}}{1+\lambda_{HT}}\right) \tag{2.95}$$

The horizontal tail root at horizontal tail-fuselage intersection:

$$w_{f\max HT} = w_{f\max}.\left(\frac{c_{rHT}-\bar{c}_{HT}}{l_A}\right) \tag{2.96}$$

The exposed horizontal tail taper ratio:

$$\lambda_{fHT} = \frac{c_{tHT}}{c_{r.fHT}} \tag{2.97}$$

Assuming constant thickness to chord ratio throughout the horizontal tail:

$$t/c)_{rHT} = t/c)_{tHT} = t/c)_{HT} \tag{2.98}$$

The exposed horizontal tail root thickness to chord ratio:

$$t/c)_{fHT} = t/c)_{HT} \tag{2.99}$$

The ratio of the tip and root thickness ratios of the exposed horizontal tail:

$$\tau_{fHT} = \frac{t/c)_{tHT}}{t/c)_{rHT}} \tag{2.100}$$

Exposed horizontal tail area:

$$S_{netHT} = \left(\frac{c_{r.fHT} + c_{tHT}}{2}\right).\left(\frac{b_{HT} - w_{f\max HT}}{\cos(\Gamma_{HT})}\right) \tag{2.101}$$

The wetted horizontal tail area:

$$S_{wetHT} = 2.S_{netHT}.\left[1 + 0.25.t/c)_{fHT}.\left(\frac{1+\tau_{fHT}.\lambda_{fHT}}{1+\lambda_{fHT}}\right)\right] \tag{2.102}$$

2.8 Landing Gears

For the UCAV, retractable tricycle landing gear configuration was selected as most of the fighter aircrafts have, like F-16.

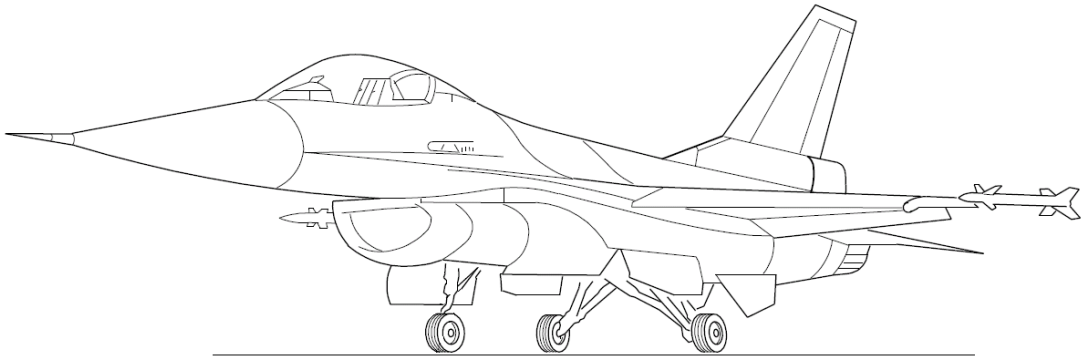

Figure 2.16 F-16

One of the plus of the tricycle landing gear may be that it allows faster acceleration during takeoff when the aircraft is at a small angle of attack so that the thrust of the engine is more parallel to the direction of travel. In addition, the nosewheel makes it impossible for the plane to tip over on its nose during landing [2].

Tricycle gear planes may also be easier to handle on the ground and reduce the possibility of a ground loop. This is due to the main gear being behind the center of mass [66].

Assuming that, nose landing gear carries 10% and main wheels carry 90% of static load of the UCAV:

$$F_N = 0.10.W_0 \tag{2.103}$$

$$F_M = 0.90.W_0 \tag{2.104}$$

Then, the wheel sizes can be determined according to the static load they carry with using Table 2.10 Ref. [46] for jet fighters.

Table 2.10 Statistical tire sizing [46]

	Diameter		Width	
	A	B	A	B
Main wheel diameter or width (cm) = AW_W^B				
Transport/Bomber	5.3	0.315	0.39	0.480
Jet Fighter/Trainer	5.1	0.302	0.36	0.467

W_w = Weight on wheel

$$D_{nosewheel} = 5.1.F_N^{0.302} \tag{2.105}$$

$$D_{mainwheel} = 5.1.\left(\frac{F_M}{2}\right)^{0.302} \tag{2.106}$$

$$w_{nosewheel} = 0.36.F_N^{0.467} \tag{2.107}$$

$$w_{mainwheel} = 0.36.\left(\frac{F_M}{2}\right)^{0.467} \tag{2.108}$$

The placement of the wheels was mentioned in section 2.10.

2.9 Aerodynamics

The airfoil of the aircraft is planned to be selected from a database as stated. It is assumed that the required lift to drag ratio during the mission can be met. However, in order to be stay in the feasible regions some properties (like lift coefficient) are also calculated for supersonic conditions. Though, in the program some checks are able to be done. And these checks served the programmer to

be able to decide on the limiting values of the constraints at the optimization part. The flexibility of the airfoil also eases the results to spread on a wide region. The used basic aerodynamic equations are not needed to be given here in detail.

Aerodynamic calculations begin with obtaining lift curve slope. The lift-curve slope is needed during conceptual design for three reasons. First, it is used to properly set the wing incidence angle. Secondly and the most important for a UCAV, the slope of the lift curve is needed while calculating drag-due-to-lift for this kind of high-performance aircrafts. The third use of the lift curve slope in conceptual design is for longitudinal-stability analysis [46].

From the Figure 2.17 Ref [46] it is seen that lift curve slope behaviour with Mach number is different for subsonic and supersonic speeds. Because the optimized UCAV is planned to be fly at supersonic conditions, supersonic equations were used for performance calculations.

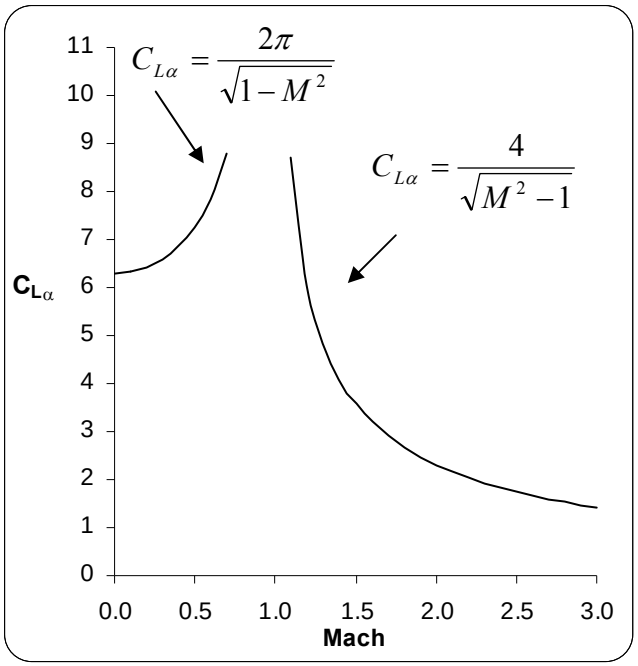

Figure 2.17 Lift curve slope vs. Mach number [46]

The following equations are from Ref. [5, 46, 48].

For a wing in supersonic flow, the lift-curve slope is ideally defined by [46]:

$$C_{L_\alpha} = 4/\beta \tag{2.109}$$

Where $\beta = \sqrt{M^2 - 1}$ when $M > 1/\cos\Lambda_{LE}$

And also, remembering that:

$$M = \frac{V}{a} \tag{2.110}$$

$$q = \frac{1}{2}\rho\ V^2 \tag{2.111}$$

Because, one of the optimization parameter is maximum velocity, $V_{\max}$, for the UCAV the required structure should be planned. For a given thrust-to-weight ratio maximum velocity is directly proportional to $\sqrt{W/S}$. The higher the wing loading the higher the maximum velocity is. However, with increasing wing loading the stalling speed, V_{stall}, is also increasing which is undesirable. The solution to this problem is increasing $C_{L\max}$ sufficiently that; in spite of the large W/S, V_{stall} will be acceptable. In turn, high-lift devices are the means to obtain the sufficient increase in $C_{L\max}$. With this knowledge, it can be said that high-lift devices make efficient high-speed flight possible [5].

For that reason, Fowler-type triple slotted flap was chosen in contrast to its complexity and high cost. Triple slotted flap is illustrated in Figure 2.18 [46].

Figure 2.18 Triple slotted flap [46]

For triple slotted flap maximum lift coefficient is interpolated from Figure 2.19 Ref. [46] as:

$$C_{L\max} \cong 3.4 - 1.4\left(\frac{\Lambda_{c/4}}{60}\right)^{1.5} \tag{2.112}$$

With using this interpolation wing sweep angle, $\Lambda_{\bar{c}/4}$, and maximum lift coefficient, $C_{L\max}$, are related, also. Where $\Lambda_{\bar{c}/4}$ was used as a design variable, so that $C_{L\max}$ was changed accordingly.

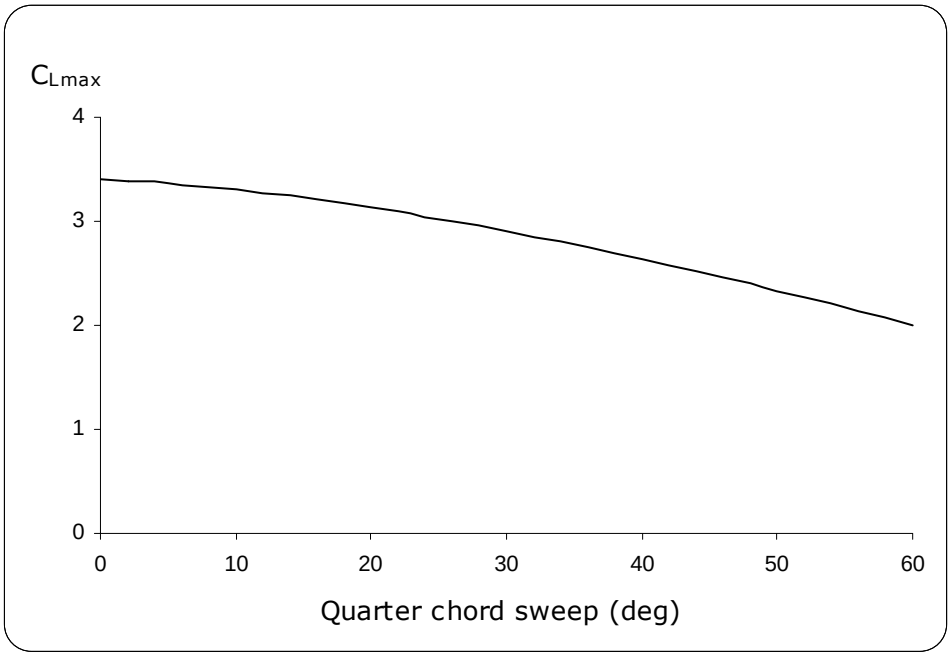

Figure 2.19 Maximum Lift Coefficient trend for triple slotted flap [46]

Then, maximum lift coefficients for takeoff and landing were calculated with the help of Table 2.11 Ref. [5, 57] for Fowler-type triple slotted flap 20° at takeoff and 40° at landing:

$$C_{L\max TO} = 2.7\cos\left(\Lambda_{c/4}\right) \tag{2.113}$$

$$C_{L\max\ Landing} = 3.5\cos\left(\Lambda_{c/4}\right) \tag{2.114}$$

Table 2.11 The effect of high-lift devices on $C_{L\max}$ [5, 57]

High Lift Device		Typical Flap Angle		$(C_L)_{\max}/\cos\Lambda$	
Trailing Edge	Leading Edge	Takeoff	Landing	Takeoff	Landing
Fowler flap					
single-slotted		15°	40°	2.0-2.2	2.5-2.9
double-slotted		20°	50°	1.7-1.95	2.3-2.7
double-slotted	slat	20°	50°	2.3-2.6	2.8-3.2
triple-slotted	slat	20°	40°	2.4-2.7	3.2-3.5

Parasite Drag was calculated as in Ref. [46]:

For the UCAV the component build up method can be used to find the supersonic parasite drag of each component. The supersonic drag includes the flat-plate supersonic skin friction drag, miscellaneous drag, leak and protuberances drag, and wave drag.

The flat-plate supersonic skin friction drag was calculated as multiplying flat-plate skin friction drag coefficient, C_{fc}, with the wetted area, S_{wetc}. Simply, it means that the component form factor, FF, and the factor Q are 1.

$$FF = 1 \tag{2.115}$$

$$Q = 1 \tag{2.116}$$

Then,

$$C_{D_{0_{\text{sup ersonic}}}} = \frac{\sum\left(C_{fc} S_{wet_C}\right)}{S_{ref}} + C_{D_{misc}} + C_{D_{L\&P}} + C_{D_{wave}} \tag{2.117}$$

The flat-plate skin friction coefficient depends on the Reynolds number, Mach number and skin roughness:

$$C_f = \frac{0.455}{\left(\log_{10} R\right)^{2.58}\left(1 + 0.144M^2\right)^{0.65}} \tag{2.118}$$

Where Reynolds number defined as:

$$R = \rho V \ell / \mu \tag{2.119}$$

For the relatively rough surface the friction coefficient is higher. So that, in the flat-plate skin friction coefficient equation the lower of the actual Reynolds number or the cut-off Reynolds number, which includes the skin roughness value, k , should be used.

For supersonic flight:

$$R_{cutoff} = 44.62\left(\ell / k\right)^{1.053} M^{1.16} \tag{2.120}$$

Because the UCAV was planned to have camouflage paint and aluminium structure skin roughness value selected from Table 2.12 Ref.[46] as :

$$k = 1.015 \ x \ 10^{-5} \tag{2.121}$$

Table 2.12 Skin roughness value (*k*) [46]

Surface	k (m)
Camouflage paint on aluminium	1.015×10^{-5}
Smooth paint	0.634×10^{-5}
Production sheet metal	0.405×10^{-5}
Polished sheet metal	0.152×10^{-5}
Smooth molded composite	0.052×10^{-5}

In order to find the weapons contribution to drag, first the number of weapons were calculated from payload weight, $W_{payload}$. Basically, two types of bombs were thought for the UCAV to carry: one of them was about 2000 lb (≅ 907 kg) in weight and other one was known as Sidewinder (Aim-9) and about 200 lb (≅ 91 kg) in weight, selected from Table 2.13 Ref.[46].

The number of 2000 lb (907 kg) bombs on wings:

$$\#_{\text{bomb.big}} = \text{int}\left(\frac{W_{payload}}{907}\right) \tag{2.122}$$

The number of Aim9 bombs:

$$\#_{\text{bomb.Aim9}} = \text{int}\left[\frac{W_{payload} - \left(\#_{\text{bomb.big}}.907\right)}{91}\right] \tag{2.123}$$

Table 2.13 Miscellaneous Weights (approximate) [46]

Component	Weight (kg)
Missiles	
Harpoon (AGM-84 A)	544
Phoenix (AIM-54 A)	454
Sparrow (AIM-7)	227
Sidewinder (AIM-9)	91
M61 Gun	
Gun	113
940 rds ammunition	250

While estimating miscellaneous drags an empirical graph from Ref. [46] was used as shown in Figure 2.20.

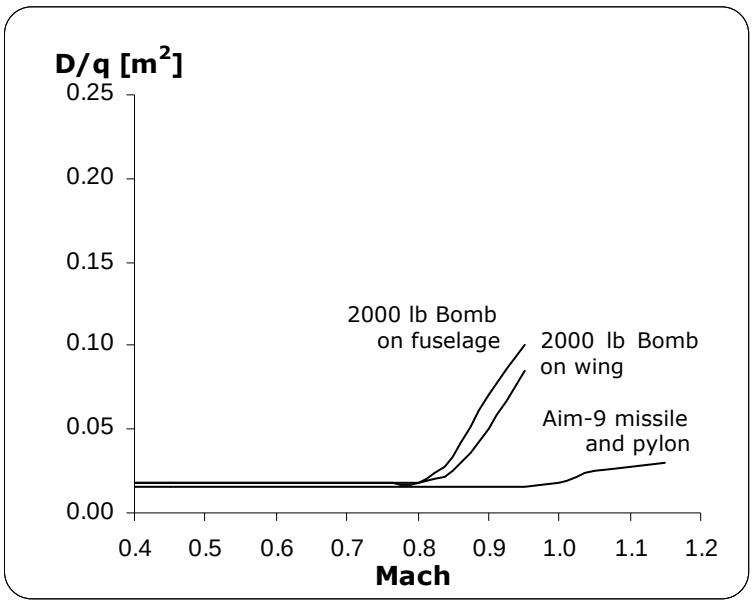

Figure 2.20 2000 lb Bomb and Aim-9 missile drag [46]

One of the important drag contributions is wave drag for the UCAV, because in supersonic flight the wave drag is often greater than all the other drag put together. The reason comes from that the wave drag is pressure drag due to shocks, and is a direct result of the way in which the aircraft's volume is distributed.

For preliminary wave drag analysis at supersonic conditions, ideally volume distributed Sears-Haack body wave drag was found initially as:

Sears-Haack body:

$$\left(D/q\right)_{Sears-Haack} = \frac{9\pi}{2}\left(\frac{A_{\max}}{\ell}\right)^2 \tag{2.124}$$

Where,

$$A_{\max} = \pi\left(\frac{D_{f\max}}{2}\right)^2 \tag{2.125}$$

Here, inlet capture area was subtracted from $A_{\max}$, and the mid section which has constant area was subtracted from length of fuselage as stated in Ref.[46]. Then,

$$\left(D/q\right)_{wave} = E_{WD}\left[1-0.386\left(M-1.2\right)^{0.57}\left(1-\frac{\pi\Lambda_{LE.\deg}{}^{0.77}}{100}\right)\right]\left(D/q\right)_{Sears-Haack} \tag{2.126}$$

Empirical wave-drag efficiency factor, E_{WD}, selected as 1.8 for the supersonic fighter.

Leaks and protuberances are difficult to predict with any method, so that they may be approximated. Leakage drag is due to the tendency of an aircraft to inhale through holes and gaps in high pressure zones, and exhale into the low pressure zones. Protuberances include antennas, lights, if exists any door edges, fuel vents, control surface external hinges, actuator fairings, and such manufacturing defects [46]. All of these contributions are estimated as 5% of the parasite drag for the UCAV.

$$C_{D.L\&P} = 0.05 \; C_{Dparasitic} \tag{2.127}$$

Induced Drag was calculated as in Ref. [46]:

To find the induced drag, Oswald span efficiency and drag-due-to-lift-factor were calculated as follows:

For swept-wing aircraft $\left(\Lambda_{LE} > 30 \;\; \text{deg}\right)$:

$$e = 4.61\left(1 - 0.045 AR^{0.68}\right)\left(\cos \Lambda_{LE}\right)^{0.15} - 3.1 \tag{2.128}$$

At supersonic speeds:

$$K = \frac{AR\left(M^2 - 1\right)}{4AR\sqrt{M^2 - 1} - 2} \cos \Lambda_{LE} \tag{2.129}$$

Then,

$$C_{D_i} = KC_L{}^2 \tag{2.130}$$

For a cambered wing, the minimum drag occurs at some positive lift not at zero lift. However, for wings of moderate camber it can be assumed that this difference is small and uncambered wing equation can be used:

$$C_D = C_{D_0} + KC_L{}^2 \tag{2.131}$$

Finally, ground effect is calculated for one meter above the ground [5]:

$$G = \frac{\left(16h/b\right)^2}{1 + \left(16h/b\right)^2} \tag{2.132}$$

2.10 Weight and Stability

The following weight and stability equations were taken from references [5, 46, 48].

Weight of the wing:

$$W_{wing} = 0.0103 K_{dw} K_{vs} \left(W_{dg} N_Z\right)^{0.5} S_w^{0.622} AR^{0.785} \left(t/c\right)_r^{-0.4} \left(1+\lambda\right)^{0.05} \left(\cos\Lambda\right)^{-1.0} S_{csw}^{0.04} \tag{2.133}$$

Where, for a swept wing $K_{dw} = 1.0$ and $K_{vs} = 1.0$.

And the ultimate load factor was calculated from: $N_Z = 1.5 n_{\max}$

Weight of the horizontal tail:

$$W_{horizontaltail} = 3.316 \left(1 + \frac{w_{f\max HT}}{b_{HT}}\right)^{-2.0} \left(\frac{W_{dg} N_z}{1000}\right)^{0.260} S_{HT}^{0.806} \tag{2.134}$$

Weight of the vertical tail:

$$\begin{aligned} W_{verticaltail} &= 0.452 K_{rHT} \left(1 + H_t/H_v\right)^{0.5} \left(W_{dg} N_z\right)^{0.488} S_{vt}^{0.718} M^{0.341} \\ &xL_f^{-1.0} \left(1 + S_r/S_{VT}\right)^{0.348} AR_{VT}^{0.223} \left(1+\lambda\right)^{0.25} \left(\cos\Lambda_{VT}\right)^{-0.323} \end{aligned} \tag{2.135}$$

Where, for conventional tail $K_{rHT} = 1.0$ and $\frac{H_t}{H_v} = 0.0$.

And $\frac{S_r}{S_{VT}} = 0.25$ like other competitor fighters F-15 and F-16 from Table 2.14 Ref. [48].

Table 2.14 Fighters vertical tail volume, rudder and aileron data [48]

Type	S (ft^2)	b (ft)	S_{VT} (ft^2)	S_r/S_{VT}	$\overline{V}_{VT}$
F-4E	530	38.4	59.6	0.20	0.054
F-15	608	42.8	143	0.25	0.098
F-16	300	31.8	62.2	0.25	0.094

Weight of the fuselage:

$$W_{fuselage} = 0.499 K_{dwf} W_{dg}^{0.35} N_z^{0.25} L^{0.5} D^{0.849} W^{0.685} \tag{2.136}$$

Where, $K_{dwf} = 1.0$ for a swept wing aircraft.

Weight of each main landing gear:

$$W_{mainlandinggear} = K_{cb} K_{tpg} \left(W_l N_l\right)^{0.25} L_m^{0.973} \tag{2.137}$$

$$L_m = \pi D_{mainwheel} \tag{2.138}$$

For tricycle landing gears $K_{cb} = 1.0$ and $K_{tpg} = 0.826$.

$$N_l = N_{gear} x\ 1.5 \tag{2.139}$$

And, $N_{gear} = 3.0$, selected from Table 2.15 Ref. [46] for Air Force Fighter.

Table 2.15 Gear load factors [46]

Aircraft type	N_{gear}
Large Bomber	2.0-3
Commercial	2.7-3
General aviation	3
Air Force Fighter	3.0-4
Navy Fighter	5.0-6

Weight of the nose landing gear:

$$W_{noselandinggear} = \left(W_l N_l\right)^{0.290} L_n^{0.5} N_{nw}^{0.525} \tag{2.140}$$

Where, number of nosewheel, $N_{nw} = 1.0$.

Weight of the engine:

$$W_{engine} = 0.8.\left(11.1 T^{1.1} M^{0.25} e^{(-0.81 BPR)}\right) \tag{2.141}$$

including 20% reduction for next-generation engines.

Total weight of the instruments:

$$W_{instruments} = 8.0 + 36.37 N_{en}^{0.676} N_t^{0.237} + 26.4\left(1 + N_{ci}\right)^{1.356} \tag{2.142}$$

Where, the number of engine, $N_{en} = 1.0$; the number of fuel tanks, $N_t = 0$; the number of crew $N_{ci} = 0$.

Total weight of the avionics:

$$W_{avionics} = 2.117 W_{uav}^{0.933} \tag{2.143}$$

With assuming the uninstalled avionics weight $W_{uav} = 800\,\text{lb}$.

Finally, weight of all the other things which were not calculated separately and the center of gravity locations were found for fighters from Table 2.16 Ref. [46].

Table 2.16 Approximate empty weight buildup [46]

Item	Fighters		Multiplier	Approximate location
	lb/ft^2	kg/m^2		
Wing	9.0	44	$S_{\text{exposed planform}}$	40% m.a.c.
Horizontal tail	4.0	20	$S_{\text{exposed planform}}$	40% m.a.c.
Vertical tail	5.3	26	$S_{\text{exposed planform}}$	40% m.a.c.
Fuselage	4.8	23	$S_{\text{wetted area}}$	40-50% length
Landing gear	0.033	-----	W_0	-----
Navy:	0.045			
Installed engine	1.3	-----	W_{engine}	-----
All-else empty	0.17	-----	W_0	40-50% length

$$W_{else} = 0.17W_0 \tag{2.144}$$

$$x_{cg.engine} = L_f - 0.5L_{eng} \tag{2.145}$$

$$x_{cg.fus} = 0.5L_f \tag{2.146}$$

$$x_{cg.else} = 0.5L_f \tag{2.147}$$

Assuming $x_{cg.wing} = x_{m.a.c-wing}$ and $x_{cg.HT} = x_{m.a.c-HT}$ for the supersonic fighter:

$$x_{cg.HT} = L_f - 0.6\bar{c}_{HT} \tag{2.148}$$

$$x_{cg.VT} = L_f - 0.6\bar{c}_{VT} \tag{2.149}$$

$$x_{cg.wing} = x_{cg.HT} - l_{HT} \tag{2.150}$$

$$x_{cg.fuel} = x_{cg.wing} \tag{2.151}$$

All the bombs were planned to be carried on wings:

$$x_{cg.payload} = x_{cg.wing} \tag{2.152}$$

Without including gears, the center of gravity was found as:

$$M_{cg1} = W_{wing}.x_{cg.wing} + W_{horizontaltail}.x_{cg.HT} + W_{verticaltail}.x_{cg.VT} + W_{fuselage}.x_{cg.fus} + W_{engine}.x_{cg.engine} + \left(W_{instruments} + W_{avionics} + W_{else}\right).x_{cg.else} + W_{payload}.x_{cg.payload} + W_{f\max w}.x_{cg.fuel} \tag{2.153}$$

$$W_{cg1} = W_{wing} + W_{horizontaltail} + W_{verticaltail} + W_{fuselage} + W_{engine} + W_{instruments} + W_{avionics} + W_{else} + W_{payload} + W_{f\max w} \tag{2.154}$$

$$x_{cg1} = M_{cg1} / W_{cg1} \tag{2.155}$$

Assuming the main wheels carry 90% and the nose wheel carries 10% of static load of the UCAV and matching the center of gravities of the wing and the main wheels:

$$x_{cg.mgears} = x_{cg.wing} \tag{2.156}$$

Then, locating the nose wheel accordingly:

$$x_{cg.ngears} = x_{cg1} - \left[\left(x_{cg.mgears} - x_{cg1}\right).9.0\right] \tag{2.157}$$

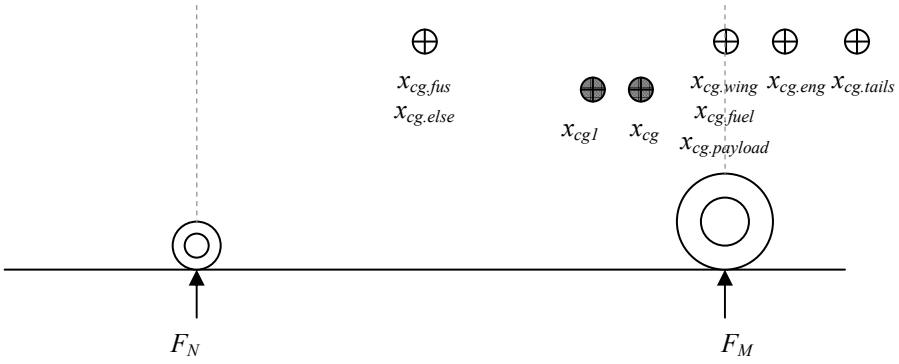

Figure 2.21 Center of gravity-exaggerated views

The resultant center of gravity location of the UCAV was found after adding landing gear values as:

$$M_{cg} = M_{cg1} + 2.W_{mainlandinggear}.x_{cg.mgears} + W_{nosselandinggear}.x_{cg.ngear} \tag{2.158}$$

$$W_{cg} = W_{cg1} + 2.W_{mainlandinggear} + W_{noselandinggear} \tag{2.159}$$

$$x_{cg} = M_{cg} / W_{cg} \tag{2.160}$$

Then the empty weight of the UCAV:

$$W_e = W_{cg} - W_{payload} - W_{f\max w} \tag{2.161}$$

Static Margin:

An assumption was made as the lift slope of the tail is equal to lift slope of the airplane:

$$\frac{a_t}{a} = 1.0 \tag{2.162}$$

and assuming $x_{acwb} = x_{cg.wing}$

Neutral point was calculated as:

$$x_n = x_{acwb} + V_{HT}\frac{a_t}{a} \tag{2.163}$$

Then,

$$Static\_margin = \frac{x_n - \bar{x}}{\bar{c}} \tag{2.164}$$

Static margin of the fighter aircrafts is usually about 5%; besides, new fighters have even minus static margins. Since, the static margin is one of the important parameter for stability and control it was inserted between the constraints in the Fortran code.

2.11 Performance

The performance calculations were made from references [5, 46, 48].

Takeoff wing loading:

$$\left.\frac{W}{S}\right)_{TO} = \frac{W_0}{S} \tag{2.165}$$

Takeoff distance:

$$s_{TO} = \frac{37.5.\left.\frac{W}{S}\right)_{TO}}{\sigma.C_{L\max TO}.\left.\frac{T}{W}\right)_{TO}} \tag{2.166}$$

Assuming the aircraft takeoffs at sea level, the density ratio:

$$\sigma = 1.0 \tag{2.167}$$

And, takeoff distance was selected as one of the constraints in the optimization part.

Wing loading at landing:

$$\left.\frac{W}{S}\right)_{Landing} = \left.\frac{W}{S}\right)_{TO} . \frac{W_{15}}{W_0} . \frac{1}{W_{15}/W_{14}} \tag{2.168}$$

Landing distance:

$$s_L = 5. \left.\frac{W}{S}\right)_{Landing} . \left(\frac{1}{\sigma . C_{L\max Landing}} \right) + S_a \tag{2.169}$$

Landing distance was also selected as one of the constraints in the optimization part.

Where,

$S_a = 137\ \ m$ was given by Ref. [46] for seven degree glideslope.

For steady-level flight:

$$\left.\frac{L}{D}\right)_{\max\_s} = \frac{1}{\sqrt{4.C_{D0}.K}} \tag{2.170}$$

For simplification of maximum rate of climb, ROC_{max}, equation, let:

$$Z = 1 + \sqrt{1 + \frac{3}{(L/D)^2_{\max} (T/W)^2}} \tag{2.171}$$

Then,

$$ROC_{\max} = \left[\frac{(W/S)Z}{3\rho_\infty C_{D0}} \right]^{1/2} \left(\frac{T}{W} \right)^{3/2} \left[1 - \frac{Z}{6} - \frac{3}{2(T/W)^2 (L/D)^2_{\max} Z} \right] \tag{2.172}$$

One important point here is that, the weight in ROC_{max} equation was stated for the weight with full payload, i.e. weapons. If this calculation had made for the weight without payload the ROC_{max} equation could be higher results.

Minimum climb angle:

$$\theta_{\max} = \arcsin\left[\frac{T}{W} - \frac{1}{(L/D)_{\max}}\right] \tag{2.173}$$

In performance calculations the available thrust was always adjusted because of the effect of the altitude change as:

$$T_{ROC} = T.\frac{\rho}{\rho_{\infty}} \tag{2.174}$$

Maximum ceiling:

Maximum ceiling was found with a control loop and caught when *ROC* equals zero. And, maximum ceiling was also inserted in constraints.

Range:

Range was calculated for separate segments before and after the combat time because of payload drop so, changing weight severely and then these ranges were summed.

$$\left(\frac{\sqrt{C_L}}{C_D}\right)_{\max} = \frac{3}{4}\left(\frac{1}{3KC_{D0}^3}\right)^{1/4} \tag{2.175}$$

$$RANGE = \frac{2}{SFC}\sqrt{\frac{2}{\rho_{\infty}S}}.\frac{\sqrt{C_L}}{C_D}\left(\sqrt{W_i} - \sqrt{W_{i+1}}\right) \tag{2.176}$$

Then, cruise range was updated as:

$$R_{cr} = \frac{RANGE - 2.R_d - s_{TO} - s_L}{2} \tag{2.177}$$

Maximum speed was calculated at 40000 ft:

$$V_{\max} = \left\{ \frac{\left[(T_A)_{\max}/W\right](W/S) + (W/S)\sqrt{\left[(T_A)_{\max}/W\right]^2 - 4C_{D0}K}}{\rho_\infty C_{D0}} \right\}^{1/2} \tag{2.178}$$

And maximum Mach number at this level:

$$M_{\max} = \frac{V_{\max}}{a} \tag{2.179}$$

Endurance:

As in the range calculation, endurance was calculated for separate segments before and after the combat time because of severe weight change at combat and then these endurances were summed. However, endurance does not include the combat time but the combat time could be added on endurance if wanted, later.

$$E = \frac{1}{SFC}.\frac{L}{D}\ln\frac{W_i}{W_{i+1}} \tag{2.180}$$

Corner Velocity:

In order to get the minimum instantaneous turn radius and the maximum instantaneous turn rate the UCAV should fly with the corner velocity, which was used while calculating maneuver radiuses and rates below:

$$V_{corner} = \sqrt{\frac{2n_{\max}}{\rho_\infty C_{L\max}}\frac{W}{S}} \tag{2.181}$$

Minimum turn radius (at sustained level turn):

$$R_{\min} = \frac{4K(W/S)}{g\rho_{\infty}(T/W)\sqrt{1-4KC_{D0}/(T/W)^2}} \tag{2.182}$$

Maximum turn rate (at sustained level turn):

$$\omega_{\max} = q\sqrt{\frac{\rho_{\infty}}{W/S}\left[\frac{T/W}{2K} - \left(\frac{C_{D0}}{K}\right)^{1/2}\right]} \tag{2.183}$$

Instantaneous turn radius (at pull up maneuver):

$$R_{\min\, pull-up} = \frac{V_{\infty}^2}{g(n-1)} \tag{2.184}$$

Instantaneous turn rate (at pull up maneuver):

$$\omega_{\max\, pull-up} = \frac{g(n-1)}{V_{\infty}} \tag{2.185}$$

Instantaneous turn radius (at pull down maneuver):

$$R_{\min\, pull-down} = \frac{V_{\infty}^2}{g(n+1)} \tag{2.186}$$

Instantaneous turn rate (at pull down maneuver):

$$\omega_{\max\, pull-down} = \frac{g(n+1)}{V_{\infty}} \tag{2.187}$$

At combat time, the lift to drag ratio should be calculated with including the load factor term [46].

$$\frac{L}{D} = \frac{1}{q\dfrac{C_{D0}}{n(W/S)} + \dfrac{n(W/S)}{q\pi A\,\mathrm{Re}}} \tag{2.188}$$

For a sustained combat turn the thrust can be calculated assuming that the thrust angle approximately aligned with the flight direction as [46]:

$$T = n.\left(\frac{L}{D}\right).W \tag{2.189}$$

Then, the combat time for known fuel weight:

$$d = \frac{W_{fc}}{SFC.T} \tag{2.190}$$

And, the number of complete turns:

$$xx = \frac{d.\omega}{2\pi} \tag{2.191}$$

In the calculations it was assumed that cruise occurs at 40000 ft and combat/strafe at 15000 ft. The atmospheric properties at these altitudes were obtained by calling the International Standard Atmosphere (ISA) subroutine, prepared with well known equations which were not needed to deal in this study.

2.12 Structural Load

It is difficult to provide a complete structural analysis at the conceptual design stage. In spite of this, some structural load parameters were calculated in order to be within feasible structural limits.

The calculations were made with in light of references [5, 46].

One of the parameter is maneuver speed defined as the maximum speed at which the control items can fully be deflected without damaging either the airframe or the controls themselves [46].

$$V_{manuever} = V_{stall} + K_p\left(V_L - V_{stall}\right) \tag{2.192}$$

Where,

$$V_{stall} = \sqrt{\frac{2}{\rho}\frac{W}{S}\frac{1}{C_{L\max}}} \tag{2.193}$$

$$K_p = 0.15 + \frac{5400}{W + 3300} \tag{2.194}$$

And the factor, K_p, should be between 0.5 and 1.0 [46]. This was controlled as deciding a constraint in the Fortran code, also.

V_L is maximum level cruise speed, which was introduced to Fortran code as a constant.

Eventually, the maximum available sustained load factor:

$$n_{\max} = \left\{ \frac{\frac{1}{2}\rho_\infty V_\infty^2}{K\left(W/S\right)}\left[\left(\frac{T}{W}\right)_{\max} - \frac{1}{2}\rho_\infty V_\infty^2 \frac{C_{D0}}{W/S}\right] \right\}^{1/2} \tag{2.195}$$

An airplane should be designed for a limit load that includes factor of safety, which is usually taken as 1.5. So as introduced in the Weight and Stability part the ultimate load factor of the UCAV is:

$$N_Z = 1.5 n_{\max} \tag{2.196}$$

2.13 Cost Model

Costs were calculated from Ref. [46] with DAPCA, the Development and Procurement Costs of Aircraft model.
DAPCA estimates the hours required for research, development, test and evaluation and production by the engineering, tooling, manufacturing, and quality control groups. These are multiplied by the appropriate hourly rates to yield costs. Development support, flight test and manufacturing material costs are directly estimated by DAPCA [46].

For the UCAV it was suggested to use aluminium as a material and camouflage paint. The cost was estimated according to this material.

In order to be able to compare with the competitor aircrafts the hourly rates were not changed and assumed they did not increase very much in dollars.

While calculating, the number of flight test aircraft was thought as a constant and equated to 2.

The number of the optimized UCAV, *Quantity*, was selected as a constant and equated to 500.

Engineering hours:

$$H_E = 7.53 W_e^{0.777} V_{\max}^{0.894} Quantity^{0.163} \quad \text{(mks)} \tag{2.197}$$

Tooling hours:

$$H_T = 10.5 W_e^{0.777} V_{\max}^{0.696} Quantity^{0.263} \quad \text{(mks)} \tag{2.198}$$

Manufacturing hours:

$$H_M = 15.2 W_e^{0.82} V_{\max}^{0.484} Quantity^{0.641} \quad \text{(mks)} \tag{2.199}$$

Quality Control hours:

$$H_Q = 0.133 H_M \quad \text{(mks)} \tag{2.200}$$

Development support cost:

$$Cost_D = 48.7 W_e^{0.630} V_{\max}^{1.3} \quad \text{(mks)} \tag{2.201}$$

Flight test cost:

$$Cost_F = 1408\ W_e^{0.325} V_{\max}^{0.822} FTA^{1.21} \quad \text{(mks)} \tag{2.202}$$

Manufacturing materials cost:

$$Cost_M = 22.6 W_e^{0.921} V_{\max}^{0.621} Quantity^{0.799} \quad \text{(mks)} \tag{2.203}$$

Engine production cost:

$$Cost_E = 2251\left[9.66 T_{\max} + 243.25 M_{\max} + 1.74 T_{turbine.inlet} - 2228\right] \quad \text{(mks)} \tag{2.204}$$

Where, the turbine inlet temperature was interpolated from Figure 2.22. This figure was based on the Table 2.17 taken from Ref. [34] and the gained knowledge from Ref. [62] and Ref. [27] for afterburning turbofan engines.

Table 2.17 Turbofan Engine Properties [34]

Engine	Thrust (kN)	Turbine Inlet Temperature (K)	BPR	W_{engine} (N)
JT8D-7B	65	853.15	1.03	14466
TF33-P-3	76	1144.26	1.55	17348
JT3D-3B	80	1144.26	1.37	19127
TF33-P-7	93	1227.59	1.21	20684
F108-CF-100	96	1493.15	6.00	20506
TF30-P-111	112	1397.04	0.73	17788
F100-PW-229	129	1755.00	0.40	13505
F101-GE-102	137	1672.04	1.91	19786

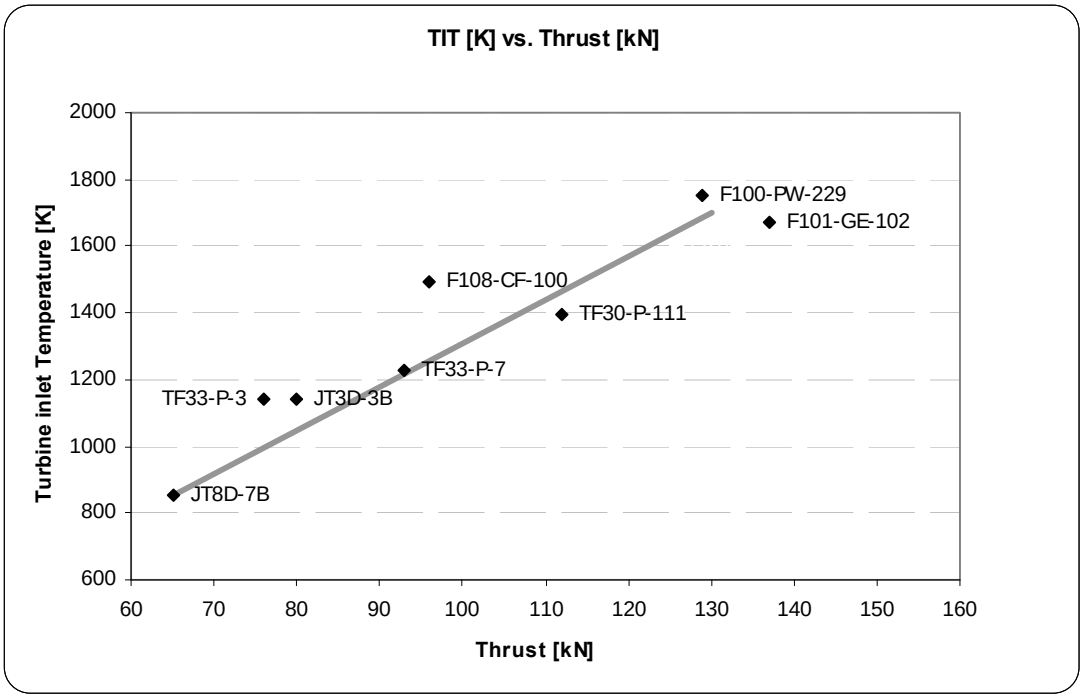

Figure 2.22 Turbine Inlet Temperature vs. Thrust for Turbofan Engines [27,34,62]

From this trend line, the turbine inlet temperature for a turbofan engine could be interpolated in Kelvin as:

$$T_i \cong 13.T + 10 \tag{2.205}$$

This interpolation was used for the rubber engine of the UCAV while finding its cost.

Avionics Cost was approximated as $7000 per kg:

$$Cost_A = 7000\ W_{avionics} Quantity \tag{2.206}$$

Average hourly rates were taken from Ref. [46] for 1999. These were adjusted to 2008 based on Consumer Price Indexes calculated from CPI inflation calculator in Ref. [59].

The CPI inflation calculator uses the average Consumer Price Index for a given calendar year. This data represents changes in prices of all goods and services purchased for consumption by urban households. For the current year, the latest monthly index value is used [59].

Engineering hourly rates in 1999 (2008):

$$R_E = \$86 \ (110)$$

Tooling hourly rates in 1999 (2008):

$$R_T = \$88 \ (112)$$

Quality control hourly rates in 1999 (2008):

$$R_Q = \$81 \ (103)$$

Manufacturing hourly rates in 1999 (2008):

$$R_M = \$73 \ (94)$$

Acquisition cost of each UCAV in $:

$$COST = {H_E R_E + H_T R_T + H_M R_M + H_Q R_Q + Cost_D + Cost_F + Cost_M + Cost_E N_E + Cost_A} \Big/ {Quantity} \quad (2.207)$$

2.14 Inputs and Outputs

Inputs and outputs of each subroutine were tabulated in Table 2.18. From this table which parameters are taken as inputs and which are served after calculations as outputs for the following subroutines and output file can be understood easily.

Table 2.18 Inputs and Outputs for each Subroutine

SUBROUTINE NAMES	INPUTS	OUTPUTS
ISA (Atmospheric Properties)	H, ρ_0 , g_0 , a_0	ρ, a
WING CONFIGURATION	D_{fmax} , Λ_w , b , AR , Γ_w , t/c)$_w$	Λ_{LE} , c_{rfw} , λ_{fw} , t_{cfw} , τ_{fw} , AR_{wet} , λ , w_{fmax} , t/c)$_{tw}$, t/c)$_{rw}$, S , c_r , c_t , $\bar{y}$, $\bar{c}$, $\bar{x}$, S_{netw} , S_{wetw} , L/D)$_{max}$, V_f , w_{fmaxw} , S_{csw}
FUSELAGE CONFIGURATION	D_{fmax} , W_0 , w_{fmax}	h_{fmax} , L_f , l_N , l_A , l_M , A_{max} , FinenessRatio, Volume, S_{wetf}
PROPULSION SYSTEM	M , W_0 , BPR , SFC	T, T_{av} , L_{eng} ,D_{eng} ,SFC_c ,T_{cruise}
HORIZONTAL and VERTICAL TAIL	$D_{f\ max}$, L_f , b , S , w_{fmax} , $\bar{c}$, l_A , Λ_w , t/c)$_{VT}$, t/c)$_{HT}$, Λ_{VT} , AR_{VT} , AR_{HT} , λ_{VT} , λ_{HT} , Γ_{VT} , Γ_{HT} , V_{VT} , V_{HT} , l_{Vtco} , l_{Htco}	l_{VT} , l_{HT} , Λ_{HT} , S_{VT} , S_{HT}, h_{VT} , c_{rVT} , c_{tVT} , $\bar{c}_{VT}$, $\bar{z}_{VT}$, c_{rfVT} , λ_{fVT} , t/c)$_{rVT}$, t/c)$_{tVT}$, t/c)$_{fVT}$, τ_{fVT} , S_{netVT} , $S_{wet\ VT}$, b_{HT} , c_{rHT} , c_{tHT} , $\bar{c}_{HT}$, $\bar{y}_{HT}$, w_{fmaxHT} , c_{rfHT} , λ_{fHT} , t/c)$_{rHT}$, t/c)$_{tHT}$, t/c)$_{fHT}$, τ_{fHT} , S_{netHT} , S_{wetHT}

Table 2.18 Inputs and Outputs for each Subroutine (continued)

SUBROUTINE NAMES	INPUTS	OUTPUTS
LANDING GEARS	W_0	$D_{nosewheel}$, $D_{mainwheel}$, F_M , F_N , $w_{nosewheel}$, $w_{mainwheel}$
AERODYNAMICS	H , ρ , a , V_{cruise}, $W_{payload}$, Λ_{LE} , Λ_w , W_0 , L_f , D_{fmax} , A_{max} , S_{wetf} , b , S , AR , $\bar{c}$, S_{wetw} , V_{VT} , V_{HT} , l_{VT} , l_{HT} , S_{VT} , S_{HT} , S_{wetVT} , S_{wetHT} , $\bar{c}_{VT}$, $\bar{c}_{HT}$	ρ$_{cruise}$, a_{cruise} , $\#_{bom\_big}$, $\#_{bomb\_aim9}$, M_{cruise}, q_{cruise}, β , Re_{fus} , $Re_{cutoff.fus}$, $C_{f.fus}$, FF_{fus} , Q_{fus}, c_{D0fus} , Re_w, $Re_{cutoff.w}$, $C_{f.w}$, FF_w , Q_w, c_{D0w} , Re_{HT} , $Re_{cutoff.HT}$, C_{fHT}, FF_{HT} , Q_{HT}, c_{D0HT} , Re_{VT}, $Re_{cutoff.VT}$, C_{fVT}, FF_{VT} , Q_{VT}, c_{D0VT} , D/q)$_{misc}$, c_{D0misc} , D/q)$_{wavesh}$, D/q)$_{wave}$, c_{D0wave} , $c_{D0parasitic}$, $c_{D0Leakage}$, $c_{D0totalclean}$, $c_{D0total}$, e , K , K_{clean} , Ground_effect, $c_{Lmaxclean}$, $c_{LacmaxTO}$, $c_{Lmax\ landing}$, c_{D0c}
WEIGHT and STABILITY	n_{max} , S , AR , t/c)$_{rw}$, λ , V_{HT} , Λ_{LE} , Λ_w , AR_{VT} , λ_{VT} , Λ_{HT} , Λ_{VT} , M , W_0 , T, T_{av} , BPR , S_{csw} , w_{fmaxHT} , D_{fmax} , h_{fmax} , b_{HT} , S_{VT} , S_{HT} , L_f , l_{VT} , l_{HT} , $D_{nosewheel}$, $D_{mainwheel}$, $\bar{c}_{HT}$, $\bar{c}_{VT}$, e , $W_{payload}$, w_{fmaxw} , L_{eng}	N_z , W_{wing} , $W_{horizontaltail}$, $W_{verticaltail}$, $W_{fuselage}$, $W_{mainlandinggear}$, $W_{noselandinggear}$, W_{engine} , $W_{instruments}$, $W_{avionics}$, W_{else} , $x_{cg.engine}$, $x_{cg.fus}$, $x_{cg.else}$, $x_{cg.HT}$, $x_{cg.VT}$, $x_{cg.wing}$, $x_{cg.fuel}$, $x_{cg.payload}$, M_{cg} , W_{cg} , x_{cg} , $x_{cg.mgear}$, $x_{cg.ngear}$, x_{acw} , Static_margin, W_e , x_n

Table 2.18 Inputs and Outputs for each Subroutine (continued)

SUBROUTINE NAMES	INPUTS	OUTPUTS
INITIAL SIZING	SFC, SFC_c , $L/D)_{max}$, w_{fmaxw} , W_e , $W_{payload}$, R_{cr} , V_{cruise} , E_{ltr} , V_{max}	W_0 , W_f , W_1/W_0 , W_2/W_1 , W_3/W_2 , W_4/W_3 , W_5/W_4 , $L/D)_{cr}$, $L/D)_{ltr}$, W_6/W_5 , W_7/W_6 , R_d , $L/D)_d$, W_8/W_7 , W_{fuel1} , W_9/W_8 , W_{fc} , W_9 , W_{10}/W_9 , W_{11}/W_{10} , W_{12}/W_{11} , W_{13}/W_{12} , W_{14}/W_{13} , W_{15}/W_{14} , W_{15}/W_0 , W_f/W_0 , $W_{0initialsizing}$, W_3
PERFORMANCE	W_0 , S, AR, $c_{Lmaxclean}$, $c_{LacmaxTO}$, $c_{Lmaxlanding}$, c_{D0c} , $c_{D0\ total}$, K , SFC , SFC_c , $L/D)_{max}$, W_{fuel1} , W_f , $W_{payload}$, W_e , W_9 , ρ_0 , ρ , e , M , W_{15}/W_{14} , W_{15}/W_0 , W_3 , H , W_{10}/W_9 , W_{fc}	$W/S)_{TO}$, T/W , T , s_{TO} , $W/S)_{Landing}$, s_L , $L/D)_{max\ s}$, ROC_{max} , θ_{max} , Maximum_ceiling, T_{ROC} , ROC , $\sqrt{c_L}/c_D)_{max}$, RANGE , V_{max} , M , M_{max} , E_{max} , V_{corner} , n_{max} , R_{min} , ω_{max} , $R_{min.pull\text{-}up}$, $\omega_{max\ pull\text{-}up}$, $R_{min.pull\text{-}down}$, $\omega_{max.pull\text{-}down}$, q_c , $L/D)_c$, T_{rc} , d , xx
STRUCTURAL LOAD	H , C_{D0c} , T , K , $c_{Lmaxclean}$, W_9 , S , ρ	$V_{manuever}$, K_p , V_{stallc} , c_{Lmaxc} , n_{max} , q_c
COSTS	W_e , $W_{avionics}$, M , V_{max} , T , Quantity, FTA , T_i , R_e , R_t , R_q , R_m	H_e , H_t , H_q , H_m , $Cost_D$, $Cost_F$, $Cost_M$, $Cost_E$, $Cost_A$, COST

In the following section, an example problem was applied to run and see the correctness of the aircraft design part before uniting with the optimization part.

2.15 Verification of the Aircraft Design Part

After constructing the related subroutines separately, all were gathered in a main program to perform the design process. This main program takes the inputs from a text file and gives outputs to another text file.

In order to prove the accuracy of the aircraft design part, a supersonic aircraft with similar missions were examined. In the end, F-16 was selected because of its known dimensions and performance characteristics. Which were taken from references [1], [3], [12], [13], [19], [36], [37], [48], [46], and [64].

Since, F-16 is not an unmanned aircraft some small adjustments were made to approximate the results.

These adjustments:

- The unmanned configuration factor of 0.7 was not used for fuselage length.
- Because F-16 is mainly composed of aluminium structure the fudge factors for composite aircrafts were not used.

In the main program of the optimization, the values of the design variables were appointed through the algorithm, and constants were taken from an input file. Here, the optimization part had not been linked to the aircraft design part yet, thus all inputs were introduced from an input file according to F-16 as shown in the Table 2.19.

Table 2.19 Design Inputs for the F-16 aircraft

Inputs	**F-16**	**UCAV**
SFC [1/h]	0.64	0.64
SFC_c [1/h]	2.06	2.06
$W_{payload}$ [kg]*	1964	1964
Quantity	>3000	3000
b [m]	9.144	9.144
AR	3.0	3.0
Λ_w [deg]	32	32
Λ_{HT} [deg]	40	40
Λ_{VT} [deg]	47.5	47.5
Γ_w [deg]	0	0
Γ_{HT} [deg]	-10	-10
Γ_{VT} [deg]	0	0
BPR	0.87	0.87
λ_{VT}	0.437	0.437
λ_{HT}	0.390	0.390
AR_{VT}	1.294	1.294
AR_{HT}	2.114	2.114

*Represents only missiles

Here, the production quantity for F-16 was found from Table 2.20, Ref. [48]. In the optimization code, this table was also used while deciding on the production "Quantity"; and a reasonable number, 500, is used there.

Table 2.20 Examples of Airplane Program Production Runs [48]

Fighters	
Type	Number produced
Gen.Dyn. F-111	563
Gen.Dyn. F-16	>3000
Gloster Meteor	3545
Gloster Javelin	435
Grumman F9F2-5	1325
Grumman F9F6-8	1985
Grumman F11F	201
Grumman F14	>900
Lockheed F-94	387
Lockheed F-80	1732
Lockheed T-33	5691
Lockheed F-104	2578
McDonnell F-4	>5000
McDD F-15	>2000
McDD F-18	>1500
SAAB JA37	329
SAAB J35A	604

Since, some necessary inputs are not known exactly, the values listed in Table 2.21 are used.

Table 2.21 Assumed Inputs

Assumed Inputs	**F-16**	**UCAV**
l_{Vtco}	unknown	0.30
l_{Htco}	unknown	0.30
V_{VT}	unknown	0.07
V_{HT}	unknown	0.40
Dfmax [m]	varying	1.5
V_{cruise} [km/h]	varying	1460
R_{cr} [km]	varying	750
E_{loiter} [h]	varying	0.5
Airfoil (wing)	NACA 64A204	NACA 64A210
Airfoil (tails)	Biconvex	NACA 64A210

The outputs obtained from the conceptual design program are tabulated in Table 2.22, together with F-16 values.

Table 2.22 Comparison table with F-16

Outputs	**F-16**	**UCAV**
S [m^2]	27.87	27.87
Λ_{LE} [deg]	40	40
λ	0.227	0.202
L_f [m]	15.0	14.9
T [kN]	111.2	112.0
L_{eng} [m]	4.67	4.18
D_{eng} [m]	0.91	0.96
$D_{nosewheel}$ [m]	0.46	0.43
$w_{nosewheel}$ [m]	0.14	0.10
$D_{mainwheel}$ [m]	0.65	0.67
$w_{mainwheel}$ [m]	0.20	0.20
W_e [kg]	8910	6328*
W_f** [kg]	3162	3078
W_{TO} [kg]	14036	11370*
n_{max} [g]	9	9
s_{TO} [m]	457	415*
s_L [m]	914	640*
$W/S)_{TO}$ [N/m^2]	4550	4002*
ROC_{max} [m/s]	254	242
Maximum ceiling [m]	15240	15724
$Range_{combat\ mission}$ [km]	1759	2148*
Maximum endurance [h]	2.42	2.35
V_{max} [km/h], (M_{max})	2175, (2.05)	2183, (2.05)
ω_{max} [deg/s]	13	13
Engine Cost [$]	~ 4.0	4.3
COST [$]	14-18 million	14.6 million

*Due to unmanned structure

** Only the internal fuel capacity

Consequently, the resultant top view of the UCAV was sketched with the prepared Excel sheet and could be checked against the top view of F-16 illustrated in the figures 2.23 and 2.24.

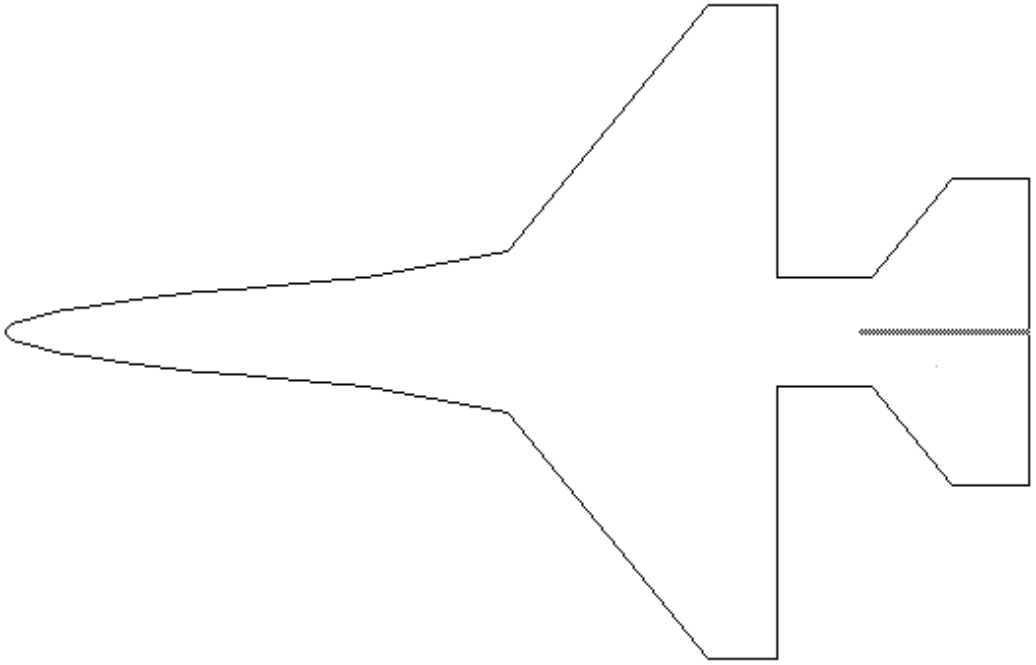

Figure 2.23 Top View of the UCAV

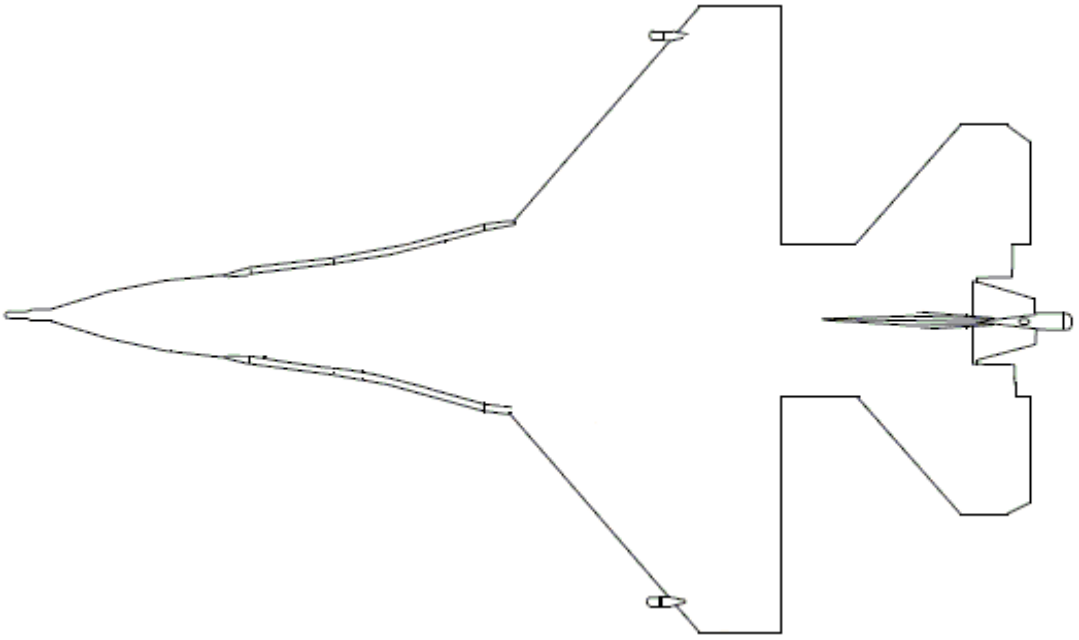

Figure 2.24 Top View of F-16

Before commenting on the results, it should be remembered that the planned mission parameters for a UCAV will normally be different. For example, the cruise segment range and the loiter time could not be found in the literature as well.

Another difference was on airfoils. Since the data for the airfoils of F-16 (NACA 64A204 for the wings and biconvex shape for the tails) were not available, thus NACA 64A210 was used for the UCAV for both the wing and the tails. It was hoped that, this airfoil would approximate the real values.

It may be observed from the table that the design code calculated results are very close to the real values. The main difference is with the empty weight only. Since the systems related to the pilot are not included in the UCAV equations the empty weight was calculated less than that of F-16. Similarly, take off gross weight was found less by the same amount. On the other hand, the performance parameters affected directly by the gross weight were improved accordingly.

The resultant shape of the UCAV approximates the real aircraft quite closely resulting into a similar external shape as F-16. In addition, it should be stated that the UCAV was found statically stable.

In summary, this work shows the design part of the code works well and ready to be integrated to the optimization part.

CHAPTER 3

OPTIMIZATION

Optimization is finding one or more feasible solutions which meet one or more objectives with the constraints. If the number of objective is only one the optimization is named as *single objective optimization*; or else, if the number of objectives are more than one than the optimization is named as *multi objective optimization.*

A multi-objective optimization problem uses a number of objective functions that are to be minimized or maximized. There are a number of constraints, which should be complied with also [54].

The general form of a multi-objective optimization problem is [54]:

Minimize/Maximize $f_m(x), \qquad m = 1,2,.....,M$ (3.1)

Subject to constraint functions

$$g_j(x) \geq 0, \qquad j = 1,2,.....,P \tag{3.2}$$

$$h_k(x) = 0, \qquad k = 1,2,.....,Q \tag{3.3}$$

And the design variables satisfies

$$x_i^L \leq x_i \leq x_i^U, \qquad i = 1,2,.....,N \tag{3.4}$$

In this chapter the optimization technique named Multiple Cooling Multi Objective Simulated Annealing Algorithm [55] was used for single, two and three objective optimizations.

In this thesis it is aimed to prove the applicability of Multiple Cooling Multi Objective Simulated Annealing Algorithm (MC-MOSA) on a supersonic multirole aircraft. The followings are the main items that distinguish this work among other studies, like Ref. [56]:

- aircraft design equations based on supersonic conditions,
- three objective optimization results were obtained,
- besides linear fitness function, elliptic and ellipsoidal fitness functions were also used and compared,
- objective couples were varied, e.g. maximizing both objectives.

As in simulated annealing the cost function is replaced by the energy of the system in MC-MOSA. The specific temperature, T_j, is used while computing the change in the energy of the system. If the energy is reduced then the trial point is accepted. However, the trial point may also be accepted without considering the energy reduction but having the probability of reduction for the next steps.

In MC-MOSA, instead of one fitness function a population of fitness functions are minimized together. Another originality of the algorithm is the assignment of a specific temperature parameter, T_j, to each fitness function, $\widetilde{F}_j$.

The MC-MOSA Algorithm is listed below [55]:

Step 0:

Initializing random number generators.

The initial test point x_0 is set and a high enough temperature T^0 is chosen. The best and next best records of the FFs : $\widetilde{F}^{best} = \widetilde{F}^{nextbest} = 0$

Step 1:

Search direction, θ^K, on the surface of a unit sphere with uniform distribution and step size, λ^K, are assigned randomly.

Setting next variables as $y^K = x^K + \lambda^K \theta^K$

Step 2:

Constructing the (linear) fitness function with added cost due to constraints:

$$\widetilde{F}_m = \sum_i^I w_{mi} \widetilde{f}_i(x) + \Omega_m, \qquad m = 1,.....,M \ , \tag{3.5}$$

$$\sum_i^I w_{mi} = 1 \tag{3.6}$$

Generating $V^K \left(0 \le V^K \le 1\right)$ from uniform distribution

Step 3:

The probability acceptance function is evaluated as

$$P_r = \min\left\{ 1, \max\left[\exp\left(\Delta \widetilde{F}_m^K / T_m^K\right)\right]\right\}, \tag{3.7}$$

$$\Delta \widetilde{F}_m^K = \widetilde{F}_m\left(x^K\right) - \widetilde{F}_m\left(y^K\right) \qquad m = 1,.....,M \tag{3.8}$$

Step 4:

Accept the trial point, y^K, with probability P_r

$$x^{K+1} = \begin{Bmatrix} y^K & if\ V^K \in (0, P_r) \\ x^K & otherwise \end{Bmatrix} \tag{3.9}$$

Step 5:

If $P_r = 1$ (i.e. any improvement in the FF):

Keep the test point, $x^{K+1} = y^K$

Update the next and best records, $\widetilde{F}_m^{\ nextbest} = \widetilde{F}_m^{\ best}$ and $\widetilde{F}_m^{\ best} = \widetilde{F}_m\left(y^K\right)$

Update the related temperature,

$$T_m = 2\left[\widetilde{F}_m\left(x^{K+1}\right) - \widetilde{F}^*{}_m\right] / \chi^2_{1-p}(d) \tag{3.10}$$

Where $\chi^2_{1-p}(d)$ is the 100(1-*p*) percentile point of the chi-square distribution with *d* degrees of freedom,

And $\widetilde{F}^*_m$ is the global minimum of the *m*th FF; estimating $\widetilde{F}^*_m$ as

$$\widetilde{F}^e_m = \widetilde{F}^{best}_m + \frac{\widetilde{F}^{best}_m - \widetilde{F}^{nextbest}_m}{(1-p)^{-d/2} - 1} \tag{3.11}$$

The estimator may also be used with upper and lower bounds in the algorithm as:

$$\widetilde{F}^*_m = \begin{cases} \widetilde{F}^{lower}_m, & if, \widetilde{F}^e_m < \widetilde{F}^{lower}_m \\ \widetilde{F}^{upper}_m, & if, \widetilde{F}^e_m < \widetilde{F}^{upper}_m \\ \widetilde{F}^e_m & otherwise \end{cases} \tag{3.12}$$

Until permitted number of function evaluations reached these steps are repeated beginning with step 2.

In this work, mainly two types of fitness function are used to reach the pareto front. First one is *linear fitness function* which uses weighted sums of objective functions (and constraints with their penalties). Aggregate weight of the objectives should be equal to 1 for each fitness function. The linear fitness function may be represented as tangent lines scanning for optimum points through feasible region. In linear fitness function while searching the points near to pareto front these tangent lines are positioned by the change in the weight of the objective functions mainly.

And the used second fitness function is *elliptic fitness function* (for 2D, and *ellipsoidal fitness function* for 3D) which uses ellipses (or ellipsoids) to find the optimum points, pareto front. A set of ellipses may be placed by uniformly

spreading their centers along a quarter circle [55]. In elliptic fitness function the search route is planned beforehand and the ellipses are perturbed by geometrical parameters on this locus. The number of fitness functions affects the sequence also. The related geometrical parameters and the number of FFs were introduced as a constant in the written code in this work. Then, the aim is to minimize the semi major axes of these ellipses or ellipsoids to reach the pareto front. The equations how these ellipses or ellipsoids are centered and proceeded on a locus are explained in Ref.[55] in detail.

These two types of FFs may be represented by figures 3.1 and 3.2. From these figures, the efficiency of the FFs can be interpreted as: linear FF may be suitable for convex pareto fronts whereas elliptic FF might search both convex and non-convex pareto front.

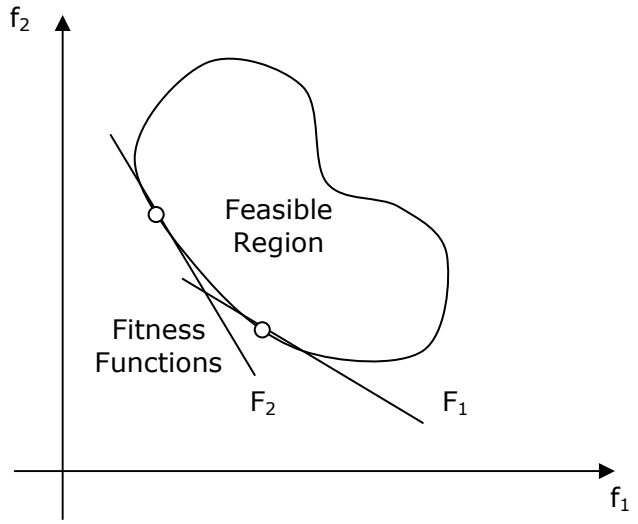

Figure 3.1 Representation of Linear Fitness Function [55]

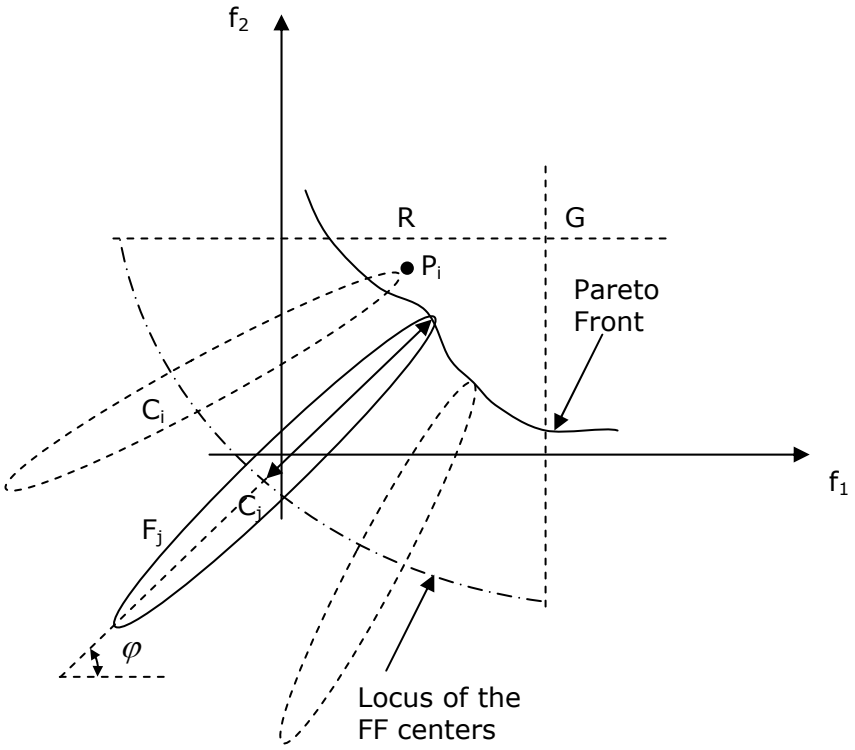

Figure 3.2 Representation of Elliptic Fitness Function [55]

In this work, the selected geometrical properties, which are given as inputs to the code, are stated for 2D and 3D problems below.

- Two objective optimization geometrical inputs:

The number of fitness functions	:	151
The eccentricity	:	0.999
Radius of the arc	:	$\sqrt{2}$
p	:	0.01

- Three objective optimization geometrical inputs:

The number of fitness functions	:	136
First eccentricity	:	0.999
Second eccentricity	:	0.999
Radius of the sphere	:	1.5
p	:	0.01
θ	:	$\pi/2$
φ	:	$\pi/2$
n_θ	:	10
n_φ	:	5

Figure 3.2 includes the locus of the elliptic FF centers for any two objective functions f_1 and f_2 which are aimed to be minimized. So, the third quarter of a circle is used and illustrated above to place the centers of the ellipses.

However, sample 2D optimizations involved in this work are done for three types of objective couples. These types and related centers for the arcs are:

- minimize (f_1) – minimize (f_2)

  Arc center: $(f_1, f_2) = (1,1)$

- maximize (f_1) – minimize (f_2)

  Arc center: $(f_1, f_2) = (0,1)$

- maximize (f_1) – maximize (f_2)

  Arc center: $(f_1, f_2) = (0,0)$

Also, for the sample 3D optimization in this work:

- maximize (f_1) – maximize (f_2) – minimize (f_3)

  Sphere center: $(f_1, f_2, f_3) = (0,0,1)$

Due to that variety, in the written program the arc is centered and turned according to the characteristic of the optimization function. Also, while finding the following ellipse centers the direction of the vector is modified accordingly.

To be sure about the correctness of the multi objective optimization results; at first, single objective optimization code is needed. But the process should begin with deciding on the objectives.

From literature survey it became clear that for an unmanned combat aerial vehicle take-off weight, W_0; total cost, $COST$; required fuel for the complete mission, W_f; maximum cruise velocity, $V_{\max}$; maximum structural load, $n_{\max}$; and maximum combat time, d, are the most important functions to optimize. Therefore, these parameters were selected as the optimization objectives.

At the beginning of the program the user is asked to enter the objectives to optimize. The optimization can be done for single, two or three objectives. These decisions are made by the user between the given objectives as stated in the previous paragraph.

These objectives are normalized with their lower and upper bounds as tabulated in Table 3.1. So that, all the objectives were weighted only due to the characteristic of the fitness functions not the number of digits. Then objectives multiplied by a variable changing from 0 to 1 with 0.1 increments for two objective optimizations while using linear FF. For three objective optimization functions increment again is 0.1 and starting from 0 to 1. However, they are arranged to result in 1.0 when summed.

Table 3.1 Upper and Lower bounds of the objectives

Objectives	**Symbol**	**Lower Value**	**Upper Value**
Take off Gross Weight [kg]	W_0	5000	10000
Acquisition Cost [$]	COST	0	50,000,000
Required Fuel [kg]	W_{fuel}	1000	9000
Maximum Velocity [km/h]	V_{max}	2750	3250
Maximum Structural Load [g]	n_{max}	5	12
Combat time [min]	d	0.7	14

Then, some constants' values are read from an input file, which can be changed easily by the user also. How these constants were selected as explained in Chapter 2 and they are tabulated in Table 3.2:

Table 3.2 Constants' Values in optimizations

Constant	**Symbol**	**Value**
Specific Fuel Consumption	SFC	0.64
By-pass Raito	BPR	0.87
Vertical Tail Volume Ratio	V_{VT}	0.40
Horizontal Tail Volume Ratio	V_{HT}	0.07
Vertical Tail Taper Ratio	λ_{VT}	0.3
Horizontal Tail Taper Ratio	λ_{HT}	0.4
Cruise Velocity [km/h]	V_{cruise}	1460
Vertical Tail Aspect Ratio	AR_{VT}	1.4
Horizontal Tail Aspect Ratio	AR_{HT}	3.4
Dash Range [km]	R_d	0.2
Production quantity	Quantity	500

And some parameters are selected as design variables, which are related with the aircraft geometry and mission characteristics. While optimizing, the values are appointed by the computer randomly in the defined ranges, which are tabulated in Table 3.3.

Table 3.3 Design Variables

Design Variables	**Symbol**	**Initial Value**	**Lower Value**	**Upper Value**
Wing Span [m]	b	10.0	8.0	15.0
Wing Aspect Ratio	AR	3.2	2.0	5.0
Wing Sweep Angle [deg]	Λ_w	32.0	30.0	50.0
Vertical Tail Sweep Angle [deg]	Λ_{VT}	45.0	35.0	55.0
Vertical Tail Moment Arm coefficient	l_{VTco}	0.40	0.40	0.45
Horizontal Tail Moment Arm coefficient	l_{HTco}	0.40	0.40	0.45
Loiter Time [h]	E_{ltr}	0.5	0.1	0.75
Payload Weight [kg]	$W_{payload}$	2000	1000	3000
Wing Dihedral [deg]	Γ_w	0	-5	5
Vertical Tail Dihedral [deg]	Γ_{VT}	0	-5	5
Horizontal Tail Dihedral [deg]	Γ_{HT}	0	-5	5

In order to get the feasible aircrafts at the end, some constraints should be imposed. The selected constraints for this study and their lower – upper values are listed in Table 3.4.

In this work, constraints are added to the FFs multiplying with penalty coefficients. In the Fortran Code these constraints were normalized with their lower and upper limits. Next, penalty coefficients are selected for these constraints. While running the program some constraints incline to stay in the boundaries and some are inclined to exceed their limits. To force this second type of constraints to stay in the limits the penalty coefficients arranged accordingly. Hence, after a number of optimization trials, the penalty coefficients are clarified with their priority and these trial results as shown in Table 3.5.

Table 3.4 Constraints

Constraints	**Symbol**	**Lower Value**	**Upper Value**
Fuselage Length [m]	L_f	5	20
Maximum Structural Load [g]	n_{max}	5	12
Take-off Wing Loading [N/m^2]	$W/S)_{TO}$	2500	7000
Static Margin [%]	Static_margin	-5	+10
Combat Time [min]	d	0.7	14
Take-off Distance [m]	s_{TO}	250	700
Landing Distance [m]	s_L	500	1000
Maximum Ceiling [m]	Maximum_ceiling	10000	20000
Range [km]	RANGE	1500	6500
Maximum Endurance [h]	E_{max}	2	6
Min. Sustained Turn Radius [m]	R_{min}	50	250
Max. Sus. Turn Rate [deg/sec]	ω_{max}	8	28
Control Items Deflection Factor	K_P	0.5	1.0

Table 3.5 Penalty Coefficients

Penalty Coefficients	Value
1	0.1
2	1.0
3	0.1
4	1.0
5	1.0
6	0.1
7	0.1
8	0.1
9	0.1
10	0.1
11	0.1
12	0.1
13	0.1

All of the functions and variables are summarized in Table 3.6 to see the resultant configuration for the optimization part.

Table 3.6 Summarized Decisions

OBJECTIVES	DESIGN VARIABLES	CONSTRAINTS	CONSTANTS
W_0	b	L_f	SFC
COST	AR	n_{max}	BPR
W_f	Λ_w	$W/S)_{TO}$	V_{HT}
V_{max}	Λ_{VT}	Static_margin	V_{VT}
n_{max}	l_{VTco}	s_{TO}	λ_{VT}
d	l_{HTco}	s_L	λ_{HT}
	E_{ltr}	Maximum_ceiling	V_{cruise}
	Wpayload	RANGE	AR_{VT}
	Γ_w	E_{max}	AR_{HT}
	Γ_{HT}	R_{min}	R_d
	Γ_{VT}	ω_{max}	Quantity
		K_P	

After settling the objectives, design variables, constants, constraints and penalty coefficients, as a next step the optimization loop was constructed. The optimization technique is described more in detail in Ref.[54,55].

The optimization code covers the aircraft design algorithm. Design variables are changed for each aircraft design. These design variables are selected by purely random walk as the single objective simulated annealing optimization algorithm Hide-and-Seek. And totally 5000 meaningful design variable combinations applied to aircraft design for linear and elliptic FF, other combinations which are not between the specified bounds are rejected before beginning the design. After reaching the number of iterations, selected aircraft designs by the optimization part are written to output files. With this output files:

- The obtained solutions for two and three objective optimizations are plotted.
- An excel sheet is prepared to sketch the outside geometry (top and side view) of the optimized vehicle configurations.

The flowchart of the design optimization code is illustrated below.

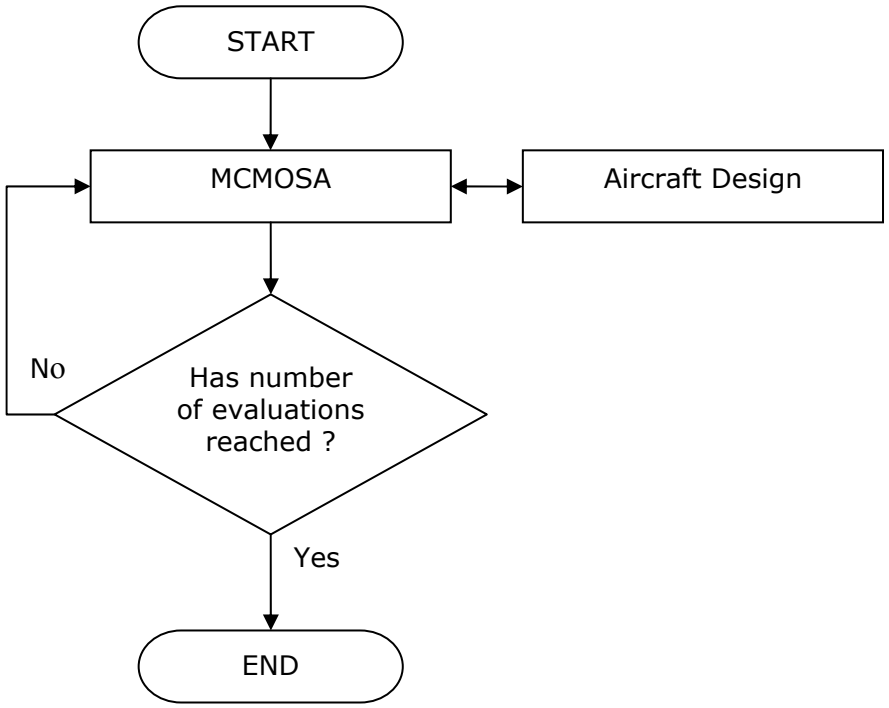

Figure 3.3 Optimization-Aircraft Design Combination Flow Chart

Using the code developed single and multiobjective optimizations are carried out. The case studies are given in the next section.

3.1 Single Objective Optimization

The UCAV has been decided to have six objectives as mentioned before: take-off weight, W_0; total cost, $COST$; required fuel for the complete mission, W_f; maximum cruise velocity, $V_{\max}$; maximum structural load, $n_{\max}$; and maximum combat time, d. The Fortran code was run for each of these objectives, and the optimized objectives and design variables are given in Table 3.7 and Table 3.8.

Table 3.7 Single-objective optimization (optimized Design Variables)

Design Variables	OBJECTIVES					
	Minimize W_0	Minimize COST	Minimize W_{fuel}	Maximize V_{max}	Maximize n_{max}	Maximize d
b [m]	8.32	8.05	9.01	8.26	8.95	15.00
AR	3.85	3.49	5.00	3.56	4.27	3.71
$\Lambda_{C/4}$ [deg]	31.6	30.1	30.0	48.6	44.0	33.3
Λ_{VT} [deg]	50.7	44.8	54.7	51.9	35.5	51.5
l_{VTco}	0.43	0.42	0.42	0.41	0.43	0.40
l_{HTco}	0.45	0.40	0.42	0.45	0.42	0.45
E_{loiter} [hour]	0.7	0.4	0.1	0.2	0.2	0.2
$W_{payload}$ [kg]	1074	1001	2131	2869	1097	1000
Γ_w [deg]	-1.6	-3.2	0.1	0.3	2.0	2.3
Γ_{HT} [deg]	-4.7	2.2	-4.9	-4.3	-4.3	3.1
Γ_{VT} [deg]	-2.5	0.5	0.6	1.2	1.1	-1.2

Table 3.8 Single-objective optimization (values of the objectives and other parameters of the designs)

Results	OBJECTIVES					
	Minimize W_0	Minimize COST	Minimize W_{fuel}	Maximize V_{max}	Maximize n_{max}	Maximize d
W_0 [kg]	**5518**	5557	6857	9550	5991	19666
COST [$]	16,487,892	**16,277,355**	20,916,240	28,412,756	18,127,982	48,700,452
W_{fuel} [kg]	1404	1535	**1053**	1717	1495	8914
V_{max} [km/h]	2810	2767	3076	**3223**	2831	2902
n_{max} [g]	11.87	11.29	11.99	11.95	**12.00**	6.49
d [min]	1.7	2.2	0.7	0.7	2.1	**14.0**
D_{fmax} [m]	0.80	0.80	0.91	1.07	0.83	1.48
Λ_{LE} [deg]	38.2	37.4	35.2	53.7	48.9	40.0
λ	0.205	0.215	0.216	0.103	0.127	0.193
$L/D)_{max}$	20.5	19.2	24.8	19.9	22.1	20.0
L_f [m]	7.80	7.83	8.48	9.66	8.06	12.85
T [kN]	60	60	79	116	66	230
L_{eng} [m]	3.34	3.33	3.81	4.51	3.47	5.87
D_{eng} [m]	0.70	0.70	0.81	0.97	0.73	1.38
h_{VT} [m]	2.10	2.12	2.00	1.98	2.19	4.15
b_{HT} [m]	4.15	4.57	3.55	4.14	4.35	8.15
$D_{nosewheel}$ [m]	0.34	0.34	0.36	0.40	0.35	0.50
$w_{nosewheel}$ [m]	0.07	0.07	0.08	0.09	0.07	0.12
$D_{mainwheel}$ [m]	0.54	0.54	0.57	0.64	0.55	0.79
$w_{mainwheel}$ [m]	0.14	0.14	0.15	0.18	0.14	0.25
$C_{D0\ total}$	0.0211	0.0209	0.0326	0.0350	0.0224	0.0182
C_{D0c}	0.0156	0.0155	0.0190	0.0215	0.0161	0.0165
K	0.215	0.221	0.215	0.164	0.177	0.211
e	0.85	0.88	0.77	0.71	0.71	0.84
Stability	stable	stable	stable	stable	stable	stable
W_e [kg]	3040	3021	3673	4965	3400	9752
K_p	0.90	0.89	0.87	0.74	0.85	0.42
s_{TO} [m]	282	273	358	527	344	283
s_L [m]	521	495	727	1022	612	458
$W/S)_{TO}$ [N/m^2]	3012	2943	4140	4885	3129	3188
ROC_{max} [m/s]	306	291	300	411	293	312
Maximum_ceiling[m]	17820	17687	17571	18358	18387	18149
RANGE [km]	2553	2470	1817	2357	2298	3180
E_{max} [hour]	2.97	2.89	2.06	2.69	2.78	3.53
R_{min} [m]	87	94	87	73	81	124
ω_{max} [deg]	17	17	16	16	17	15
$R_{min.pull\text{-}up}$ [m]	705	685	840	1203	874	704
$\omega_{max.pull\text{-}up}$ [deg]	12	12	11	9	11	10
$R_{min.pull\text{-}down}$ [m]	648	627	773	1106	804	603
$\omega_{max.pull\text{-}down}$ [deg]	13	13	12	10	12	12
xx	5	6	2	2	6	34

In Table 3.7 each column shows the attained values of the design variables for the selected objective runs.

In Table 3.8 each column shows the resultant values of the objectives and other calculated parameters related to the optimization. The attained objectives are printed bold.

For example, first column gives the results from minimizing the take off gross weight, W_0. The objective value attained under the imposed constraints listed in Table 3.2 is 5518 kg.

While minimizing the take off gross weight (W_0) the fuel weight (W_{fuel}) is also reduced causing reduction in the range (*RANGE*), endurance (E_{max}), combat time (d), and number of combat turns (xx). Although, these parameters approached to their lower values, they were not reduced to the levels attained in the minimizing W_{fuel} case, because W_0 is not as sensitive as W_{fuel} against these parameters. Besides, the cost for minimum W_0 was also reduced but not as much as in the minimizing *COST* case. Rather, the take off gross weight (W_0) is very sensitive to dimensional variables like $D_{nosewheel}$, $D_{mainwheel}$, $w_{nosewheel}$, $w_{mainwheel}$, D_{fmax}, L_f, L_{eng}, D_{eng}, b and b_{HT}, which build up empty weight (W_e) of the aircraft. While reducing W_0, these variables also decrease to their lower bounds.

Then, the resultant dimensions were entered on the prepared excel sheet, and figures 3.4 and 3.5 are obtained for each objective.

Note that, airplane shapes plotted in the figures all have the same scale. From these figures it may be observed that the minimization of the take-off gross weight (W_0) results in the smallest dimensions or the smallest configuration compared with others.

For the second objective, the acquisition cost (*COST*) is minimized. *COST* is very sensitive to V_{max}; as a result thrust (T) reaches the lowest value to reduce the maximum velocity so that the cost (*COST*). Then, V_{max} and T took their lowest values at this configuration. As in the minimizing W_0 case the dimensions were also reduced. Then, W_e and $W_{payload}$ were also reduced. The resultant shape looks

like a conventional airplane which is for reducing suchlike manufacturing hours (H_M), engineering hours (H_E), manufacturing materials cost ($Cost_M$) and so the cost (*COST*).

For the third objective, the fuel (W_{fuel}) is minimized. Consequently, the combat time (*d*), *RANGE*, number of combat turns (*xx*), loiter time (E_{loiter}) and the maximum endurance (E_{max}) were reduced to their lowest limits by the algorithm as expected. So that, the other dimensions and as well as the wing area are also reduced.

The fourth objective was to maximize the maximum velocity (V_{max}). It can be observed that rate of climb (ROC_{max}) is also increased. Also, the sweep angles for the wing and tail (Λ_{LE}, Λ_{VT}, Λ_{HT}) and wing loading $(W/S)_{TO}$) took higher values, because V_{max} is very sensitive to these variables mutually. However, drag-due-to-lift-factor (*K*) was reduced as expected. The thrust and engine dimensions increased to catch the highest value for the maximum velocity. The shape of the aircraft resembles to a flying wing configuration, which is distinguishing from other views. On the other hand, cost is also increased due to the direct relation between maximum velocity and cost.

The fifth single-objective case presented is to maximize the structural load (n_{max}). The permitted structural load was limited to 12g. In this study a simple structural model is prepared, however the structural analysis is a big issue which should be considered in detailed and this is not the main subject matter for this study for the present. A more detailed analysis shall be added in the future work. From gained results, maximum lift to drag ratio $L/D)_{max}$ was found as increased while the total and combat drag coefficients were reduced. Examining the top view of the optimized aircraft for structural load it is observed that the leading edge sweep angle (Λ_{LE}) and aspect ratio (*AR*) were high and horizontal tail moment arm coefficient (l_{HTco}) was reduced so that the wing and the horizontal tail are joined together. As well as the vertical tail sweep angle (Λ_{VT}) almost reduced to it lowest value. The size of the aircraft seems small and the shape gives the impression of a highly maneuverable aircraft.

The sixth single-objective case was the maximization of the combat time (d). As expected, to increase the combat time the size of the aircraft increases to carry more fuel. So that the empty weight and the total fuel consumed were increased. Thus, the wing area increases as well as the area of the tail surfaces, because these tail areas are related to the area (S), mean chord length ($\bar{c}$) and span of the wing (b) according to the formulations given in Ref. [46]. A commend may be made as that, the tail moment arm coefficients could be selected as constants in stead of being design variables to obtain a more reasonable tail shape especially for this kind of large configurations; or could be limited to change with in a narrower range. In addition, the increase in weight (W_0) also increases the thrust (T) because of direct relation set. As a result engine dimensions were also increased. By the way, the number of combat turns was also so high. However, the maximum structural load and K_p were reduced for this heavy configuration. To reduce the required fuel for other segments the payload was pulled to its lowest limit and so the drag due to these payloads are also minimized.

In summary, from the top and side views it can be interpreted as that, if the objective is to minimize the take gross weight (W_0), cost ($COST$) or the required fuel (W_{fuel}), the aircraft is small and has a conventional shape.

Conversely, while optimizing the combat time (d), the sweep angle (Λ_{LE}) and the volume of the wing are increased to store more fuel to have high number of combat turns (xx).

When the objective is to increase the maximum velocity and the maximum structural load, the distance between the wing and the tails is decreased; so the optimized aircraft shape resembled more to a flying wing. Remembering that, the moment arms were changing with the limited moment arm coefficients, which were selected as design variables; a comment may be made as if these design variables' limits are extended the aircraft shape may be very much similar to a flying wing.

Optimizing an UCAV for just one objective results in losing the control over other important objectives. To defeat this problem, multi-objective optimization should

be used to be able to reach a trade off between more than one objective. This issue is examined in the next section.

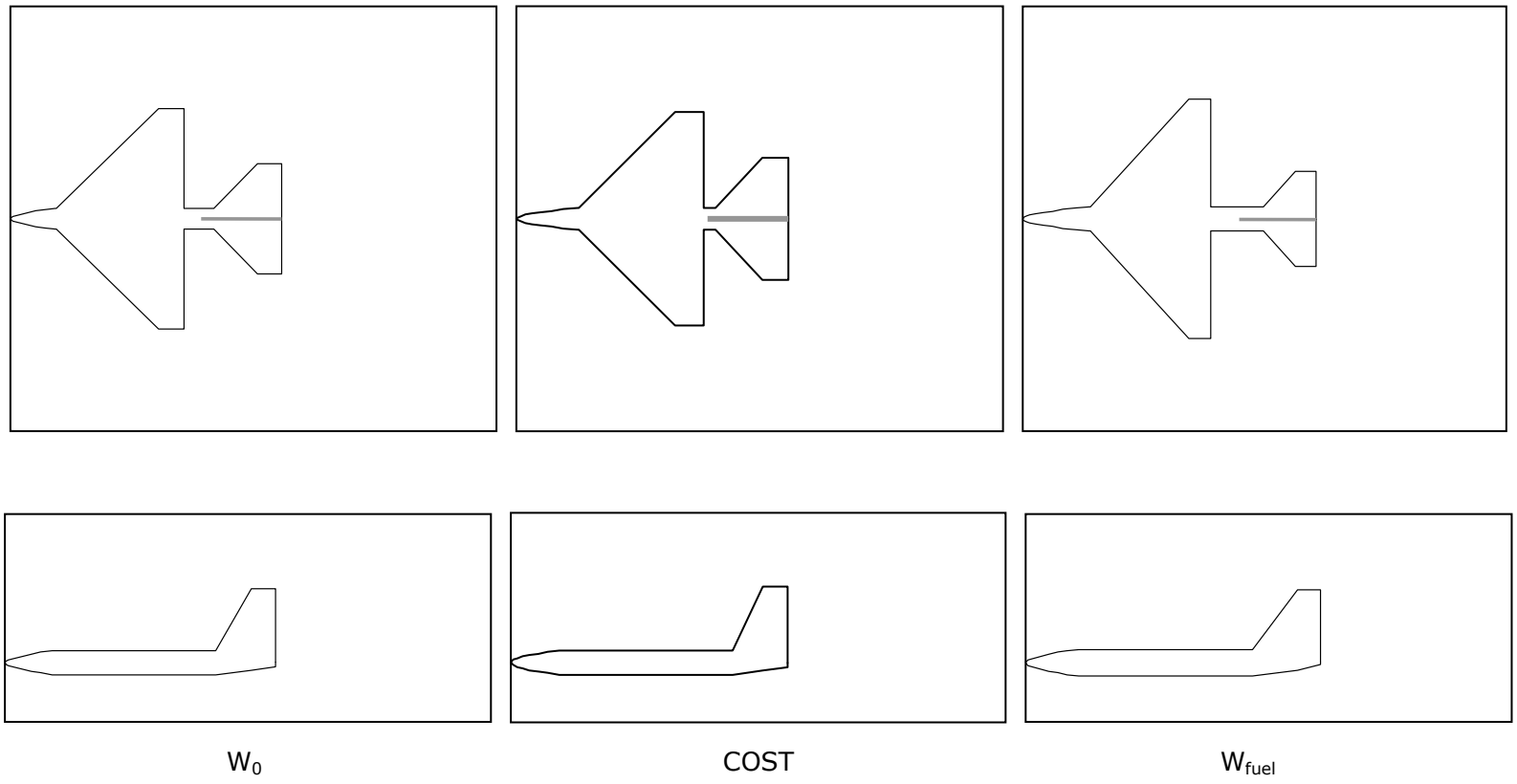

Figure 3.4 Single-objective optimization results for minimizing W_0 , COST and W_{fuel}

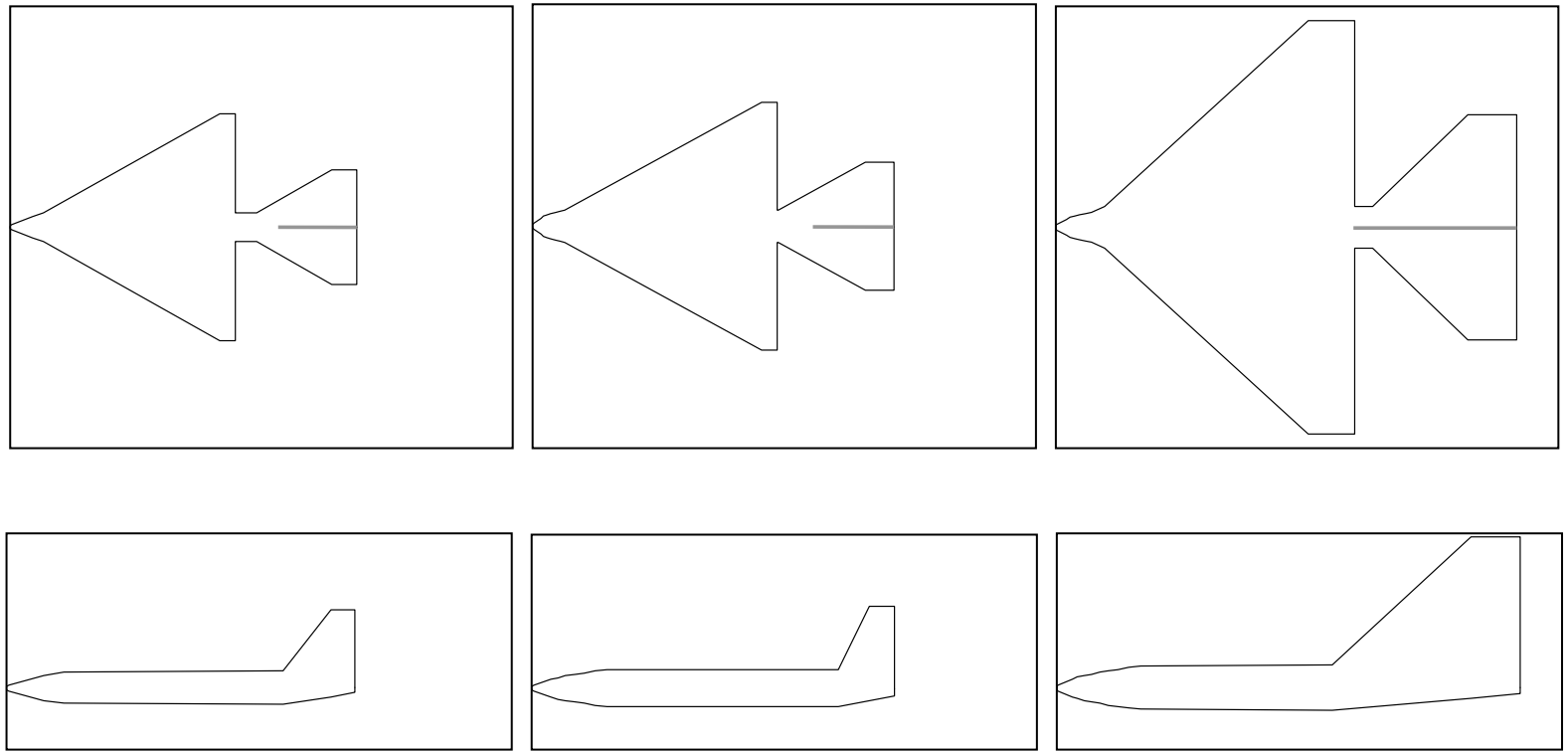

V_{max} n_{max} d

Figure 3.5 Single-objective optimization results for maximizing V_{max} , n_{max} and d

3.2 Two Objective Optimization

In this section two objective design studies are presented. The objective pairs are selected to conflict with each other. In this vein, the following combinations are chosen:

- Minimize W_0 – Maximize V_{max}
- Minimize COST – Maximize V_{max}
- Minimize W_f – Maximize d
- Maximize V_{max} – Maximize d
- Minimize COST – Maximize d

For each objective set, two types of fitness functions were employed. First set of results and charts were obtained using Linear Fitness Function; and the second set of results and charts were obtained using Elliptic Fitness Functions. In addition, fronts were obtained by selecting non-dominated points. The third charts include only these points which compose the fronts.

While using Linear Fitness Functions in the program, each iteration is done for one design variable set. And each fitness functions is calculated using a separate weight set combination. These weight couples are directly introduced in the linear fitness function used in MCMOSA algorithm. In a loop the weights are changed for the next step to build up next fitness function. The changing weight sets can be summarized in Table 3.9. These weight sets were only used with linear fitness functions, for elliptic fitness functions there is no need.

For two-objective optimization with Linear Fitness Functions, 5000 iterations and 11 FFs were employed for each objective set. Each optimization process took about 8 minutes. On the other hand 5000 iterations and 151 FFs were used for Elliptic Fitness Function optimization runs. And each optimization process took about 10 minutes at most. However the durations might be strongly affected by the complexity of the aircraft design part and so the iterations in itself.

Table 3.9 Weight sets for Linear Fitness Function

Weight Sets	Weight 1	Weight 2
1	0.0	1.0
2	0.1	0.9
3	0.2	0.8
4	0.3	0.7
5	0.4	0.6
6	0.5	0.5
7	0.6	0.4
8	0.7	0.3
9	0.8	0.2
10	0.9	0.1
11	1.0	0.0

First two-objective optimization is carried out to minimize take-off gross weight while maximizing the maximum velocity of the aircraft. Results are shown in Figure 3.6. Remembering also that, the take-off gross weight (W_0) conflicts with the maximum velocity (V_{max}); because the maximum velocity is influenced by the thrust and thrust is related to take-off gross weight directly. So, the result was expected to have the shape of a lower right quarter-circle.
From the mutual chart of linear and elliptic fitness functions non-dominated points shows that linear fitness function exhibit good performance for convex parts; but elliptic FF dominates linear one through out the limits. And also, the number of points on the front is fairly high. Though, it is stipulated that elliptic FF converges to the real front more than the linear FF for this objective couple.

The second objective couple was maximizing maximum velocity (V_{max}) while minimizing the cost (*COST*): the fastest but cheaper UCAV. Since in the design model the acquisition cost directly and strongly imposed by the maximum velocity; these two objectives are conflicting. The linear FF approximated the Pareto front with well spread solutions as shown on the first chart of Figure 3.7.

Whereas, elliptic FF performed much more better and formed a front which is closer to the Pareto front.

The third two-objective optimization run was for minimizing required fuel for the complete mission (W_{fuel}) while maximizing the combat time (d). The results are shown on Figure 3.8. These two objectives are directly related with each other. Indeed, while maximizing the combat time the required fuel also tends to increase: highly conflicting couple. Thus, the actual Pareto front should have the shape of a forth quarter circle. From the related charts, the elliptic FF dominated the linear FF by scanning the whole front laying between the limit values of the objectives. The linear FF seems worked poor for these coupled objectives spreading to a small area. Anyway, the elliptic FF performed much better than the linear FF. Again elliptic FF is performed better in approaching to the actual front.

The fourth objective couple is to maximize the maximum velocity (V_{max}) and combat time (d). The purpose was to obtain the Pareto front of maximizing both maximum velocity and combat time. This problem is original for this work from other research [56]. The obtained front should resemble the first quarter circle. These two objectives do not affect each other, directly; whilst, they use the same parameters which result in indirect effect. From Figure 3.9 it is seen that linear FF again tend to find points on a convex front, because of that it converged in a small area. However, the couple formed on an almost straight and non-convex line. Hence, elliptic FF is very successful to catch non-dominated and well spread points closer to the actual Pareto front throughout the limits. Again, the linear FF tends to find a convex shape so the front directed to find points on this kind of curve. On the other hand elliptic FF succeeded to find points on concave parts and also continue to search for further solutions.

Figure 3.10 shows the results of two-objective optimization for maximizing combat time (d) while minimizing the acquisition cost ($COST$): searching for the cheaper UCAVs which have higher combat duration. In the design model, no direct relation exists between these objectives. The front of elliptic FF is well populated except a few small intervals. Though, these intervals were dominated by the found neighbouring non-dominated points by the elliptic FF.

From the presented two-objective combinations, the applicability of the MC-MOSA algorithm and the effectiveness of it with two kinds of fitness functions can be summarized as the obvious superiority of the elliptic FF over the linear FF with this algorithm. It caught the well populated and spread points between the desired bounds. Moreover, elliptic FF's results were observed to be closer to the results of single-objective runs gained separately, which also proves the high performance of elliptic FF while approaching the actual Pareto front.

For the combinations which tend to have highly convex parts throughout the front, linear FF can be used with elliptic FF to get the benefit from both [55]. Since, for highly convex fronts or zones the linear FF can be interpreted as performing well inherently.

The figures in the following pages are the mentioned results for two objective optimizations.

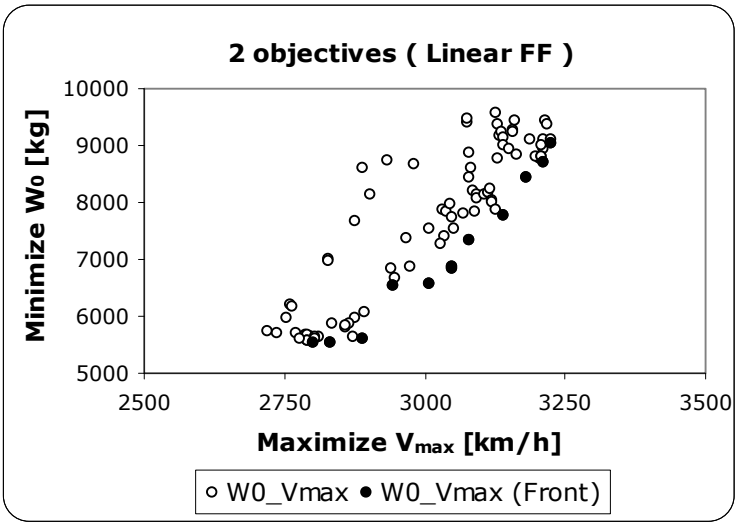

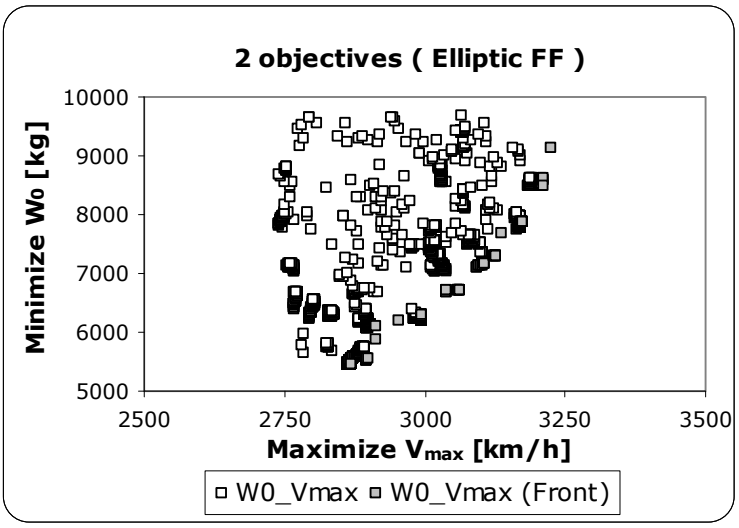

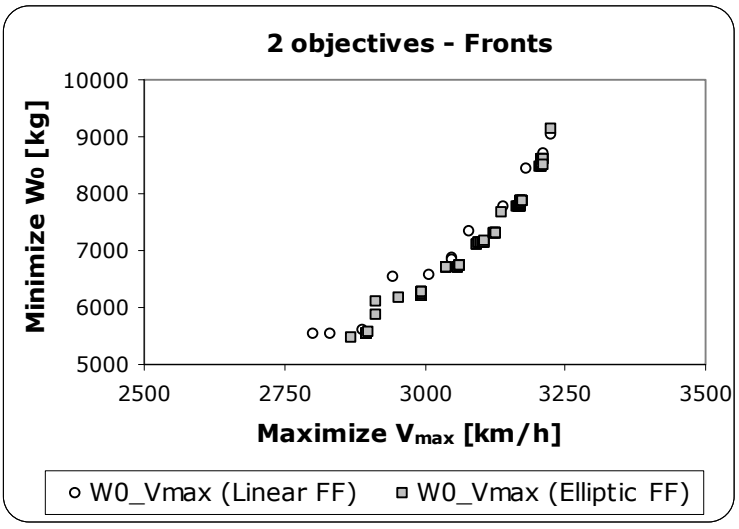

Figure 3.6 Double-objective (W_0 and V_{max}) optimization results

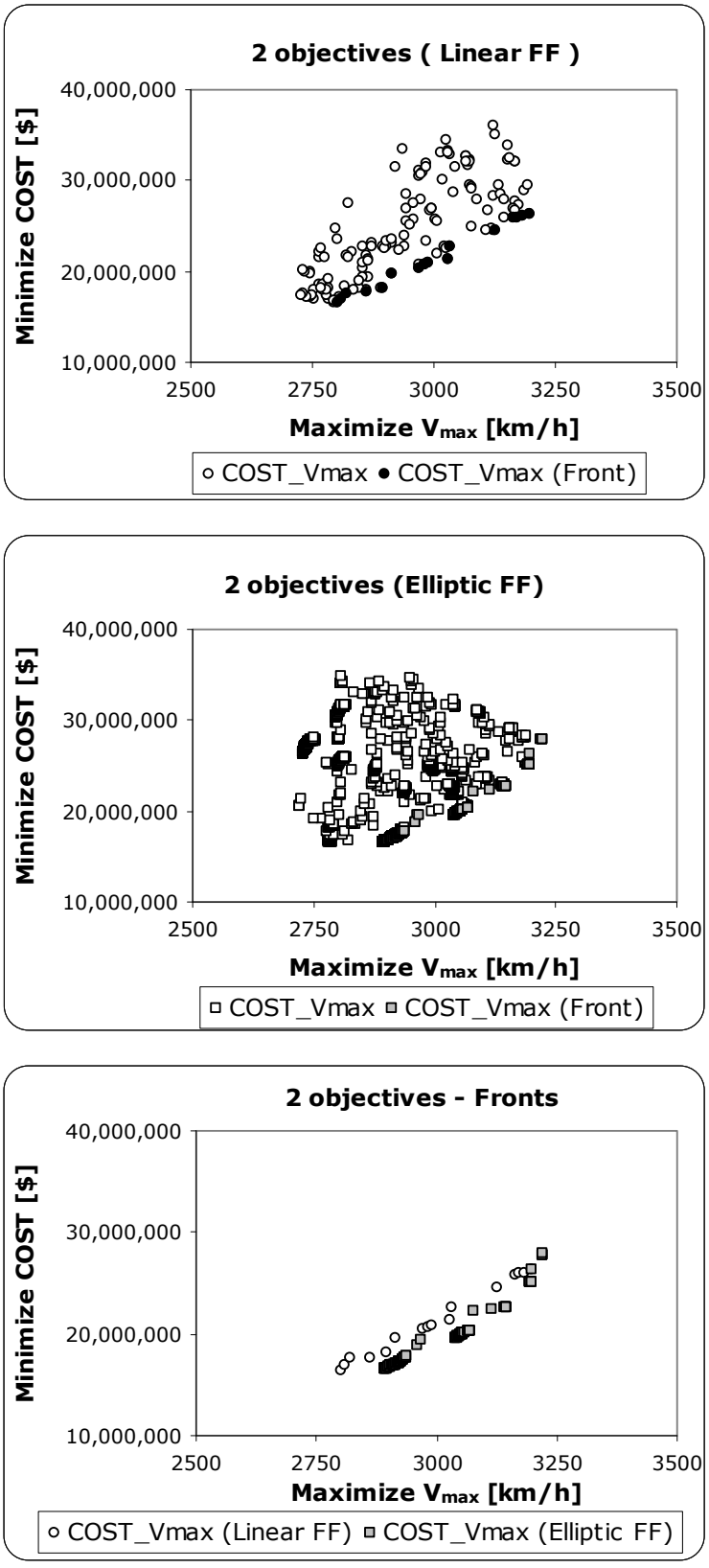

Figure 3.7 Double-objective (COST and V_{max}) optimization results

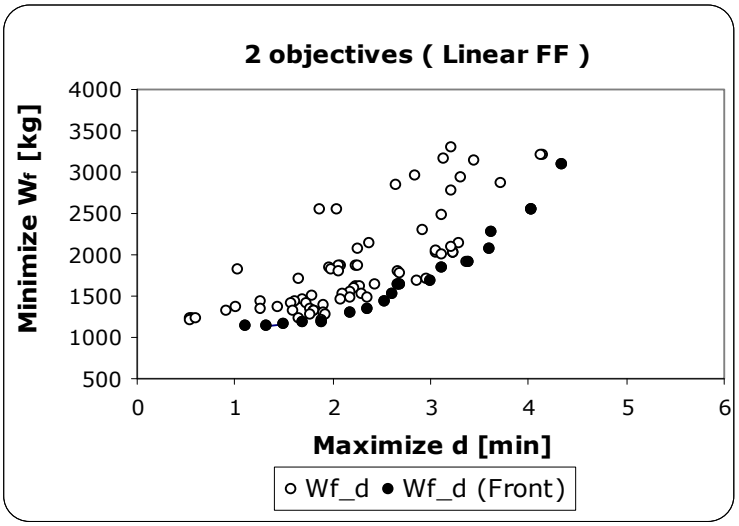

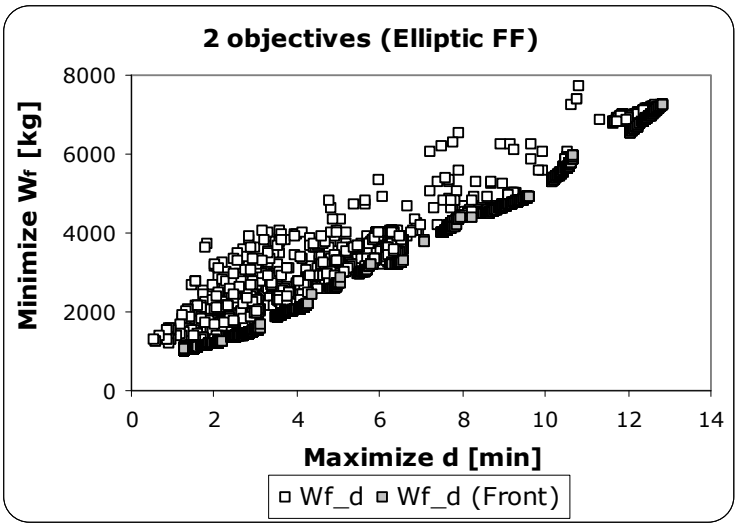

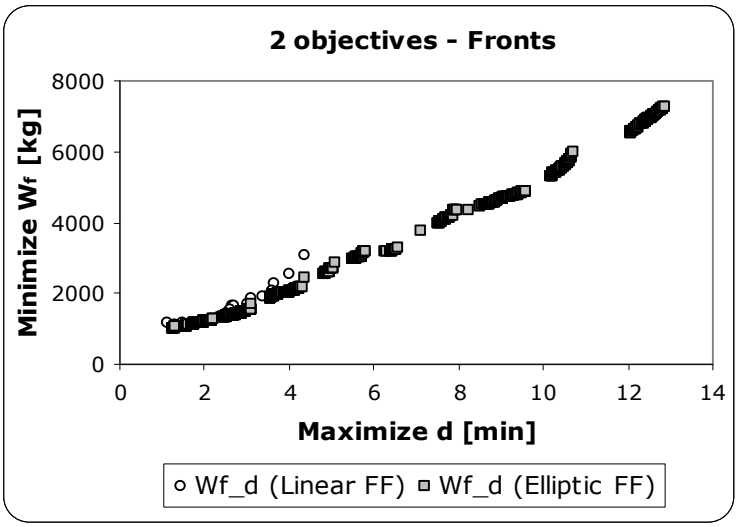

Figure 3.8 Double-objective (W_f and d) optimization results

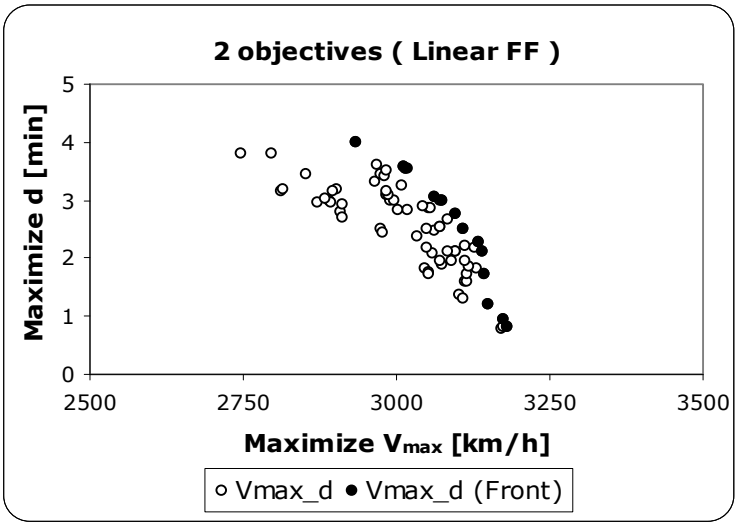

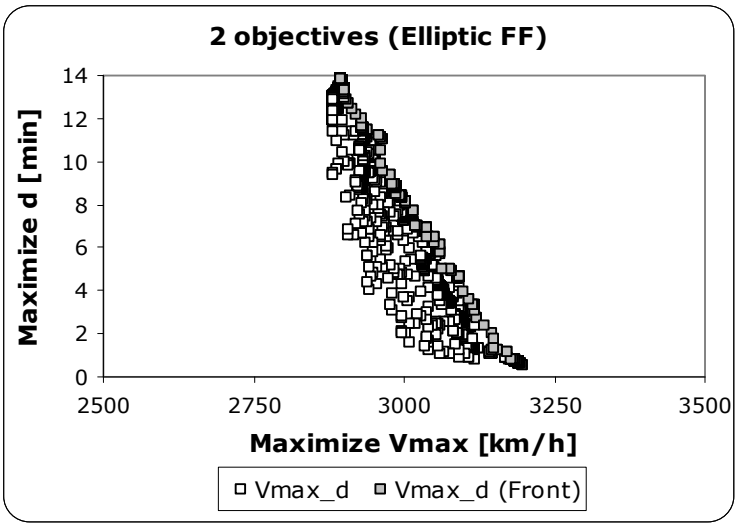

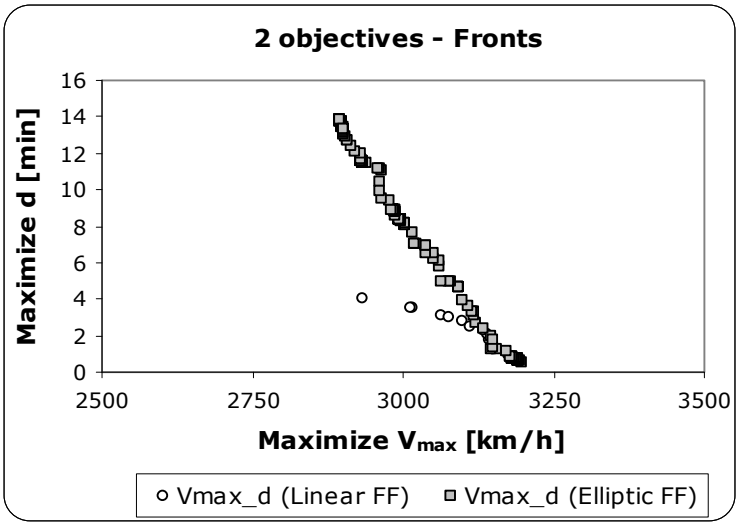

Figure 3.9 Double-objective (V_{max} and d) optimization results

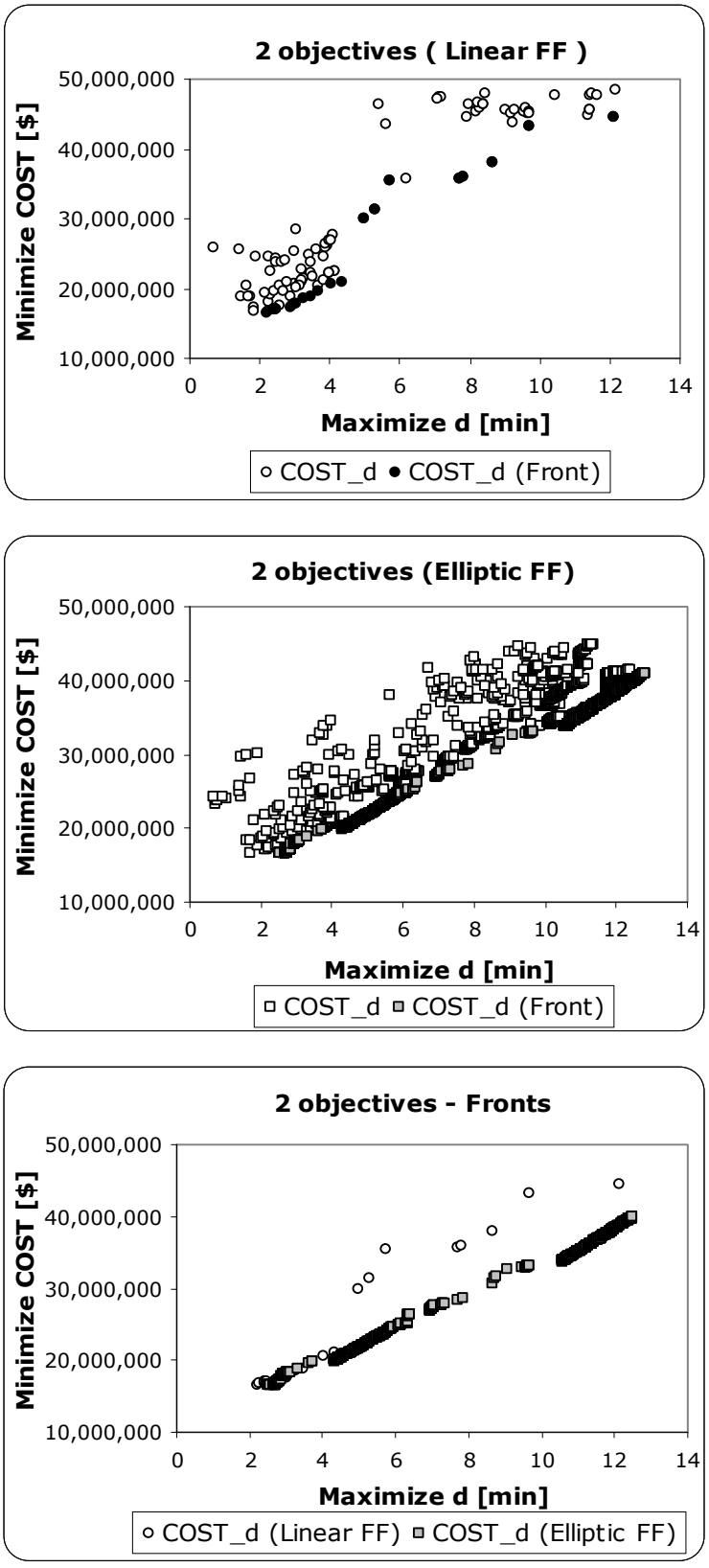

Figure 3.10 Double-objective (COST and d) optimization results

3.3 Three Objective Optimization

To observe the applicability of the MC-MOSA algorithm in three dimensional space, three conflicting objectives were chosen as: maximize acquisition cost (*COST*), maximize maximum velocity (V_{max}) and maximize combat time (*d*). In other words, to obtain cheaper UCAVs which have higher maximum velocity and combat duration. Two types of fitness functions were employed to this 3D-optimizaiton.
While attaining three-objective optimization with Linear Fitness Functions, 5000 iterations and 121 FFs were employed, duration was 6.5 minutes; whereas 5000 iterations and with 136 Ellipsoidal Fitness Functions duration of the run was 8 minutes.

The front was expected to have the shape of the surface of an eight of a sphere. To ease the readability of this 3D front, 2D views are also included as top and two side views. Afterwards, 3D view was supplemented. First four views are the results of linear fitness functions and the following five views are the results of ellipsoidal fitness function (3D version for elliptic fitness function). And the last figure of this section was the mutual chart of front with the linear and ellipsoidal FFs' results together.

Figure 3.11 represents 2D views of linear FF result for COST_V_{max}_d optimization. Further, Figure 3.12 exhibited 3D view of this optimization run. The front is almost uniformly separated but not extending until the bounds. The surface is highly convex.

Figure 3.13 and 3.14 represent elliptic FF result for this three objective optimization. The resultant points are highly separated between the upper and lower limits of the objectives. The shape is not purely convex, there are points which can only be reached on a non-convex surface.

From the mutual figure, Figure 3.15, the efficiency of the elliptic FF can be seen more clearly. Whereas the linear FF's points converged to a narrow area at the lower left, the elliptic FF scanned the other areas and found non-dominated points which are closer to the actual Pareto front. Indeed, it can be said that

elliptic FF's results highly dominate the results of linear FF in 3D environment, also.

The success of elliptic FF in three-objective optimization environment is mainly due to the sensitivity of the ellipsoidal FF. The number of non-dominated points can be increased by increasing the FF's points. The increase in the number of iterations would also result in an increase of non-dominated points as well as shifting the front closer to the actual Pareto front. By the way, this will also increase the run time [55].

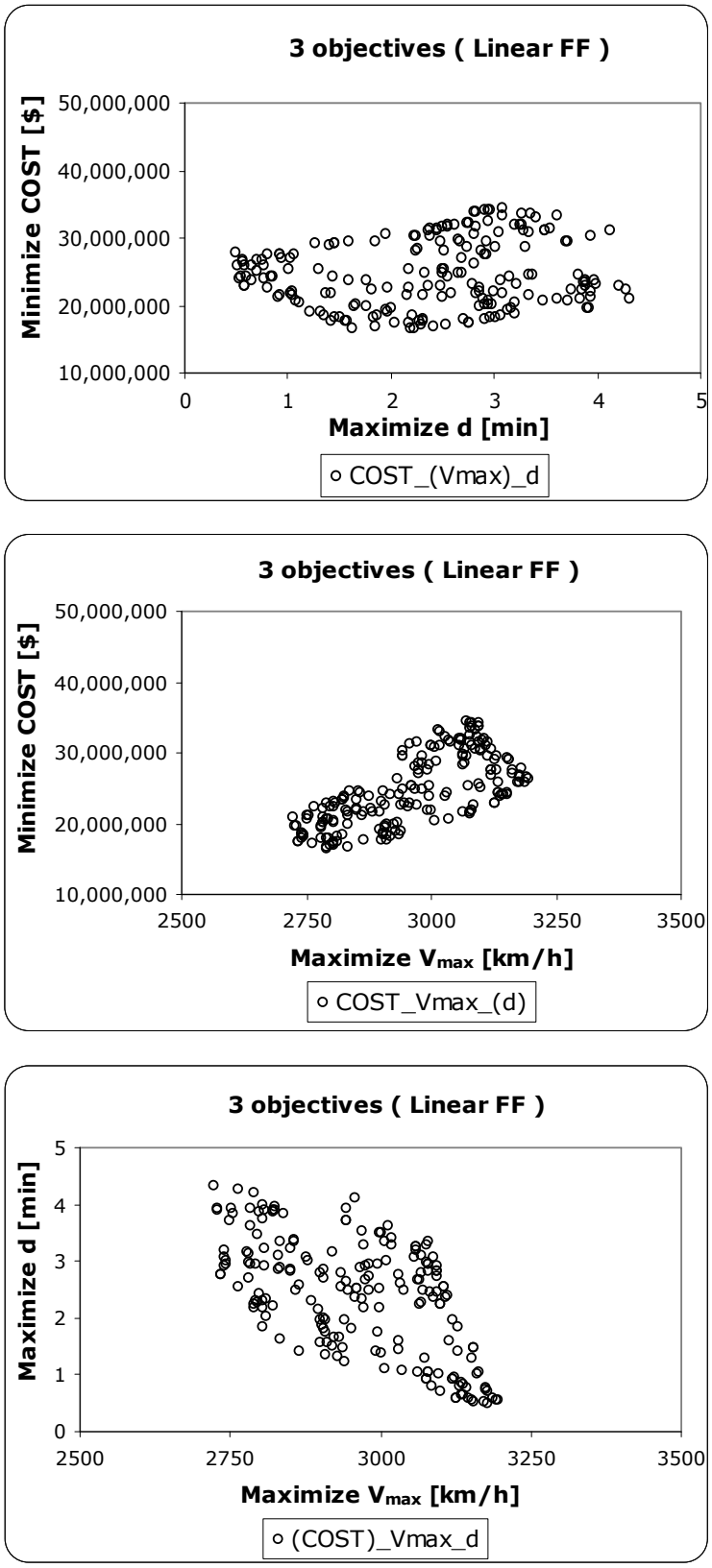

Figure 3.11 Triple-objective optimization results (2D, Linear FF)

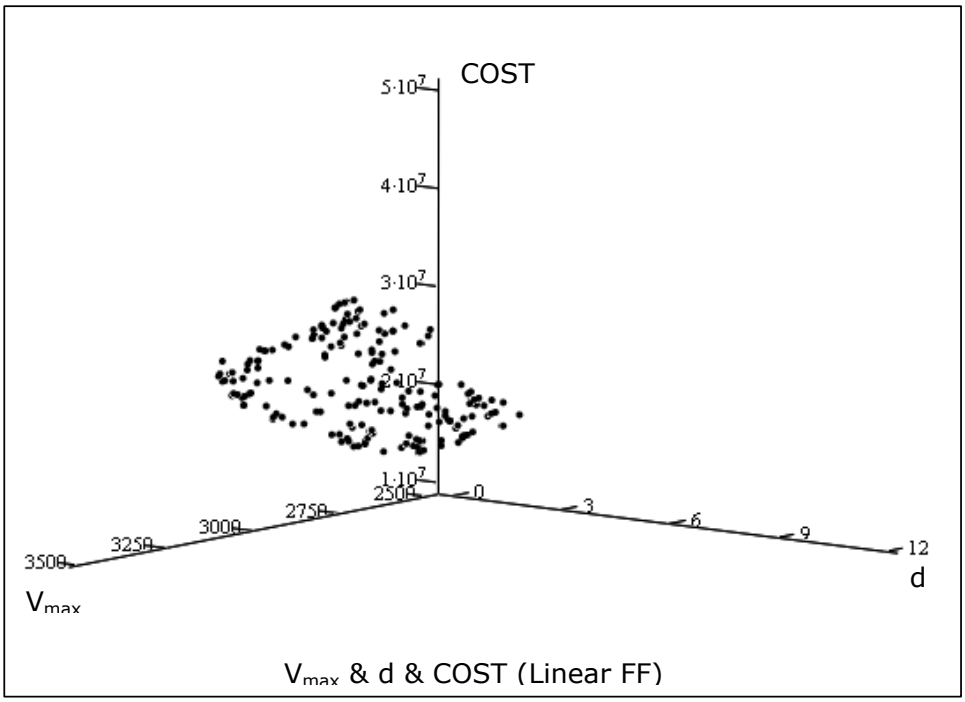

Figure 3.12 Triple-objective optimization results (3D, Linear FF)

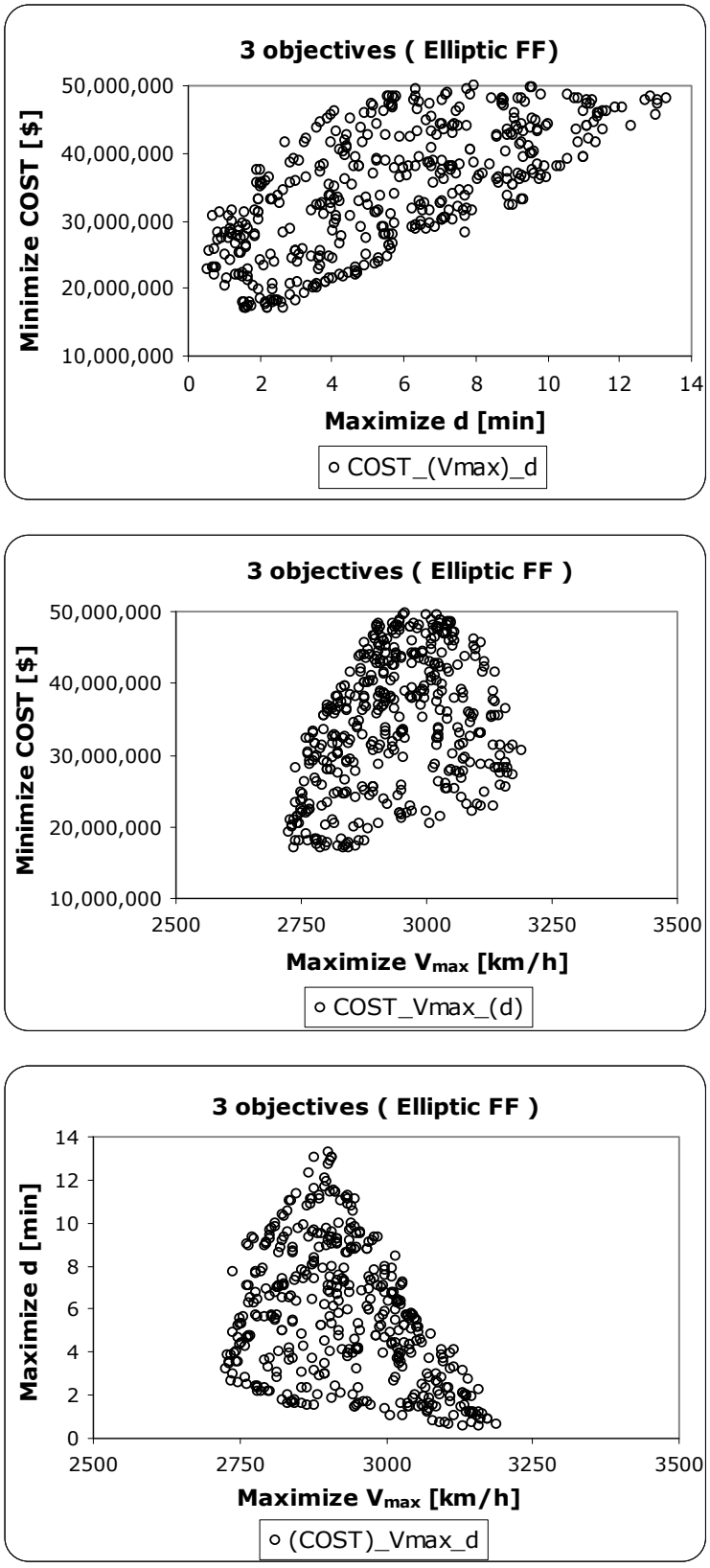

Figure 3.13 Triple-objective optimization results (2D, Elliptic FF)

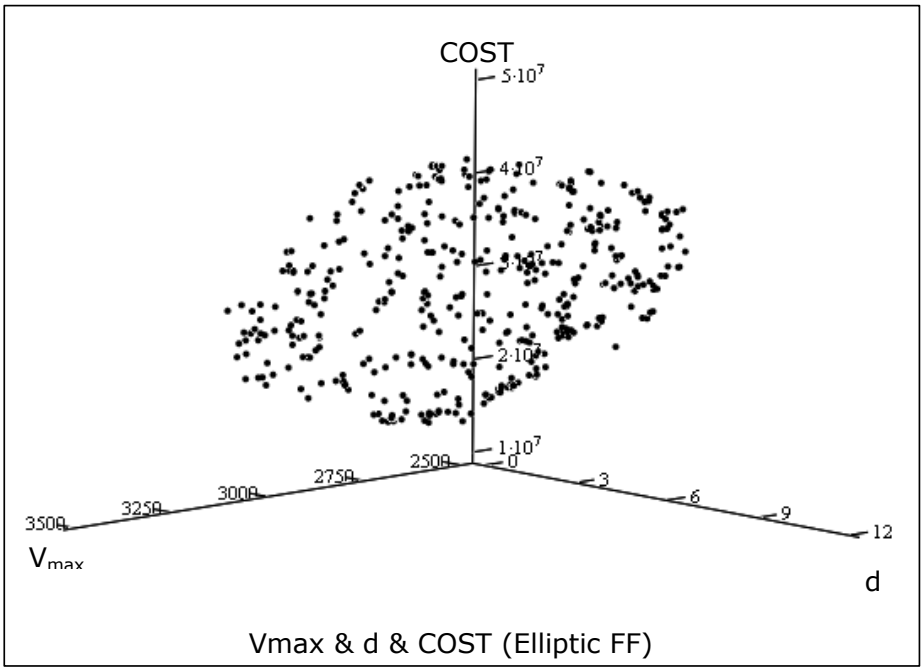

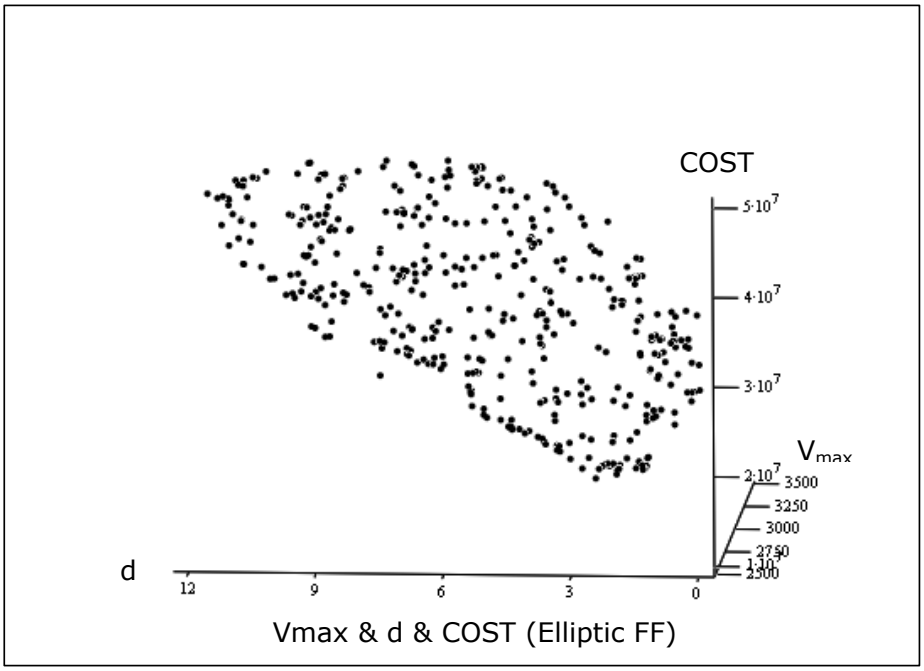

Figure 3.14 Triple-objective optimization results (3D, Elliptic FF)

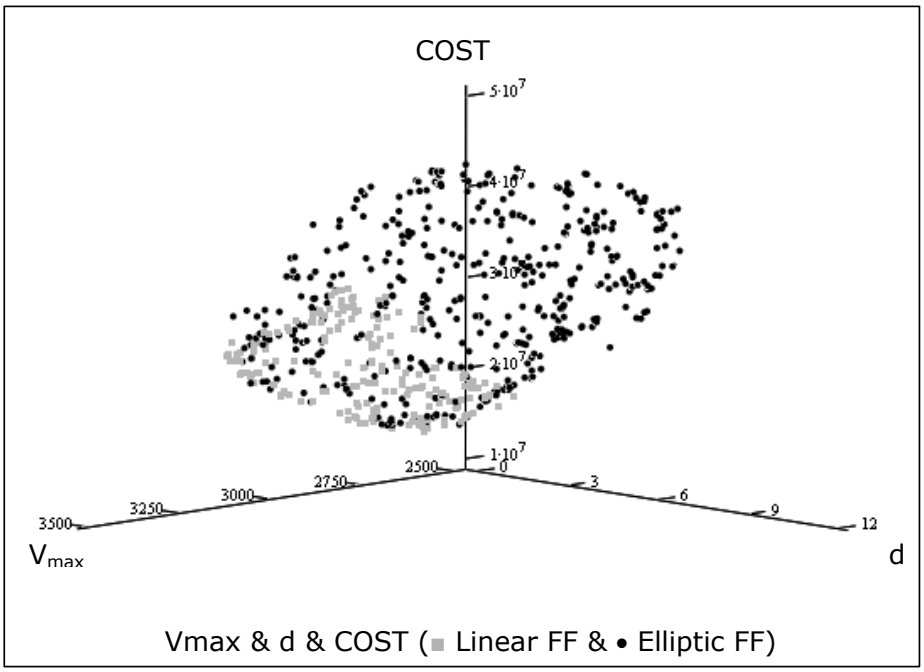

Figure 3.15 Triple-objective optimization results comparison (3D, Linear and Elliptic FFs)

CHAPTER 4

CONCLUSION

In this thesis a supersonic multi-role unmanned aerial vehicle conceptual design optimization is addressed. The UCAV is planned to have a combat mission which includes Engine Start and Warm-up, Taxi, Take-off, Climb, Cruise-out, Loiter, Descent, Dash-out, Combat (strafe), Dash-in, Climb, Cruise-in, Descent, Landing-Taxi and Shutdown. It was required to carry two types of bombs as payloads which are changing in weight and the number of these bombs is determined by the design process. The structure is composed of aluminium and some composite parts. It has a turbofan engine which was also designed for thrust, length and diameter. The aircraft is remotely piloted with a mounted Ground Control System on the vehicle. It is also capable of switching to autonomous flight in a case if the ground station contact is lost.

In the aircraft design part, fuselage, wing, horizontal and vertical tails, landing gears and engine were designed for the planned but flexible mission (the flexibility comes from the included mission parameters in design variables). Weight, static stability, performance, and structural load were also taken into account. At the end, the acquisition cost considering 500 unit productions is calculated for the designed UCAV.

The design code is verified with a simple application of the parameters of F-16 aircraft. The results obtained were reasonable enough to continue with this design configuration.

The optimization algorithm used is Multiple Cooling Multi Objective Simulated Algorithm whose performance was demonstrated previously in the references [54, 55, 56] with sample problems including a subsonic unmanned agricultural aerial robot.

In this study, the success of MC-MOSA algorithm is investigated with two kinds of fitness functions. The applicability and success of this algorithm to this kind of design problems is demonstrated with case studies given. The resultant shapes for some sample aircraft design results were also sketched with the prepared Excel sheet. The aircraft shapes obtained were very reasonable and to build confidence on the design code as well as optimization code .

The effectiveness of the algorithm was demonstrated first by applying it to a single objective optimization. Six parameters were selected as objectives: Minimizing take-off gross weight, minimizing the acquisition cost, minimizing the required fuel to complete the mission, maximizing the maximum velocity, maximizing the structural load, and maximizing the combat time. In addition, twelve constraints were selected to make sure that the design remains in the eligible bounds. The assigned design variables by the optimization loop and related results gave an idea about how approachable the desired limits for these objectives.

For the two-objective optimization part coupled-combinations of conflicting objectives were examined:
Minimize W_0 – Maximize V_{max} , Minimize COST – Maximize V_{max} , Minimize W_f – Maximize d , Maximize V_{max} – Maximize d, Minimize COST – Maximize d

And for the three-objective part the following conflicting three objectives was selected: Minimize COST – Maximize V_{max} – Maximize d.
This three-objective optimization was examined both with linear and ellipsoidal FFs.

The results demonstrate that the MC-MOSA algorithm can be effectively used in aerospace applications involving a supersonic multi-role unmanned combat aerial vehicle.

The effectiveness of the algorithm based on the type of fitness function that is used, the number of FFs and the number of iterations.

Generally, the elliptic and ellipsoidal fitness functions performed better than linear FFs.

The number of the iterations is also another parameter that helps to find a better front. However, this parameter is not addressed in this study; the experience with the code has shown that it is an important parameter.

As a future work, the design model may be improved to include a structural analysis part. In addition, cost and propulsion parts may also be improved.

REFERENCES

[1] Aeroflight, "Lockheed Martin F-16 Fighting Falcon", http://www.aeroflight.co.uk/types/usa/lockheed_martin/f-16/F-16.htm , (Last accessed date: May 19, 2008)

[2] Aerospaceweb.org, "Aircraft Landing Gear Layouts", http://www.aerospaceweb.org/question/design/q0200.shtml , (Last accessed date: April 23, 2008)

[3] Aerospaceweb.org , "F-16 Fighting Falcon Multi-Role Fighter", http://www.aerospaceweb.org/aircraft/fighter/f16/ , (Last accessed date: April 23, 2008)

[4] Ahn, J., Lee, S., and Kim, J., "A Robust Approach to Pre-Concept Design of UCAV Considering Survivability", 9th AIAA/ISSMO Symposium on Multidisciplinary Analysis and Optimization, Atlanta, Georgia, September 2002. AIAA 2002-5605

[5] Anderson Jr., J.D., Aircraft Performance and Design, McGraw-Hill, 1999

[6] Bingöl, M., Trajectory and Multidisciplinary Design Optimization of Missiles Using Simulated Annealing, M.S. Thesis, Aeronautical Engineering Department, METU, Ankara, January 2000

[7] Cabral, L.V., Paglione, P., Mattos, B.S., "Multi-Objective Design Optimization Framework for Conceptual Design of Families of Aircraft", 44th AIAA Aerospace Sciences Meeting and Exhibit, Reno, Nevada, January 2006. AIAA 2006-1328

[8] Crawford, C.A., and Simm, S.E., "Conceptual Design and Optimisation of Modern Combat Aircraft", Paper 8, RTO AVT Symposium on Aerodynamic Design and Optimization of Flight Vehicles in a Concurrent Multi-Disciplinary Environment, Ottawa, Canada, October 1999

[9] Dovi, A.R., Wrenn, G.A., "Aircraft Design for Mission Performance Using Nonlinear Multiobjective Optimization Methods", Journal of Aircraft, Vol.27, No.12, pp. 1043-1049, December 1990

[10] Epstein, B., Jameson, A., Peigin, S., Roman, D., Harrison, N., Vassberg, J., "Comparative Study of 3D Wing Drag Minimization by Different Optimization Techniques", 46th AIAA Aerospace Sciences Meeting and Exhibit, Reno, Nevada, January 2008. AIAA 2008-326

[11] Erkan, S., Kandemir, M., and Giger, G., "Advanced Task Assignment for Unmanned Combat Aerial Vehicles Targeting Cost Efficiency and Survivability", 46th AIAA Aerospace Sciences Meeting and Exhibit, Reno, Nevada, January 2008. AIAA 2008-873

[12] F16 Falcon.com, "Lockheed Martin F-16C/D", http://www.f16falcon.com/ , (Last accessed date: May 19, 2008)

[13] F-16.net The Ultimate F-16 Reference, "F-16C/D", http://www.f-16.net/f-16_versions_article5.html , (Last accessed date: May 19, 2008)

[14] Fenwick, S.V., and Harris, J. ap C., "The Application of Pareto Frontier Methods in the Multidisciplinary Wing Design of a Generic Modern Military Delta Aircraft", Paper 13, RTO AVT Symposium on Aerodynamic Design and Optimization of Flight Vehicles in a Concurrent Multi-Disciplinary Environment, Ottawa, Canada, October 1999

[15] Flug Revue, "Boeing X-45C", http://www.flug-revue.rotor.com/FRtypen/FRX-45C.htm, (Last accessed date: May 19, 2008)

[16] Flug Revue, "Northrop Grumman X-47B", http://www.flug-revue.rotor.com/FRtypen/FRX-47B.htm , (Last accessed date: May 19, 2008)

[17] Galloway, J.D.Jr., Optimization of Conceptual Aircraft Design for Stability/Control and Performance, Master Thesis, Department of Aeronautics and Astronautics, University of Washington, 2000

[18] Giunta, A.A., Aircraft Multidisciplinary Design Optimization Using Design of Experiments Theory and Response Surface Modeling Methods, PHD Thesis, Virginia Polytechnic Institute and State University, Blacksburg, Virginia, May 1997

[19] GlobalSecurity.org,"F-16 Fighting Falcon", http://www.globalsecurity.org/military/systems/aircraft/f-16.htm , (Last accessed date: May 19, 2008)

[20] Gonzalez, L.F., Périaux, J., Srinivas, K., and Whitney, E.J., "A Generic Framework for the Design Optimisation of Multidisciplinary UAV Intelligent Systems Using Evolutionary Computing", 44th AIAA Aerospace Sciences Meeting and Exhibit, Reno, Nevada, January 2006. AIAA 2006-1475

[21] Gonzáles, L.F., Srinivas, K., Périaux, J., and Whitney, E.J., "Multidisciplinary Design Optimisation of Unmanned Aerial Vehicles (UAV) Using Multi-Criteria Evolutionary Algorithms", 6th World Congresses of Structural and Multidisciplinary Optimization, Rio de Janeiro, Brazil, May-June 2005

[22] Gödel, H., and Hörnlein, H., Aeroelasticity and Optimization in Fighter Aircraft Design, Messerschmitt-Bölkow-Blohm GmbH., Helicopter and Military Aircraft Group, Germany

[23] Gundlach, J.F.IV, Multi-Disciplinary Design Optimization of Subsonic Fixed-Wing Unmanned Aerial Vehicles Projected Through 2025, Aerospace Engineering, Virginia Polytechnic Institute and State University, Virginia, February 2004

[24] Introduction to Cape Cod Documentary by Stuart Kline, "John Polando", http://www.earlyaviators.com/epolando.htm , (Last accessed date: July 9, 2008)

[25] Kim, Y., Jeon, Y.H., and Lee, D.H., "Multi-Objective and Multidisciplinary Design Optimization of Supersonic Fighter Wing", Journal of Aircraft, Vol.43, No.3, page 817, May-June 2006

[26] Kirkpatrick, S., Gelatt, C.D., Vechi, M.P., "Optimization by simulated annealing", Science 220(4598), 671–680, 1983

[27] Koenig R.W., Kraft G.A., Influence of High Turbine Inlet Temperature Engines In a Methane-Fueled SST When Takeoff Jet Noise Limits are Considered, Lewis Research Center, NASA Technical Note

[28] Kroo, I., Altus, S., Braun, R., Gage, P., and Sobieski, I., Multidisciplinary Optimization Methods for Aircraft Preliminary

Design, American Institute of Aeronautics and Astronautics, Inc., 1994. AIAA-94-4325-CP

[29] Lee, D.S., Gonzalez, L.F., Srinivas, K., Auld, D.J., and Periaux, J., "Multi-Objective/Multidisciplinary Design Optimisation of Blended Wing Body UAV via Advanced Evolutionary Algorithms", 45th AIAA Aerospace Sciences Meeting and Exhibit, Reno, Nevada, January 2007. AIAA 2007-36

[30] Lee, D.S., Gonzalez, L.F., Srinivas, K., Auld, D.J., and Wong, K.C., "Aerodynamic Shape Optimisation of Unmanned Aerial Vehicles Using Hierarchical Asynchronous Parallel Evolutionary Algorithms", International Journal of Computational Intelligence Research, Vol.3, No.3, pp. 231-252, 2007

[31] Lombardi, G., Mengali, G., and Beux, F., "Optimization Procedure for the Conceptual Analysis of Different Aerodynamic Configurations", Paper 6, RTO AVT Symposium on Aerodynamic Design and Optimization of Flight Vehicles in a Concurrent Multi-Disciplinary Environment, Ottawa, Canada, October 1999

[32] MacMillin, P.E., Golovidov, O.B., Mason, W.H., Grossman, B., and Haftka, R.T., "An MDO Investigation of the Impact of Practical Constraints on an HSCT Configuration", 35th Aerospace Sciences Meeting and Exhibit, Reno, Nevada, January 1997. AIAA 97-0098

[33] Malachowski, Ryszard J., "Designing Process of Unmanned Aerial Vehicles", Warsaw University of Technology, ICAS-96-4.2.3

[34] Mattingly,J.,D., Heiser, W.H., and Pratt, D.T., Aircraft Engine Design, 2nd edition, American Institute of Aeronautics and Astronautics, Inc., Reston, Virginia, 2002

[35] McKay, K., "Eurofighter: Aerodynamics within a Multi-Disciplinary Design Environment", Paper 1, RTO AVT Symposium on Aerodynamic Design and Optimization of Flight Vehicles in a Concurrent Multi-Disciplinary Environment, Ottawa, Canada, October 1999

[36] Military Aviation, "Lockheed (General Dynamics) F-16 Fighting Falcon", http://sirviper.com/index.php?page=fighters/f-16/index , (Last accessed date: May 19, 2008)

[37] Mirage-jet.com, "Flight Data", http://www.mirage-jet.com/COMPAR_1/compar_1.htm , (Last accessed date: May 19, 2008)

[38] Monge, F., and Varona, J.J., "Design and Optimization of Wings in Subsonic and Transonic Regime", Paper 21, RTO AVT Symposium on Aerodynamic Design and Optimization of Flight Vehicles in a Concurrent Multi-Disciplinary Environment, Ottawa, Canada, October 1999

[39] Nangia, R.K., and Palmer, M.E., "A Comparative Study of UCAV Type Wing Planforms-Aero Performance & Stability Considerations", 23rd AIAA Applied Aerodynamics Conference, Toronto, Ontario Canada, June 2005. AIAA 2005-5078

[40] Nangia, R.K., and Palmer, M.E., "Leading-Edge Vortex Flaps on Moderate Sweep Wings-UCAV Flow Improvement at High Lift", 45th AIAA Aerospace Sciences Meeting and Exhibit, Reno, Nevada, January 2007. AIAA 2007-267

[41] Newcome, L.R., Unmanned Aviation: A Brief History of Unmanned Aerial Vehicles, American Institute of Aeronautics and Astronautics, Inc., Reston, Virginia, 2004.

[42] Orlowski, M., and Tang, W., "A System for the Aerodynamic Optimization of Three-Dimensional Configurations", Paper 19, RTO AVT Symposium on Aerodynamic Design and Optimization of Flight Vehicles in a Concurrent Multi-Disciplinary Environment, Ottawa, Canada, October 1999

[43] Perez, R.E., Liu, H.H.T., and Behdinan K., "Evaluation of Multidisciplinary Optimization Approaches for Aircraft Conceptual Design", 10th AIAA/ISSMO Multidisciplinary Analysis and Optimization Conference, Albany, New York, August-September 2004. AIAA 2004-4537

[44] Piperni, P., Abdo, M., and Kafyeke, F., "The Application of Multi-Disciplinary Optimization Technologies to the Design of a Business Jet", 10th AIAA/ISSMO Multidisciplinary Analysis and Optimization Conference, Albany, New York, August-September 2004. AIAA 2004-4370

[45] Probert, B., "Aspects of Aerodynamic Optimisation for Military Aircraft Design", Paper 11, RTO AVT Symposium on Aerodynamic

Design and Optimization of Flight Vehicles in a Concurrent Multi-Disciplinary Environment, Ottawa, Canada, October 1999

[46] Raymer, Daniel P., Aircraft Design: A Conceptual Approach, 3rd edition, AIAA Education Series, American Institute of Aeronautics and Astronautics, Virginia, 1999

[47] Raymer, D.P., Enhancing Aircraft Conceptual Design Using Multidisciplinary Optimization, Doctoral Thesis, Department of Aeronautics, Royal Institute of Technology, Sweden, May 2002

[48] Roskam, J., Airplane Design Part I-VII, DAR Corporation, Lawrence, Kansas, USA, 2000

[49] Selmin, V., Vitagliano, P.L., Pennavaria, A., and Crosetta, L., "Alenia Multidisciplinary Design Optimisation-Topics and Approaches", Paper 20, RTO AVT Symposium on Aerodynamic Design and Optimization of Flight Vehicles in a Concurrent Multi-Disciplinary Environment, Ottawa, Canada, October 1999

[50] Sherer, S.E., Gordnier, R.E., and Visbal, M.R., "Computational Study of a UCAV Configuration Using a High-Order Overset-Grid Algorithm", 46th AIAA Aerospace Sciences Meeting and Exhibit, Reno, Nevada, January 2008. AIAA 2008-626

[51] Stettner, M., and Haase, W., "Multi-Objective Aeroelastic Optimization", Paper 24, RTO AVT Symposium on Aerodynamic Design and Optimization of Flight Vehicles in a Concurrent Multi-Disciplinary Environment, Ottawa, Canada, October 1999

[52] Talley, D.N., Shellpfeffer, N., Johnson, C., and Mavris, D.N., "Methodology for the Mission Requirement Determination and Conceptual Design of a Morphing UCAV", AIAA 3rd Unmanned Unlimited Technical Conference, Workshop and Exhibit, Chicago, Illinois, September 2004. AIAA 2004-6597

[53] Tekinalp O., Bingöl M., "Simulated Annealing for Missile Optimization: Developing Method and Formulation Techniques", Journal of Guidance, Control, and Dynamics, 2003

[54] Karslı G., Simulated Annealing for the Generation of Pareto Fronts with Aerospace Applications, M.S. Thesis, Aerospace Engineering Department, METU, Ankara, January 2004

[55] Tekinalp O., Karslı G., "A new Multiobjective Simulated Annealing Algorithm", J Glob Optim, 2006

[56] Özdemir S., Multi Objective Conceptual Design Optimization of an Agricultural Aerial Robot (AAR), M.S. Thesis, Aerospace Engineering Department, METU, Ankara, September 2005

[57] Torenbeek, E., Synthesis of Subsonic Airplane Design, Kluwer Academic Publishers, 1982

[58] Tse, D.C.M., and Chan, L.Y.Y., "Application of Micro Genetic Algorithms and Neural Networks for Airfoil Design Optimization", Paper 23, RTO AVT Symposium on Aerodynamic Design and Optimization of Flight Vehicles in a Concurrent Multi-Disciplinary Environment, Ottawa, Canada, October 1999

[59] U.S. Department of Labour, "Consumer Price Indexes, Inflation Calculator", http://www.bls.gov/CPI/#data , (Last accessed date: May 19, 2008)

[60] Vanderplaats, G.N., Numerical Optimization Techniques for Engineering Design, McGraw-Hill Series in Mechanical Engineering, 1984.

[61] Vicini, A., and Quagliarella, D., "A Multiobjective Approach to Transonic Wing Design by means of Genetic Algorithms", Paper 22, RTO AVT Symposium on Aerodynamic Design and Optimization of Flight Vehicles in a Concurrent Multi-Disciplinary Environment, Ottawa, Canada, October 1999

[62] Whitford, R., Fundemantals of Fighter Design, The Crowood Press Ltd., Ramsbury, Marlborough, Wiltshire, 2004

[63] Wikipedia The Free Encyclopedia, "Boing X-45", http://en.wikipedia.org/wiki/Boeing_X-45 , (Last accessed date: July 9, 2008)

[64] Wikipedia The Free Encyclopedia, "F-16 Fighting Falcon", http://en.wikipedia.org/wiki/F-16 , (Last accessed date: May 19, 2008)

[65] Wikipedia The Free Encyclopedia, "MQ-9 Reaper", http://en.wikipedia.org/wiki/MQ-9_Reaper , (Last accessed date: July 9, 2008)

[66] Wikipedia The Free Encyclopedia, "Tricycle Gear", http://en.wikipedia.org/wiki/Tricycle_landing_gear , (Last accessed date: April 23, 2008)

[67] Wikipedia The Free Encyclopedia, "Unmanned combat air vehicle", http://en.wikipedia.org/wiki/UCAV , (Last accessed date: April 23, 2008)

[68] Woolvin, S.J., "A Conceptual Design Study of the 1303 UCAV Configuration", 24th Applied Aerodynamics Conference, San Francisco, California, June 2006. AIAA 2006-2991

[69] Woolvin, S.J., "UCAV Configuration & Performance Trade-offs", 44th AIAA Aerospace Sciences Meeting and Exhibit, Reno, Nevada, January 2006. AIAA 2006-1264

[70] Yenne, B., Attack Drones: A History of Unmanned Aerial Combat, Zenith Press, USA, 2004

[71] Sobieski, J.S., and Chopra, I., "Multidisciplinary Optimization of Aeronautical Systems", Journal of Aircraft, Vol.27, No.12, pp. 997-998, December 1990

[72] Defense Advanced Research Projects Agency, "Joint Unmanned Combat Air Systems J-UCAS Overview", http://www.darpa.mil/j-ucas/fact_sheet.htm , (Last accessed date: August 9, 2008)

[73] Defense Industry Daily, "Britain Requests 10 MQ-9 Reapers for over $1B", http://www.defenseindustrydaily.com/britain-requests-10-mq-9-reapers-for-over-1b-04536/ , (Last accessed date: August 9, 2008)

APPENDIX A

INPUT and OUTPUT SAMPLES

A.1 A Sample Input File

```
&initialize
p=0.01,
Temperature = 150*10000000.,
fdim = 12,
ffdim = 121,
accuracy_required = 0.0000001,
n_of_loops = 1,
fe_per_loop = 5000,
loop_factor = 1.,.5,0.25, 147*0.1
x0 = 10.0,3.2,32.0,45.0,0.40,0.40,0.5,3000.0,2000.0,0.0,0.0,0.0
xupper = 15.0,5.0,50.0,55.0,0.45,0.45,0.75,4000.0,3000.0,5.0,5.0,5.0
xlower = 8.0,2.0,30.0,35.0,0.40,0.40,0.1,100.0,1000.0,-5.0,-5.0,-5.0
fmax = 10000000.,
fmin = -10000000.,
stopcriteria = 78000,
ftest = -1000.
weights=0.0,0.0,0.0,0.0,0.0,0.0,0.0,0.0,0.0,0.0,0.0,0.1,0.1,0.1,0.1,0.1,0.1,0.1,
0.1,0.1,0.1,0.1,0.2,0.2,0.2,0.2,0.2,0.2,0.2,0.2,0.2,0.2,0.2,0.3,0.3,0.3,0.3,0.3,0.
3,0.3,0.3,0.3,0.3,0.3,0.4,0.4,0.4,0.4,0.4,0.4,0.4,0.4,0.4,0.4,0.4,0.5,0.5,0.5,0.5,
0.5,0.5,0.5,0.5,0.5,0.5,0.5,0.6,0.6,0.6,0.6,0.6,0.6,0.6,0.6,0.6,0.6,0.6,0.7,0.7,0.
7,0.7,0.7,0.7,0.7,0.7,0.7,0.7,0.7,0.8,0.8,0.8,0.8,0.8,0.8,0.8,0.8,0.8,0.8,0.8,0.9,
0.9,0.9,0.9,0.9,0.9,0.9,0.9,0.9,0.9,0.9,1.0,1.0,1.0,1.0,1.0,1.0,1.0,1.0,1.0,1.0,1.
0
penalty_coeff = 0.1, 1.0, 0.1, 1.0, 1.0, 0.1, 0.1, 0.1, 0.1, 0.1, 0.1, 0.1, 0.1
/
```

A.2 A Sample Output File

```
-----------------------------------------------

Design Variables :
y(1)=   8.953996
y(2)=   4.266974
y(3)=   44.02119
y(4)=   35.50978
y(5)=  0.4258094
y(6)=  0.4211011
y(7)=  0.1643288
y(8)=   1096.548
y(9)=   2.001251
y(10)=  -4.299292
y(11)=   1.070643

-----------------------------------------------

Constraints:
constraints(1)=  0.0000000E+00
constraints(2)=  0.0000000E+00
constraints(3)=  0.0000000E+00
constraints(4)=  0.0000000E+00
constraints(5)=  0.0000000E+00
constraints(6)=  0.0000000E+00
constraints(7)=  0.0000000E+00
constraints(8)=  0.0000000E+00
constraints(9)=  0.0000000E+00
constraints(10)=  0.0000000E+00
constraints(11)=  0.0000000E+00
constraints(12)=  0.0000000E+00
constraints(13)=  0.0000000E+00

-----------------------------------------------
```

WingConfiguration

S= 18.78943
cr= 3.724461
ct= 0.4724221
ybar= 1.660317
cbar= 2.518426
xbar= 1.905972
sweep_angle_LE= 48.94190
Taper_ratio= 0.1268431
Snetw= 17.31100
Swetw= 35.48756
ARwet= 2.259215
L_Dmax= 22.09307
VFueltankw= 1.916452
Wfmaxw= 1494.833

FuselageConfiguration

Lf= 8.059099
lN= 1.427646
LM= 4.388009
LA= 2.243444
FinenessRatio= 9.878794
VOLUME= 3.359576
Swet_f= 17.94475

PropulsionSystem

T= 65.73273
Leng= 3.471266
Deng= 0.7344167
SFC= 0.6400000
SFCc= 1.527117

HorizontalandVerticalTailSize

SVT= 3.431839
hVT= 2.191934
crVT= 2.408719
ctVT= 0.7226157
zbarVT= 0.8992549
cbarVT= 1.716984
SnetVT= 3.349854
SwetVT= 6.867202

SHT= 5.577377
bHT= 4.354662
crHT= 1.829690
ctHT= 0.7318760
ybarHT= 0.9331418
cbarHT= 1.359198
wfmaxHT= 0.0855439
SnetHT= 5.437079
SwetHT= 11.14601

LandingGear

D_nosewheel= 0.3506204
w_nosewheel= 0.0709605
D_mainwheel= 0.5522140
w_mainwheel= 0.1432409

Aerodynamics

CD0_fuselage= 0.0021275
CD0_w= 0.0049906
CD0_HT= 0.0017241
CD0_VT= 0.0010242
CD0_misc= 0.0063866

CD0_wave= 0.0051185
CD0_total= 0.0224399
CD0c= 0.0160534
K= 0.1768093
e= 0.7059147
CL_ac_alpha= 4.242167
Mcruise= 1.374441
bomb_big= 1
bomb_aim9= 2
Ground_effect= 0.7615103

CLmax_clean= 2.520180
CL_ac_max_TO= 1.941566
CLmax_landing= 2.516845

WeightandStability

Static_margin= -0.0246654 "acceptable"
Wwing= 630.0856
Whorizontaltail= 132.7665
Wverticaltail= 149.2681
Wfuselage= 269.8283
Wengine= 544.6189
Winstruments= 15.60357
Wavionics= 490.8732
Wmainlandinggear= 60.18327
Wnoselandinggear= 39.57265
Welse= 1006.597
We= 3399.580
Wfmaxw= 1494.833

InitialSizing

W0= 5990.960
Wf= 1494.833

Wfmaxw= 1494.833
We= 3399.580
Wpayload= 1096.548

StructuralLoad
nmax= 11.99996
Vmanuever= 1297.633
Kp= 0.8504344

Performance
TakeoffDist= 343.7356
LandingDist= 611.4811
WS_TO= 3127.89
MAX_ROC= 293.4244
Maximum Ceiling= 18387.00
RANGE= 2297.895
Maximum_endurance= 2.778683
Vmax= 2830.923
Mmax= 2.665025
Vcorner= 607.0861
nmax= 11.99996
R_sus_turn_min= 81.02170
sus_turn_rate_max= 16.86093
R_pup_turn= 874.0395
pup_turn_rate= 11.05532
R_pdown_turn= 803.9991
pdown_turn_rate= 12.01840
d= 2.065573
xx= 6.0

Costs
Quantity= 500
CostE= 1,259,480
COST= 18,127,982

APPENDIX B

UCAV SAMPLES

B.1 Boing X-45C

These properties were taken from Ref. [15]:

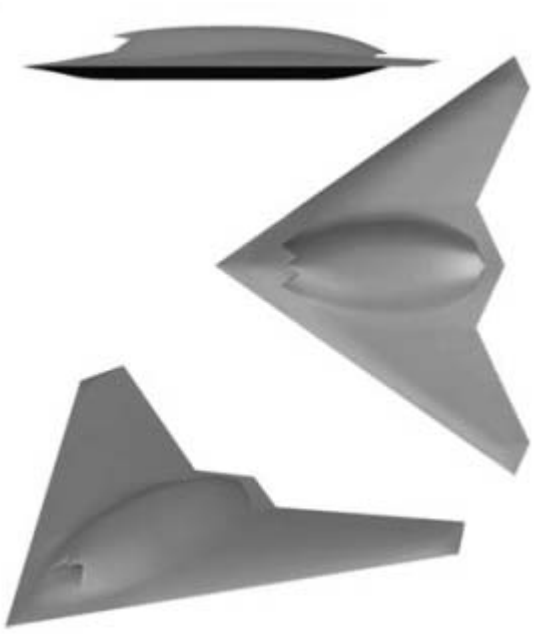

Figure B.1 Boing X-45C [72]

Type: UCAV (Unmanned Combat Air Vehicle)

Country: USA

Manufacturer : Boeing Integrated Defense Systems PO Box 516 St. Louis, Missouri 63166 USA

Crew: 0
Weapons: it can carry up to 8 SDBs (Small Diameter Bombs) or two 910 kg JDAMs

Power plant: 1 x General Electric F404-GE-102D
Thrust: about 50 kN dry

Dimensions
Length: 11,9 m
Span: 14,95 m

Weights
Empty weight: 8165 kg
Weapons laod: 2040 kg
Max. gross weight: about 16555 kg

Performance
Cruise speed: Mach 0.8
Service ceiling: 12190 m (40000 ft)
Combat radius: over 2220 km

Costs ??

B.2 Northrop Grumman X-47B

These properties were taken from Ref. [16]:

Figure B.2 Northrop Grumman X-47B [72]

Type: UCAV (Unmanned Combat Air Vehicle)

Country : USA
Manufacturer: Northrop Grumman (Integrated Systems) PO Box 509066 San Diego, CA 92150-9066 USA
Phone: 001-858/618-4405
Internet: www.northropgrumman.com

Crew: 0

Weapons: 2 x JDAM (905 kg each) or 12 of the Small Diameter Bombs (113 kg each).

Power plant: 1 x Pratt & Whitney F100-220
Thrust: 105,7 kN

Dimensions
Length: 11,63 m
Height: 3,10 m
Span: 18,92 m

Weights
Weapons load: 2040 kg internal
Max. gross weight: ca 19050 kg (up to 21790 kg have been mentioned)

Performance
Cruise speed: high subsonic
Service ceiling: 12190 m (40000 ft)
Combat radius: over 2775 km (1500 NM) for ISR missions
Ferry range: 6500 km
Flight time: about 7 hours

Costs : ?? (under development)

B.3 General Atomics Aeronautical Systems MQ-9 Reaper

These properties were taken from Ref. [65]:

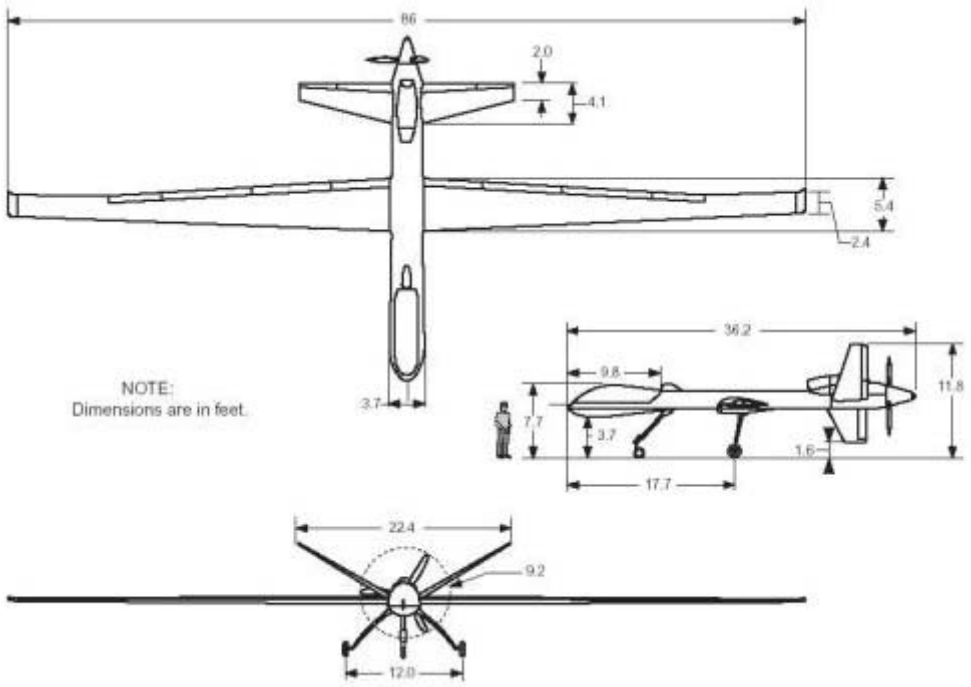

Figure B.3 General Atomics Aeronautical Systems MQ-9 Reaper [73]

Type: UCAV (Unmanned Combat Air Vehicle)
Contractor: General Atomics Aeronautical Systems Incorporated

General Characteristics
Landing Type: runway
Launch Type: runway
Power Plant: Honeywell TP331-10 turboprop engine, 670 kW

Performance
Ceiling: 50,000 ft (15 km)
Operational altitude: 25,000 ft (7.5 km)

Endurance: 16-28 h
Range: 3682 mi (3200 nmi, 5926 km)
Maximum speed: 400 km/h (250 mph, 220 knots)
Cruise speed: 160 km/h (100 mph, 85 knots)

Weight: 1676 kg (3700 lb) empty; 4760 kg (10,500 lb) max
Fuel Capacity: 1,300 kg (3,907 lb)
Payload: 1700 kg (3800 lb)
Wingspan: 20 m (66 ft)
Length: 11 m (36 ft)

Armanent
6 Hardpoints under the wings, can carry a payload mix of 1,500 lb. on each of its two inboard weapons stations, 500-600 lb. on the two middle stations and 150-200 lb. on the outboard stations.
Up to 14x AGM-114 Hellfire air to ground missiles can be carried or 4 Hellfire missiles and 2 500lbs GBU-12 Paveway II laser-guided bombs. The ability to carry the JDAM in the future is also possible.

Unit cost: USD 8 million (approximate, varies by configuration)